Breakdown of GABAergic control in thalamocortical epilepsies

Peter Malcolm Klein
St. Louis Park, MN

Bachelor of Science in Neuroscience, Bates College, 2008

A Dissertation presented to the Graduate Faculty
Of the University of Virginia in Candidacy for the Degree of
Doctor of Philosophy

Neuroscience Graduate Program and
Department of Pharmacology

University of Virginia
May, 2018

Abstract

Breakdown of GABAergic control in thalamocortical epilepsies

Peter M. Klein

Adviser: Mark P. Beenhakker, Ph.D.

Absence epilepsy, characterized by brief seizures that spread throughout the brain, results from abnormal rhythmic activity between networks of thalamic and cortical neurons. Inhibitory GABAergic signaling among neurons of the reticular thalamic (***RT***) nucleus is proposed to form a critical choke point that normally prevents the generation of seizures. Neurons need to maintain low intracellular Cl^- concentrations ($\boldsymbol{[Cl^-]_i}$) to enable inhibitory neuronal responses to $GABA_A$ receptor-mediated signaling. The Cl^- transporter KCC2 and extracellular impermeant anions ($\boldsymbol{[A]_o}$) of the extracellular matrix maintain a low $[Cl^-]_i$ in RT neurons under basal conditions. However, low KCC2 expression reduces the Cl^- extrusion capacity of RT neurons and facilitates $[Cl^-]_i$ accumulation during periods of elevated GABAergic signaling. The thalamic choke point breaks down, allowing seizures to occur, when the $[Cl^-]_i$ of RT neurons becomes sufficiently elevated to produce excitatory GABAergic signaling. The seizure-prone WAG/Rij strain of rats has reduced RT expression of both KCC2 and $[A]_o$, potentially promoting the occurrence of spontaneous absence seizures. A more complete understanding of the mechanisms that enable inhibitory GABAergic signaling among RT neurons to form a critical seizure choke point has the potential to improve the treatments available to patients with absence epilepsy.

Acknowledgements

Family. I am incredibly thankful for the strong support I have always received from my parents for all of my endeavors. You have taught me to always value the pursuit of knowledge and to be a careful observer of the world around me. I partially trace my interest in understanding the underlying mechanisms of complex neurological systems to the early experiences you provided me with disassembling old appliances. Daniel and Sophie, thank you for being wonderful siblings.

Friends. I have been fortunate to shared my time in Charlottesville with a fantastic group of friends. Whether it was through kickball games, biweekly bar trivia, hikes, beer festivals or late-night pizza, you have made six years of grad school fly by.

Lab. Without question, there is no other lab environment like that of the Beenhakker Lab. Between watching looping videos of bigfoot sightings and debating what makes a great burrito, we still find time to conduct research in a way I am proud to be part of. Katie, you have been an integral part of the Beenhakker lab since before my rotation (not that you would ever let me forget it) and it has been great to see you mature as a scientist. Lise, we've been through a lot since we took the plunge together, but we're close to the finish line. Adam, you are an island of calm amongst the storm and your analytical insights have elevated all of our research. Ashley, I'm grateful for your critical help as I have been wrapping up my own time in the lab. Thank you for tolerating the not always controlled chaos. You have all made our lab feel more like a family than a group of coworkers.

Mark. I am endlessly grateful for the mentorship, guidance and support you have provided me throughout my graduate training. I appreciate the freedom you always gave me to pursue the research questions that excited me. Thank you for putting up with me irregardless of my occasional stubbornness and passion for arguing over minutia. You are an inspiration for the kind of researcher I hope to become.

Committee. Thank you to the members of my committee: Drs. Jaideep Kapur, Doug Bayliss, Howard Goodkin, Bimal Desai and Paula Barrett. While I could have been better at seeking out your advice, I appreciate how you were always supportive of my growth as a scientist.

Program. I am grateful for the strong training I received in the Neuroscience Graduate Program under the leadership of Drs. Bettina Winkler, Manoj Patel and Chris Deppmann and through the administrative support of Nadia Badr Cempré. Thank you as well to Jolene Kidd, Antoinette Denise Reid, Deborah Steele and Tammy Snow who made the Department of Pharmacology an incredibly welcoming and supportive environment.

Princess. You are truly rat royalty. Thank you for always providing a calming influence for the lab and for the selfless contributions of your kin.

Funding. This work was supported by the Epilepsy Foundation, and NIH 5T32GM008328-22 and 1R01NS099586.

Table of contents

Chapter 1: Introduction

Epilepsy Overview

Current estimates indicate that 1 in 26 people will develop epilepsy in their lifetime (Hesdorffer et al., 2011). By this measure, epilepsy burdens approximately 70 million people worldwide (Ngugi et al., 2010), establishing epilepsy as the fourth most prevalent neurological disorder in the world (Hirtz et al., 2007). While the precise definition of epilepsy continues to evolve (Fisher et al., 2005, 2014), epilepsy can generally be characterized as a disorder in which patients experience spontaneously occurring seizures. Individual seizures are periods of brain activity during which populations of neurons are excessively active and synchronized. An individual experiencing multiple, recurrent seizures is classified as having epilepsy. Furthermore, having a high probability of experiencing a subsequent seizure or being diagnosed with an underlying syndrome that is linked to epilepsy can also lead to a patient being considered epileptic (Fisher et al., 2014).

Overall, epilepsy encompasses a wide spectrum of more than 25 distinct syndromes (Berg et al., 2010). These syndromes result from a diverse range of genetic, metabolic, immunological, structural or even currently unknown etiologies (Scheffer et al., 2017). More broadly, the majority of epilepsy syndromes are associated with either focal or generalized seizures. Focal seizures are typically isolated to a single, or a small number of brain regions, whereas generalized seizures spread widely throughout the brain (Scheffer et al., 2017). In this document, I will focus on the mechanisms involved in a specific subgroup of generalized seizures associated with absence epilepsy.

Absence Epilepsy

Absence epilepsy has been a recognized disorder for nearly 250 years, yet even today there is much that remains to be learned about this condition. While brief impairments of consciousness were previously considered as a common accompaniment of other epilepsies, the Swiss physician Samuel Tissot was the first to describe these clinical features as an independent condition (Tissot, 1770; Eadie and Blandin, 2001). These brief impairments of consciousness were only later termed ‘absences’ (Calmeil, 1824). Gibbs, Davis and Lennox later used the still very new technology of electroencephalography (***EEG***) to capture the first recordings of the underlying electrical activity of the brain that occurs during an absence seizure (1935). The seizures observed in twelve different patients all shared characteristic 3 Hz oscillations, with combined spike and wave elements (**Fig. 1A**). To this day, absence epilepsy is defined by the simultaneous occurrence of bilateral and symmetrical 2-4 Hz spike-and-wave discharges (***SWDs***) (**Fig. 1B**), and brief behavioral absences characterized by loss of consciousness, pausing, staring, and in some cases mild automatisms (Panayiotopoulos, 2008).

Absence epilepsy fits within the classification of the *genetic generalized epilepsies*, and includes the syndromes of both childhood absence epilepsy and juvenile absence epilepsy, which are largely differentiated based on age of onset (Beghi et al., 2006; Gallentine and Mikati, 2012). Patients with absence epilepsy generally have more favorable outcomes than individuals experiencing tonic-clonic seizures, as well as a higher likelihood of undergoing remission (Seneviratne et al., 2012). However, nearly 15% of patients with absence epilepsy eventually

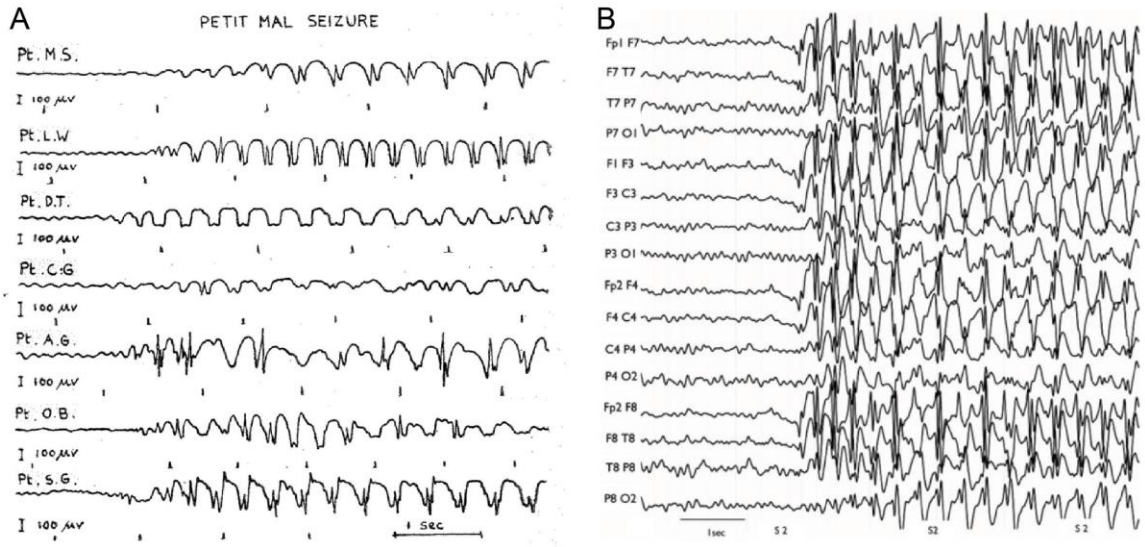

Figure 1. Early and modern examples of absence epilepsy EEG. ***A***, Early recording of EEG activity associated with absence seizures observed in paired electrode recordings from a number of different patients (i.e. Pt. M. S., Pt. L. W.). These absence seizures display a clear 3 Hz spike-and-wave discharge pattern of activity (figure modified from Gibbs et al., 1935). ***B***, Modern example of an EEG recording showing the absence seizure activity of a patient, obtained from a set of 30 scalp electrodes (figure modified from Moeller et al., 2008).

develop myoclonic epilepsy and an even greater number are at risk of developing generalized tonic-clonic seizures (Trinka et al., 2004). In addition to seizures, patients with absence epilepsy often display comorbidities such as cognitive and linguistic deficits, and an increased incidence of attention-deficit hyperactivity disorder. However, these comorbidities can be ameliorated when seizures are effectively controlled with antiepileptic drugs (Caplan et al., 2008; Hughes, 2009).

Currently, both the antiepileptic drugs ethosuximide and valproate have some established efficacy in the treatment of absence epilepsy, and clinical trials indicate lamotrigine is also possibly effective at reducing absence seizures (Glauser et al., 2013a). However, over half of all patients taking one of these three drugs will either continue to experience seizures or will need to stop treatment due to intolerable side effects (Glauser et al., 2013b). Thus, while absence epilepsy is in some cases one of the more tractable forms of epilepsy, there remains a clear need to continue developing tools and strategies to further our understanding of absence epilepsy and to seek new cures. While there are many potential mechanisms involved in generating absence seizures, the specific role of the thalamus is of particular interest to me.

The Thalamus and Absence Epilepsy

Longstanding evidence links absence epilepsy to altered activity in the thalamus. A defining characteristic of absence epilepsy is that seizure activity is generalized and can be detected simultaneously throughout the brain (Gallentine and Mikati, 2012). Some of the first experimental evidence to link the thalamus to

seizure-like activity in the cortex came from extracellular recordings performed in nembutalized cats (Morison et al., 1943). In these recordings, spontaneous bouts of 5-10 Hz synchronized electrical activity were observed in multiple regions of the cortex, while similar activity could be recorded simultaneously by an electrode placed in the thalamus (**Fig. 2A**). Later experiments in decorticated cats indicated that even in the absence of cortical input, the thalamus was capable of spontaneously generating periods of synchronized neuronal activation (Morison and Bassett, 1945) (**Fig. 2B**).

The first direct evidence that specific waveforms generated by the thalamus were sufficient to induce generalized, seizure-like, cortical responses came from experiments in which various brain regions in cats were stimulated with rhythmic electrical pulses. Electrical stimulation of the midline and intralaminar thalamus at 3 Hz was found to be sufficient to generate bilateral 3 Hz SWDs in the cortex that recapitulated the electrical signature of EEG from human patients with absence epilepsy (Jasper and Droogleever-Fortuyn, 1947) (**Fig. 2C**). The development of the feline generalized penicillin epilepsy model, in which intramuscular injections of penicillin induced seizures that behaviorally, electrophysiologically, and pharmacologically replicate characteristics of human absence epilepsy, permitted seizure studies without the need for direct electrical stimulation (Prince and Farrell, 1969; Kostopoulos, 2000). Penicillin is believed to evoke seizure activity through antagonizing inhibitory GABAergic signaling (MacDonald and Barker, 1977; Kostopoulos et al., 1981). Experiments conducted with feline and rodent models demonstrate that the generation of absence seizures requires altered patterns of

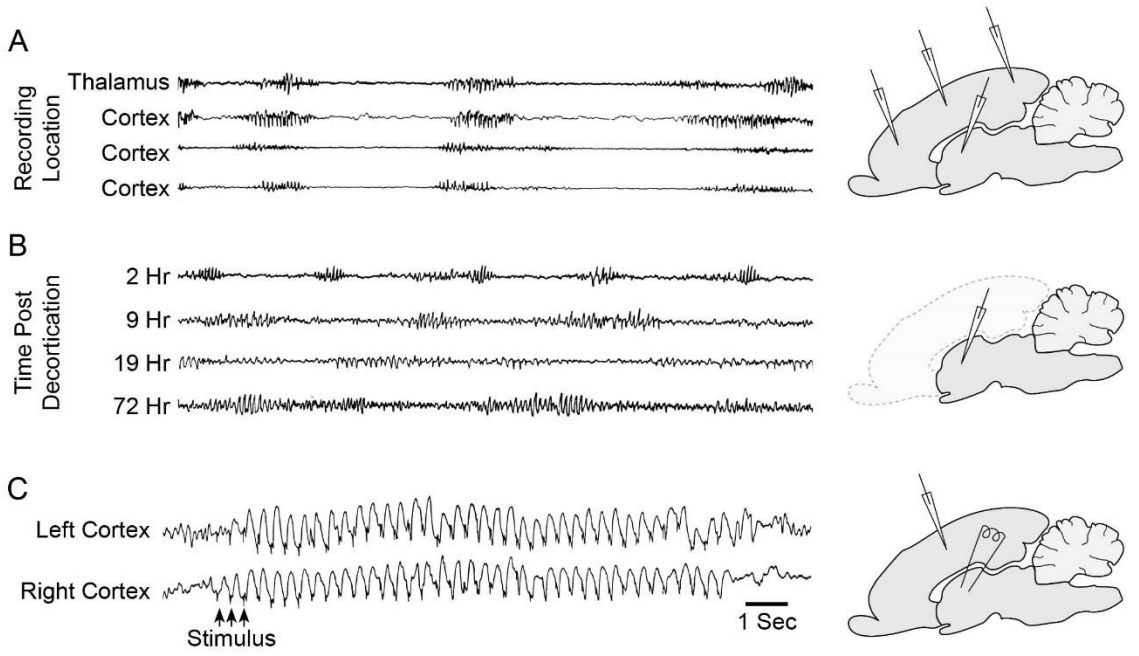

Figure 2. Early evidence of thalamic involvement in absence seizures. ***A***, (*left*) *in vivo* recording of electrical activity in a nembutalized cat indicates that intermittent bursts of activity could be recorded simultaneously on both cortical and thalamic electrodes (figure modified from Morison et al., 1943). (*right*) Diagram roughly indicating the presence of three cortical and one thalamic electrode in this recording. ***B***, (*left*) *in vivo* recording of electrical activity in a nembutalized cat following decortication suggests that the thalamus can generate intermittent bursts of activity independent of cortical inputs (figure modified from Morison et al., 1945). (*right*) Diagram roughly indicating the presence of one thalamic electrode in this recording from a decorticated cat. ***C***, (*left*) *in vivo* recording of electrical activity in a nembutalized cat in response to 3 Hz electrical stimulation of the thalamus produced an absence seizure-like pattern of cortical activity that persisted beyond the end of stimulation (figure modified from Jasper and Droogleever-Fortuyn, 1947). This indicates that thalamic activation is sufficient to evoke seizure-like activity. (*right*) Diagram roughly indicating the presence of one thalamic stimulating electrode and one cortical recording electrode in this experiment.

electrical activity in both the cortex and thalamus, with the cortex likely initiating seizure-like events and the thalamus then maintaining the observed 3 Hz rhythm of SWDs (Contreras and Steriade, 1995; Meeren et al., 2002; Avoli, 2012). In both the WAG/Rij and GAERS rats, two genetic models of absence epilepsy, seizures likely originate in the perioral region of the somatosensory cortex before spreading to other cortical and thalamic regions (Meeren et al., 2002; Polack et al., 2007; Leresche et al., 2012).

In addition to animal studies, the role of the thalamus in the generation of absence seizures has also been studied in humans. When recordings were acquired from patients implanted with depth electrodes, thalamic 3 Hz spike-and-wave discharges originated prior to, or coincident with, activation of the cortex (Williams, 1953). More recent, combined EEG-fMRI studies of patients with absence epilepsy found that increased activation of the thalamus correlates with the occurrence of seizures (Labate et al., 2005; Moeller et al., 2008). Collectively, studies conducted in cats, rats and humans provide abundant evidence that the thalamus holds an important and necessary role in the generation of absence seizures.

As a vast number of studies indicate that the thalamus plays a key role in the generation of absence seizures, significant effort has focused on understanding the particular mechanisms through which the thalamus propagates generalized epileptiform activity. Research into the rhythmogenic mechanisms within the thalamus that generate absence seizures have garnered much insight from studies into how the thalamus produces another pattern of rhythmic activity

known as sleep spindles. Unlike the 3 Hz activity of absence seizures, sleep spindles are spontaneous bouts of 12-14 Hz rhythmic oscillations (Loomis et al., 1935). Electrographically, sleep spindles wax and wane in amplitude, thereby resembling the shape of a spindle of yarn, and occur during non-REM sleep (De Gennaro and Ferrara, 2003). Informed by earlier EEG experiments, a hypothesis emerged that the same thalamic circuits normally involved in generating sleep spindles could, if perturbed, produce the cortical hypersynchrony that likely underlies the loss of consciousness associated with absence seizures (Gloor, 1978; Kostopoulos, 2000).

As described above (see **Fig. 2B**), the thalamus is capable of generating 5-10 Hz rhythmic oscillations even in the absence of cortical connections. The thalamic oscillations in decorticated cats resemble sleep spindles and suggest that the essential neural circuitry required to produce sleep spindle oscillations is located entirely within the thalamus (Morison and Bassett, 1945). Understanding the organization of neural circuits within the thalamus therefore appears critical for determining how one brain region can produce both benign sleep spindles and the pathological rhythmic activity of absence seizures.

Oscillatory Circuits in the Thalamus

While earlier studies demonstrated that isolated thalamic circuits are sufficient to sustain sleep spindles (Morison and Bassett, 1945; Andersen et al., 1967; Andersson et al., 1971), it remained unclear precisely how thalamic neurons generated oscillatory activity patterns. Lesioning the reticular thalamic (***RT***)

nucleus in cats prevents the remaining thalamic regions from generating further sleep spindle or other oscillatory activity (Steriade and Deschênes, 1984; Steriade et al., 1985). These results implicated the RT nucleus as an essential component of the pacemaking circuitry responsible for generating rhythmic thalamic activity. However, further studies found that thalamocortical neurons are also required for the generation of 12-14 Hz activity, informing a model where sleep spindles require interactions between RT and thalamocortical neurons (Buzsáki, 1991; McCormick and Bal, 1997).

The RT nucleus is a component of the ventral thalamus and forms a thin shell of neurons that covers many surfaces of the dorsal thalamus (Jones, 2007). RT neurons appear to receive collaterals from nearly every passing corticothalamic and thalamocortical projection (Steriade and Deschênes, 1984; Oh et al., 2014), yet are believed to only send projections to the dorsal thalamus (Jones, 1975). Thalamocortical neurons are largely located within the dorsal thalamus, and are responsible for relaying sensory, motor and association signals from the thalamus to various regions of the cortex (Steriade and Deschênes, 1984; Jones, 2007). The ventroposterior medial and ventroposterior lateral nuclei within the dorsal thalamus are collectively known as the ventrobasal (***VB***) complex and transmit somatosensory stimuli to the cortex (Rose and Mountcastle, 1952; Jones, 2007) (**Fig. 3A**). The specific interactions between RT and VB neurons have been studied extensively in the context of absence epilepsy (Huguenard and Prince, 1994; Cox et al., 1996; Gentet and Ulrich, 2003).

RT neurons form GABAergic connections onto VB neurons (Houser et al., 1980; Pinault and Deschênes, 1998), while VB neurons send excitatory glutamatergic afferents to both the cortex and back to RT neurons (Ottersen et al., 1983; Kaneko and Mizuno, 1988; Kharazia and Weinberg, 1994). The network formed among RT and VB neurons forms a central pattern generator-like circuit that at the most basic level produces alternating firing of VB and RT neurons (**Fig. 3B**). Central pattern generating circuits are certain neural circuits that are intrinsically capable of generating rhythmic activity, even in the absence of descending inputs carrying timing information (Wilson, 1961; Marder and Bucher, 2001). Similarly, even isolated networks of RT and VB neurons are capable of generating robust rhythmic activity. Acute brain sections containing only the thalamus can still generate both spindle-like and SWD-like oscillations (von Krosigk et al., 1993; Huguenard and Prince, 1994). Next, I will present a prevailing model that describes how interactions between RT and VB neurons can sustain network oscillations.

Activated RT neurons fire action potentials that trigger the release of GABA onto VB neurons. GABA release inhibits VB neurons by activating post-synaptic $GABA_A$ and $GABA_B$ receptors (Huguenard and Prince, 1994). Although RT activity briefly inhibits VB neurons, hyperpolarization also primes the VB neuron for a T-type Ca^{2+} channel-dependent, post-inhibitory rebound burst of action potentials (further described below). As VB neurons are glutamatergic and send excitatory projections to RT neurons, post-inhibitory rebound bursting of VB neurons is often sufficient to reactivate RT neurons. RT neurons also express T-type Ca^{2+} channels

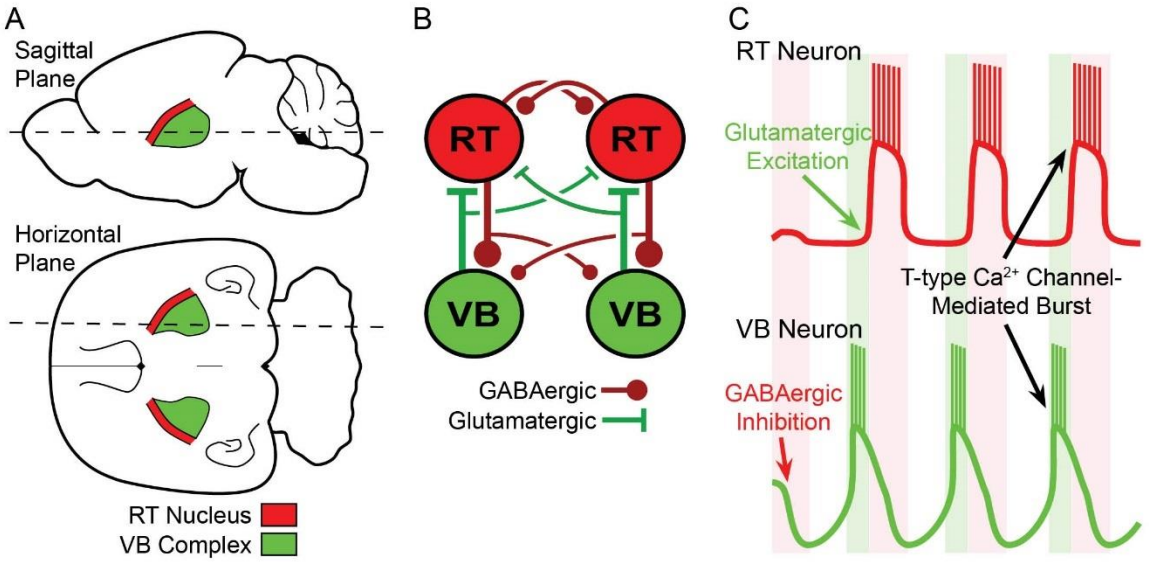

Figure 3. Overview of the thalamic oscillatory circuit. ***A***, Approximate location of the reticular thalamic (RT) nucleus and the ventrobasal (VB) complex within the rat brain. Dashed lines indicate the orientations at which the two projected planes would intersect ***B***, Simplified diagram of the synaptic connectivity of the thalamic oscillatory network. Only projections among thalamic neurons are included, thus corticothalamic and thalamocortical connectivity is not shown ***C***, Schematic of oscillatory network activity between an RT and a VB neuron. An initial inhibitory GABAergic input onto a VB neuron produces hyperpolarization that is followed by a T-type Ca^{2+} channel-mediated rebound burst of action potentials. Excitatory glutamatergic signaling from this VB neuron depolarizes the RT neuron sufficiently to induce the firing of action potentials that are further aided by activation of T-type Ca^{2+} channels. GABAergic inhibition from the RT neuron again hyperpolarizes the VB neuron and primes the circuit for another round of oscillatory activity. Shaded regions indicate times when GABAergic (red) or glutamatergic (green) signaling is occurring.

(von Krosigk et al., 1993; Talley et al., 1999; Huguenard and McCormick, 2007), and therefor produce bursts of activity in response to VB-mediated excitation (**Fig. 3C**). In the thalamus, the specific molecular properties of T-type Ca^{2+} channels provide a critical contribution that enables sustained recurrent network oscillations.

T-type Ca^{2+} channels are composed entirely of a single α1G, α1H or α1I pore forming subunit (Cribbs et al., 1998; Perez-Reyes et al., 1998; Lee et al., 1999), which form channels referred to as $Ca_V3.1$, $Ca_V3.2$ and $Ca_V3.3$, respectively (Ertel et al., 2000; Zamponi et al., 2010). T-type Ca^{2+} channels are characterized by their low voltage threshold for activation, fast inactivation and slow deinactivation kinetics, and small conductances (Huguenard, 1996; Talley et al., 1999). In contrast, high voltage-activated Ca^{2+} channels require a larger membrane depolarization to evoke activation and can contain β, α2δ and γ subunits in addition to the pore forming α1 subunit (Zamponi et al., 2010).

Due to their low threshold for activation and rapid inactivation, nearly half of all T-type Ca^{2+} channels in VB neurons are often already inactivated at the resting membrane potential of -81 mV, with the remainder quickly inactivating when the neuron further depolarizes (Huguenard and McCormick, 1992; Huguenard and Prince, 1992; Huguenard, 1996). Robust GABAergic input from RT neurons onto VB neurons produces $GABA_B$ receptor-mediated inhibitory postsynaptic potentials (***IPSPs***) that persists for >200 ms (Huguenard and Prince, 1994). Such prolonged hyperpolarization is sufficient to deinactivate a large proportion of T-type Ca^{2+} channels in VB neurons (Coulter et al., 1989; Huguenard and McCormick, 1992; Huguenard, 1996). As RT neurons cease firing and GABA-mediated inhibition

wanes, VB neurons return towards their resting membrane potential, allowing reprimed T-type Ca^{2+} channels to open in a voltage-dependent manner. As T-type Ca^{2+} channels open, a regenerative low-threshold spike (***LTS***) is produced (Llinas and Jahnsen, 1982; Coulter et al., 1989). The ensuing LTS drives VB neurons towards depolarized membrane potentials that are sufficient to activate voltage-gated Na^{+} channels and enable a post-inhibitory rebound burst of action potentials in VB neurons. The action potentials generated by VB neurons can then activate postsynaptic RT neurons through the release of the excitatory neurotransmitter glutamate. Post-inhibitory rebound bursting of VB neurons ceases as the voltage-dependent inactivation of T-type Ca^{2+} channels in VB neurons terminate the LTS (Huguenard, 1996).

Of the three T-type Ca^{2+} channel subtypes, $Ca_V3.1$ is typically expressed in VB neurons. Mutant VB neurons lacking $Ca_V3.1$ are incapable of generating post-inhibitory rebound bursts (Kim et al., 2001; Huguenard and McCormick, 2007). Conversely, $Ca_V3.2$ and $Ca_V3.3$ localize to the dendrites of RT neurons (Talley et al., 1999; Liu et al., 2011). While $Ca_V3.2$ knockout mice display a mild disruption in RT bursting activity (Liao et al., 2011), RT neurons from mice lacking $Ca_V3.3$ are unable to generate oscillatory burst firing and the capacity of the RT-VB circuit to produce sleep spindles is greatly compromised (Astori et al., 2011). Targeted disruption of T-type Ca^{2+} channel activity in the thalamus demonstrates that the capacity to generate post-inhibitory rebound bursts in both RT and VB neurons is required for the proper typical of the thalamic oscillatory circuitry.

While the oscillatory thalamic circuit is most simply conceptualized as a reciprocally connected pair of RT and VB neurons (e.g. **Fig. 3B**), the biological network contains a much greater degree of complexity due to extensive convergent and divergent connectivity among RT and VB neurons (**Fig. 4A**). Calculations based on a combination of physiological and anatomical measurements estimate that each RT neuron synapses onto roughly 150 VB neurons and that each VB neuron in turn receives input from 10-20 RT neurons (Kim and McCormick, 1998). This skewed connectivity ratio appears reasonable as the 300 VB neurons in a thalamic barreloid that relay sensory information from a single whisker (Land et al., 1995) converge onto a much smaller whisker receptive field of only 30 RT neurons (Shosaku, 1986; Gentet and Ulrich, 2003). There is little evidence to suggest that collateral connectivity exists among VB neurons (Jones, 2007). Furthermore, each RT neuron is innervated by approximately 30 VB neurons (Kim and McCormick, 1998), with inputs from VB neurons accounting for about 25% of the synapses found on RT neurons (Liu and Jones 1999). A majority of the remaining synapses onto RT neurons are from glutamatergic corticothalamic projections.

RT neurons likely form both recurrent GABAergic synapses (Ahlsén and Lindström, 1982; Yen et al., 1985) and connexin-mediated electrical connections (Landisman et al., 2002) with other RT neurons. While anatomical evidence suggests that intra-RT connectivity may be relatively sparse (Cox et al., 1996) (**Fig. 4B**), a number of studies have demonstrated that spontaneous or evoked GABAergic IPSCs occur in RT neurons (Ulrich and Huguenard, 1995; Huntsman

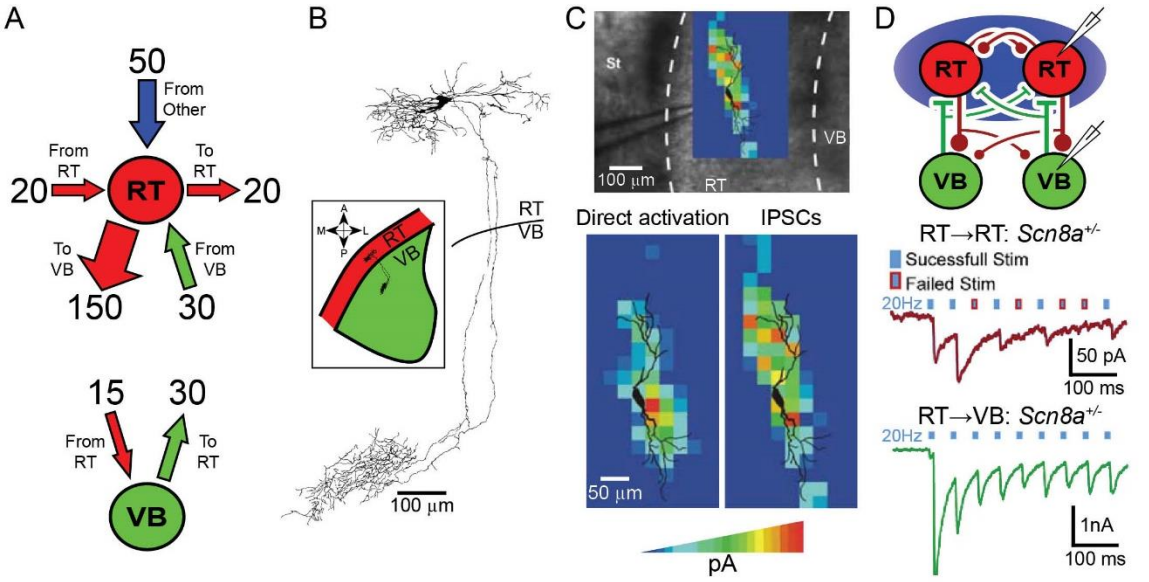

Figure 4. Evidence of intra-RT GABAergic signaling. ***A***, schematic displaying the number of neuronal projections originating from and projecting to RT and VB neurons. ***B***, Camera lucida drawing of a biocytin-filled RT neuron (figure modified from Cox et al., 1996). Inset shows neuronal localization within a horizontal thalamic section. Extensively branched axon-like dendrites and axon collaterals that remain within the RT nucleus suggest the existence of intra-RT GABAergic synapses ***C***, Laser scanning photostimulation of an RT neuron using caged glutamate (figure modified from Deleuze and Huguenard, 2006). (*top*) Whole-cell recording of an RT neuron performed using biocytin-filled electrodes, allowing localization within the RT nucleus and reconstruction of neuronal morphology. Colormaps indicate the amplitude of either direct glutamatergic activation of the recorded neuron (*bottom left*) or disynaptic GABAergic IPSCs evoked by stimulation of presynaptic RT neurons (*bottom right*) during laser uncaging in the indicated location relative to the recorded neuron ***D***, (*top*) Optogenetic stimulation of ChETA targeted to RT neurons was combined with whole-cell recordings. Stimulation of the RT nucleus evoked IPSCs in both RT (*middle*) and VB neurons (*bottom*), although the failure rate was substantially higher in RT neurons (figure modified from Makinson et al., 2017).

et al., 1999; Huguenard and McCormick, 2007). Several presynaptic sources can account for IPSCs recorded in RT neurons. Extrathalamic projection from the substantia nigra pars reticulata (Paré et al., 1990), globus pallidus (Nauta, 1979) and basal forebrain (Asanuma and Porter, 1990) all provide important sources of GABAergic signaling onto RT neurons. Additionally, RT neurons may form GABAergic connections with each other to establish a network of recurrent inhibition within the RT nucleus. I elaborate on the latter, more contentious possibility below.

Electrical stimulation of corticothalamic fibers produces both disynaptic and polysynaptic IPSCs in RT neurons (Zhang and Jones, 2004). One interpretation of this observation is that stimulation of glutamatergic, corticothalamic fibers initially activates some RT neurons that can then directly inhibit other, connected RT neurons. If true, then a direct assay of neuronal connectivity using paired intracellular recordings should expose connections among paired RT neurons. However, paired-cell recordings of RT neurons reveal inhibitory chemical synapse in only 3% of intra-RT neuron pairs recorded in rats younger than P9 (Parker et al., 2009). Furthermore, no such connections are observed in older animals (Landisman et al., 2002; Parker et al., 2009).

Arguably, paired whole-cell recordings of RT neurons may not provide the best approach to detect sparse GABAergic connectivity among RT neurons. Methods that rapidly assess connections among a large number of RT neurons can more readily gauge sparse connectivity probabilities. Indeed, laser-scanning photostimulation experiments reveal that an average RT neuron chemically

synapses with 20 other RT neurons over a distance of 355 µm from the cell body and electrically synapses with 13 RT neurons over 220 µm (Deleuze and Huguenard, 2006) (**Fig. 4C**). Targeted optogenetic stimulation of the RT nucleus also successfully evokes IPSCs in nearby RT neurons in P12 mice (Hou et al., 2016). However, optogenetic stimulation of neither RT neurons (Hou et al., 2016) nor corticothalamic inputs to RT neurons (Cruikshank et al., 2010) can resolve such intra-RT connectivity beyond the second postnatal week. Recent evidence suggests that intra-RT GABAergic signaling can still be observed in mice older than three months when evoked by low-intensity or sparse stimulation, although there is a higher failure rate of GABAergic IPSCs during more intensive stimulation paradigms (Makinson et al., 2017) (**Fig. 4D**). Further research is still required to fully characterize the nature of GABAergic connectivity among RT neurons.

Although the thalamic oscillatory circuit is highly interconnected and is believed to require bidirectional signaling between VB and RT neurons, repetitive closed-loop firing between specific pairs of neurons only occurs in as few as 7% of all paired RT-VB recordings in acute brain slices (Gentet and Ulrich, 2003; Pinault, 2004). Some of the sparse reciprocal connectivity among RT and VB neurons likely results from the severing of connections as the brain is sectioned. However, limited reciprocal RT-VB connectivity also suggests that the thalamic network may be largely distributed, rather than existing through discrete iterative and interlaced units. Nevertheless, the features of the oscillatory network formed between VB and RT neurons produces a core circuit capable of generating the oscillatory bursts of activity associated with both sleep spindles and absence

seizures. The exact mechanisms underlying the transition between network states responsible for producing sleep spindles and absence seizures remains an important area of study.

GABAergic Signaling in the Thalamus

Sleep spindles are important for many brain functions, including the consolidation of new memories (Gais et al., 2002; Tamminen et al., 2010), yet disrupting the underlying circuitry of sleep spindles is hypothesized to generate the pathological activity of absence seizures (Buzsáki et al., 1990; McCormick and Bal, 1997). Sleep spindles and absence seizures both generalize widely throughout the brain and last for only a few seconds, with the shift in oscillation frequency (from 10 Hz to 3 Hz) potentially representing a perversion of typical signaling within the thalamic oscillatory circuit (Kandel and Buzsáki, 1997; McCormick and Bal, 1997; Beenhakker and Huguenard, 2009). Notably, the transformation between sleep spindles and SWDs largely depends on GABAergic signaling in the thalamus. Disrupting GABAergic signaling in the thalamus is sufficient to transform sleep spindle activity into a pattern resembling absence seizures (von Krosigk et al., 1993). Thus, understanding the role of GABAergic signaling in the thalamus has the potential to improve treatments for absence epilepsy.

While neurons in both the RT and VB nuclei express GABA receptors, the relative distribution of the $GABA_A$ and $GABA_B$ receptor subtypes varies between these two regions of the thalamus. $GABA_A$ receptors are found in practically every region of the brain, including in both RT and VB neurons (Bowery et al., 1987;

Pirker et al., 2000). In contrast, $GABA_B$ receptor expression is highly regional. Both binding and *in situ* hybridization studies demonstrate that $GABA_B$ receptors are enriched in VB neurons, while there is little evidence of $GABA_B$ receptors in RT neurons (Bowery et al., 1987; Bischoff et al., 1999; Ferreira-Gomes et al., 2004).

Recordings of thalamic slices demonstrate that the same neurons which fire sleep spindle-like bursts of action potentials initially begin to fire bursts of action potentials at a slower rate of 2-4 Hz, resembling absence seizure activity, when exposed to the $GABA_A$ receptor antagonist bicuculline (von Krosigk et al., 1993; Huguenard and Prince, 1994). The remaining, unaffected $GABA_B$ receptor-mediated IPSPs have a much longer duration of ~300 ms (Huguenard and Prince, 1994; Sanchez-Vives and McCormick, 1997) than do the faster (~100 ms) $GABA_A$ receptor-mediated IPSPs (Huntsman et al., 1999; Huntsman and Huguenard, 2006). The prolonged inhibition mediated by $GABA_B$ receptors delays when rebound bursting of VB neurons can initiate another round of reciprocal firing involving RT neurons. *In vivo* experiments where $GABA_A$ receptor mediated inhibition of VB neurons is disrupted by a direct infusion of bicuculline into the thalamus produce a similar shift to a seizure-like pattern of 3 Hz cortical activity (Castro-Alamancos, 1999). Thus, $GABA_B$ receptor activation appears to be an essential component of the shift to the slower thalamic oscillations associated with absence seizures.

While bicuculine eliminates the $GABA_A$ component of RT to VB signaling, it also fully blocks intra-RT GABAergic signaling that is entirely mediated by the $GABA_A$ receptor. Intra-RT GABAergic signaling is proposed to serve an important

role in regulating the transition from normal sleep spindle rhythms to seizure activity by desynchronizing the thalamic network (Sohal and Huguenard, 2003; Beenhakker and Huguenard, 2009). When an RT neuron fires a burst of action potentials, it not only hyperpolarizes VB neurons, priming them for post-inhibitory rebound firing, but also activates GABAergic synapses on other RT neurons. This effect reduces the probability that neighboring RT neurons will fire in response to recurrent excitation from VB neurons. Computational studies suggest that such a burst-vetoing mechanism limits the number of simultaneously firing RT neurons, thereby reducing the ability of the circuit to support additional cycles of oscillatory firing (Sohal and Huguenard, 2003).

Together, these studies informed the hypothesis that while GABA-mediated signaling from RT to VB neurons is required for the generation or rhythmic thalamic activity, it may specifically be intra-RT $GABA_A$-mediated signaling that prevents benign thalamic oscillations from becoming absence seizures. However, the abovementioned studies were unable to fully isolate the impact of pharmacological manipulations that had diverse impacts on both RT and VB neurons.

Bicuculline likely promotes synchronous bursting activity by inhibiting $GABA_A$ receptors in the thalamus. However, bicuculline is known to have other non-specific effects (Debarbieux et al., 1998; Kleiman-Weiner et al., 2009), and it is hard to disentangle the combined impact on both RT and VB neurons of bicuculline broadly applied to the thalamus. To more directly examine the role of intra-RT GABAergic signaling as a desynchronization mechanism, experiments were conducted using $GABA_A$ receptor β_3 subunit knock-out mice. The $GABA_A$

receptor is pentameric and in most cases requires at least one α, one β and one γ (or δ/ε/θ/π) subunit to be functional. While VB neurons express both β_1 and β_2 subunits, only the β_3 subunit is found in RT neurons (Pirker et al., 2000). Therefore, a β_3 subunit knock-out mouse will eliminate all functional GABAergic signaling among RT neurons. Disruption of intra-RT GABAergic signaling is manifested by a significant reduction in the amplitude and frequency of spontaneous IPSCs in the RT neurons of β_3 subunit knock-out mice, while spontaneous IPSCs are unaltered in VB neurons (Huntsman et al., 1999). Importantly, β_3 subunit knock-out mice generate hypersynchronous, epileptiform thalamic oscillations that resemble absence seizures.

Overall evidence for the outsized role of intra-RT GABAergic signaling in preventing the propagation of seizures has led some to describe the structure as a seizure choke point (Paz and Huguenard, 2015). Conceptually, seizure chokepoints refer to the small number of specific neural circuits throughout the brain that are likely critically responsible for inhibiting the occurrence of seizures. Therefore, when these chokepoints break down, seizure activity can emerge and propagate throughout the brain. Support for the importance of intra-RT GABAergic signaling as a seizure chokepoint is bolstered by the finding that deleting *Scn8a,* the gene responsible for encoding the voltage-gated sodium channel $Na_v1.6$, alters thalamic activity (Makinson et al., 2017). A global deletion of *Scn8a* in inhibitory neurons is sufficient to produce spontaneous absence seizures in mice. *Scn8a* deletion is also associated with an increased failure rate in inhibitory synaptic signaling among RT neurons, while not altering RT to VB signaling. Furthermore,

selective knockdown of *Scn8a* in RT neurons using RNAi is sufficient to cause mice to experience spontaneous absence seizures. This study provides the first evidence directly linking a specifically targeted disruption of GABAergic signaling among RT neurons to absence epilepsy (Makinson et al., 2017). As intra-RT GABAergic signaling appears to form a critical seizure chokepoint, the mechanisms underlying inhibitory responses in RT neurons are worthy of further consideration.

Regulation of Intracellular Chloride

Many of the aforementioned hypotheses regarding the mechanisms by which the thalamus produces absence seizures are predicated on GABA acting as an inhibitory neurotransmitter within the reticular thalamus. The $GABA_A$ receptor is a ligand-gated channel selective for Cl^- ions. When the equilibrium potential of Cl^- ($\boldsymbol{E_{Cl}}$) is more negative than the resting membrane potential, Cl^- enters the neuron through activated $GABA_A$ receptors, leading to hyperpolarization and decreased probability of action potential initiation (**Fig. 5A**). Even a slightly depolarizing E_{Cl} is still capable of supporting shunting inhibition, as activated $GABA_A$ receptors locally reduce the membrane resistance and attenuate the amplitude of concurrent excitatory postsynaptic potentials (Edwards, 1990; Staley and Mody, 1992; Blaesse et al., 2009). However, if the intracellular concentration of Cl^- ($\boldsymbol{[Cl^-]_i}$) of a neuron is sufficiently elevated, such that E_{Cl} is depolarized relative to the action potential threshold, then GABAergic signaling becomes excitatory.

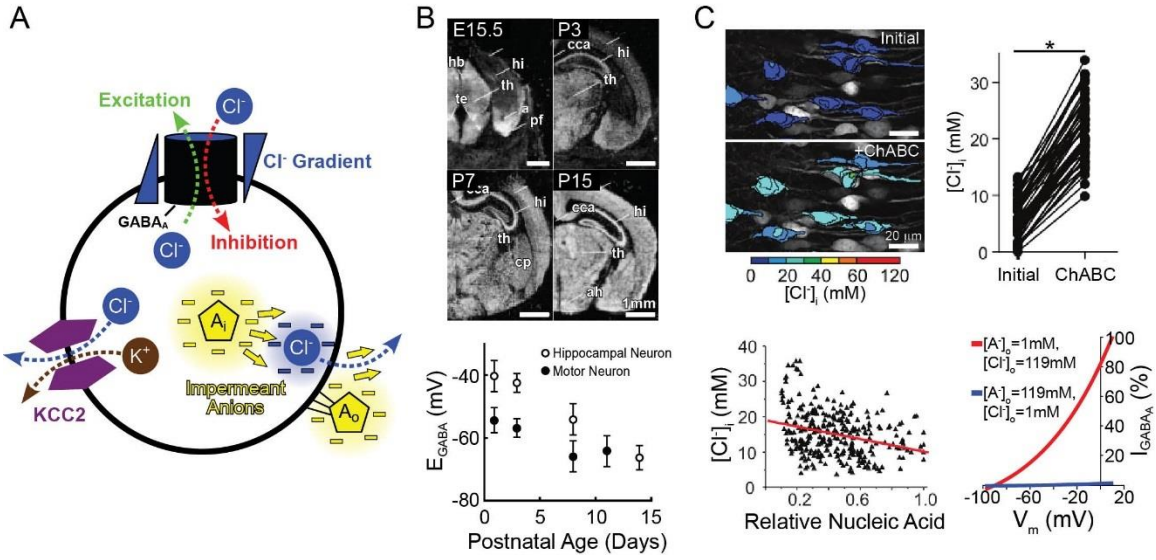

Figure 5. Mechanisms of Cl^- regulations in neurons. ***A***, Schematic of the mechanisms by which KCC2 and impermeant anions can maintain low $[Cl^-]_i$ within neurons. Low $[Cl^-]_i$ is required for sustaining inhibitory responses to activation of the $GABA_A$ receptor. Sufficient elevation of $[Cl^-]_i$ can result in GABAergic excitation. ***B***, (*top*) *in situ* hybridization indicates that KCC2 mRNA expression increases during mouse brain development. ah, arcuate hypothalamic nucleus; cca, corpus callosum; cp, caudate putamen; hb, habenula; hi, hippocampus; pf, piriform cortex; te, thalamic eminence; th, thalamus. (*bottom*) E_{GABA} of hippocampal pyramidal neurons and spinal motor neurons becomes increasingly hyperpolarized postnatally, corresponding to rising KCC2 expression (figures modified from Stein et al., 2004). ***C***, (*top left*) Pseudo-colored images of organotypic hippocampal slices from mice expressing the Clomeleon Cl^- sensor. (*top*) Enzymatic reduction of $[A]_o$, resulting from incubation in chondroitinase ABC (ChABC), produced an increase in $[Cl^-]_i$. (*bottom left*) Higher intracellular concentrations of nucleic acids, a major component of $[A]_i$, corresponded to lower $[Cl^-]_i$ in organotypic hippocampal slices. (*bottom right*) Theoretical relationship between $[A]_o$ and the ability of the $GABA_A$ receptor to conduct current (figures modified from Glykys et al., 2014, and Delpire and Staley, 2014).

Most mature neurons have a relatively low $[Cl^-]_i$ due to an abundance of K-Cl cotransporters that pump Cl^- out of the neuron (Blaesse et al., 2009). Two isoforms of a K-Cl cotransporter were identified in short succession (Gillen et al., 1996; Payne et al., 1996) and the second isoform (***KCC2***) is neuron-specific, with expression throughout the brain (Payne et al., 1996). KCC2 is an electroneutral cotransporter, which uses the energy provided by the electrochemical gradient that drives K^+ efflux to also drive the extrusion of an equal number of Cl^- ions (**Fig. 5A**), thereby not altering the membrane potential (Payne, 1997). KCC2 is initially upregulated perinatally and increased expression corresponds to a shift from excitatory to inhibitory responses to GABAergic signaling in most neurons (Rivera et al., 1999; Stein et al., 2004; Kaila et al., 2014) (**Fig. 5B**).

Impermeant anions refer to fixed negative charges produced by a variety of sources that are also proposed to play an important role in regulating $[Cl^-]_i$ (Donnan, 1911; Delpire and Staley, 2014). Intracellular impermeant anions (***[A]$_i$***) include phosphate groups on nucleic acids and cytoplasmic proteins (Gianazza and Righetti, 1980). A major source of extracellular impermeant anions (***[A]$_o$***) are the highly sulfated proteoglycan components of the extracellular matrix (Bandtlow and Zimmermann, 2000). Fixed negative charges within and outside of neurons form clouds of negativity that repel the more mobile negatively-charged Cl^- away from the neuron, promoting a reduced $[Cl^-]_i$ (Delpire and Staley, 2014) (**Fig. 5A**). An additional impact of locally displacing extracellular Cl^-, is that $[A]_o$ reduce the available pool of charge carriers for anionic influx during $GABA_A$ receptor activation. Therefore, elevating $[A]_o$ will produce a corresponding decrease in the

conductance of Cl^- through $GABA_A$ receptors, reducing the amplitude of $GABA_A$-mediated postsynaptic potentials (**Fig. 5C**). Recent studies in the hippocampus suggested that altering either $[A]_o$ or $[A]_i$ may more effectively shift $[Cl^-]_i$ than blocking KCC2 in neurons (Glykys et al., 2014a) (**Fig. 5C**).

Interestingly, the RT nucleus stands out as one of the few regions in the adult rat brain with minimal KCC2 mRNA expression (Kanaka et al., 2001). Likewise, expression of KCC2 protein in the RT nucleus of adult rats (Barthó et al., 2004) and mice (Sun et al., 2012) is noticeably lower than in surrounding brain regions. The reduced expression of KCC2 in RT neurons suggests a more limited capacity to extrude Cl^-, which could result in an elevated $[Cl^-]_i$ and excitatory responses to GABAergic signaling. Gramicidin perforated patch recordings are used to measure $[Cl^-]_i$, as the cation-specific pores formed by the linear polypeptide antibiotic gramicidin A (Myers and Haydon, 1972; Ulrich and Huguenard, 1997) prevents Cl^- from passing between the recording electrode and the neuron being recorded. The E_{Cl} of a neuron can then be assessed by measuring the membrane currents evoked by $GABA_A$ receptor activation while the neuron is held at a range of command potentials.

Previous, gramicidin perforated patch recordings have provided divergent measurements of $[Cl^-]_i$ in RT neurons. Experiments in P9-12 rats measure an E_{Cl} of -70 mV for RT neurons, which suggests that $GABA_A$ receptor activation promotes Cl^- influx and inhibition (Ulrich and Huguenard, 1997). However, similar studies in P13-35 mice report an E_{Cl} of -45 mV, suggesting that $GABA_A$ receptor activation excites RT neurons (Sun et al., 2012). Indeed, cell attached recording

techniques that leave the membrane of the patched cell intact also indicate that $GABA_A$ receptor activation can cause both depolarizing post-synaptic potentials and the firing of action potentials in RT neurons (Sun et al., 2012). The limited expression of KCC2 in RT neurons and inconsistent measurements of E_{Cl} call into question how $[Cl^-]_i$ is regulated in RT neurons, and how inefficient Cl^- extrusion may impact the ability of the RT nucleus to function as a seizure choke point.

Conclusions

While multiple lines of research indicate that GABAergic signaling among RT neurons forms a critical seizure choke point that prevents seizure generation (Castro-Alamancos, 1999; Huntsman et al., 1999; Sohal and Huguenard, 2003; Paz and Huguenard, 2015; Makinson et al., 2017), the specific mechanisms that allow the RT nucleus to serve as a seizure choke point remain elusive. Overall, the goals of my research included determining: (**1**) how $[Cl^-]_i$ is regulated in RT neurons, (**2**) what impact RT $[Cl^-]_i$ regulatory mechanisms have on the ability of RT neurons to maintain inhibitory responses to GABAergic signaling, and (**3**) if modulating the ability of RT neurons to maintain a low $[Cl^-]_i$ is correlated with the ability of the RT nucleus to serve as a seizure choke point in absence epilepsy.

In Chapter 2 of my dissertation, I address the first two of these goals. I have determined that while KCC2 protein expression is low between P5-40 in RT neurons, basal $[Cl^-]_i$ in RT remains sufficiently low to support inhibitory GABAergic signaling based on both gramicidin perforated patch recordings and calcium imaging experiments. $[A]_o$ are elevated surrounding RT neurons, yet appear to

contribute little to maintaining an inhibitory E_{Cl}. However, even the low levels of KCC2 expressed in RT neurons helps to maintain a low basal $[Cl^-]_i$, but leave RT neurons with a compromised ability to handle the large influxes of Cl^- that accompany prolonged GABAergic signaling. Using computational modeling, I provide conceptual support for the possibility that slowed Cl^- extrusion associated with low KCC2 expression weakens the RT seizure choke point and allows prolonged excitatory inputs to trigger a seizure-like spread of synchronized thalamus activity. My findings suggest that enhancing the ability of RT neurons to maintain inhibitory responses to GABAergic signaling should strengthen the RT seizure choke point to aid in preventing absence seizures.

Chapter 3 of this dissertation addresses my third goal of determining whether modulating Cl^- regulation in RT neurons alters the capacity of the RT nucleus to serve as a seizure choke point. I have determined that the WAG/Rij rat model of genetic absence seizures has reduced KCC2 and $[A]_o$ expression within the RT nucleus relative to wild type rats. I have also begun to investigate whether supplementing the Cl^- extrusion capacity of KCC2 in RT neurons of WAG/Rij rats is sufficient to strengthen the RT seizure choke point and reduce the frequency of spontaneous absence seizures.

Altogether, this dissertation addresses a critical gap in our knowledge of how GABAergic signaling among RT neurons is able to prevent the occurrence of absence seizures. My research indicates that therapies that can enhance the ability of RT neurons to set and maintain a low $[Cl^-]_i$ have the potential to reduce the frequency of seizures in patients suffering from absence epilepsy.

References

Ahlsén G, Lindström S (1982) Mutal inhibition between perigeniculate neurones. Brain Res 236:482–486.

Andersen P, Andersson SA, Lømo T (1967) Some factors involved in the thalamic control of spontaneous barbiturate spindles. J Physiol 192:257–281.

Andersson SA, Holmgren E, Manson JR (1971) Synchronization and desynchronization in the thalamus of the unanaesthetized decorticate cat. Electroencephalogr Clin Neurophysiol 31:335–345.

Asanuma C, Porter LL (1990) Light and electron microscopic evidence for a GABAergic projection from the caudal basal forebrain to the thalamic reticular nucleus in rats. J Comp Neurol 302:159–172.

Astori S, Wimmer RD, Prosser HM, Corti C, Corsi M, Liaudet N, Volterra A, Franken P, Adelman JP, Lüthi A (2011) The Ca(V)3.3 calcium channel is the major sleep spindle pacemaker in thalamus. Proc Natl Acad Sci 108:13823–13828.

Avoli M (2012) A brief history on the oscillating roles of thalamus and cortex in absence seizures. Epilepsia 53:779–789.

Bandtlow CE, Zimmermann DR (2000) Proteoglycans in the developing brain: new conceptual insights for old proteins. Physiol Rev 80:1267–1290.

Barthó P, Payne JA, Freund TF, Acsády L (2004) Differential distribution of the KCl cotransporter KCC2 in thalamic relay and reticular nuclei. Eur J Neurosci 20:965–975.

Beenhakker MP, Huguenard JR (2009) Neurons that fire together also conspire

together: is normal sleep circuitry hijacked to generate epilepsy? Neuron 62:612–632.

Beghi M, Beghi E, Cornaggia CM, Gobbi G (2006) Idiopathic generalized epilepsies of adolescence. Epilepsia 47 Suppl 2:107–110.

Berg AT, Berkovic SF, Brodie MJ, Buchhalter J, Cross JH, van Emde Boas W, Engel J, French JA, Glauser TA, Mathern GW, Moshé SL, Nordli D, Plouin P, Scheffer IE (2010) Revised terminology and concepts for organization of seizures and epilepsies: report of the ILAE Commission on Classification and Terminology, 2005-2009. Epilepsia 51:676–685.

Bischoff S, Leonhard S, Reymann N, Schuler V, Shigemoto R, Kaupmann K, Bettler B (1999) Spatial distribution of GABA(B)R1 receptor mRNA and binding sites in the rat brain. J Comp Neurol 412:1–16.

Blaesse P, Airaksinen MS, Rivera C, Kaila K (2009) Cation-chloride cotransporters and neuronal function. Neuron 61:820–838.

Bowery NG, Hudson LA, Price GW (1987) GABAA and GABAB receptor site distribution in the rat central nervous system. Neuroscience 20:365–383.

Buzsáki G (1991) The thalamic clock: emergent network properties. Neuroscience 41:351–364.

Buzsáki G, Smith A, Berger S, Fisher LJ, Gage FH (1990) Petit mal epilepsy and parkinsonian tremor: hypothesis of a common pacemaker. Neuroscience 36:1–14.

Calmeil LF (1824) De l’épilepsie, étudiée sous le rapport de son siège et de son influence sur la production de l’aliénation mentale. Paris Theses 110:1–35.

Caplan R, Siddarth P, Stahl L, Lanphier E, Vona P, Gurbani S, Koh S, Sankar R, Shields WD (2008) Childhood absence epilepsy: behavioral, cognitive, and linguistic comorbidities. Epilepsia 49:1838–1846.

Castro-Alamancos MA (1999) Neocortical synchronized oscillations induced by thalamic disinhibition in vivo. J Neurosci 19:RC27.

Contreras D, Steriade M (1995) Cellular basis of EEG slow rhythms: corticothalamic relationships. J Neurosci 15:604–622.

Coulter DA, Huguenard JR, Prince DA (1989) Calcium currents in rat thalamocortical relay neurones: kinetic properties of the transient, low-threshold current. J Physiol 414:587–604.

Cox CL, Huguenard JR, Prince DA (1996) Heterogeneous axonal arborizations of rat thalamic reticular neurons in the ventrobasal nucleus. J Comp Neurol 366:416–430.

Cribbs LL, Lee J-H, Yang J, Satin J, Zhang Y, Daud A, Barclay J, Williamson MP, Fox M, Rees M, Perez-Reyes E (1998) Cloning and characterization of alpha1H from human heart, a member of the T-type Ca2+ channel gene family. Circ Res 83:103–109.

Cruikshank SJ, Urabe H, Nurmikko A V, Connors BW (2010) Pathway-specific feedforward circuits between thalamus and neocortex revealed by selective optical stimulation of axons. Neuron 65:230–245.

De Gennaro L, Ferrara M (2003) Sleep spindles: an overview. Sleep Med Rev 7:423–440.

Debarbieux F, Brunton J, Charpak S (1998) Effect of bicuculline on thalamic

activity : a direct blockade of I(AHP) in reticularis neurons. J Neurophysiol 79:2911–2918.

Deleuze C, Huguenard JR (2006) Distinct electrical and chemical connectivity maps in the thalamic reticular nucleus: potential roles in synchronization and sensation. J Neurosci 26:8633–8645.

Delpire E, Staley KJ (2014) Novel determinants of the neuronal Cl- concentration. J Physiol 592:4099–4114.

Donnan FG (1911) Theorie der membran gleichgewichte und membran potentiale bei vorhandernsein von nicht dialysierenden elektrolyten. Zeitschrift für Elektrochimie und Angewandlte Phys Chemie 17:572–581.

Eadie MJ, Blandin PF (2001) A disease once sacred : a history of the medical understanding of epilepsy. Eastleigh, England: John Libbey.

Edwards DH (1990) Mechanisms of depolarizing inhibition at the crayfish giant motor synapse. I. Electrophysiology. J Neurophysiol 64:541–550.

Ertel EA, Campbell KP, Harpold MM, Hofmann F, Mori Y, Perez-Reyes E, Schwartz A, Snutch TP, Tanabe T, Birnbaumer L, Tsien RW, Catterall WA (2000) Nomenclature of voltage-gated calcium channels. Neuron 25:533–535.

Ferreira-Gomes J, Neto FL, Castro-Lopes JM (2004) Differential expression of GABA(B(1b)) receptor mRNA in the thalamus of normal and monoarthritic animals. Biochem Pharmacol 68:1603–1611.

Fisher RS, Acevedo C, Arzimanoglou A, Bogacz A, Cross JH, Elger CE, Engel J, Forsgren L, French JA, Glynn M, Hesdorffer DC, Lee BI, Mathern GW, Moshé SL, Perucca E, Scheffer IE, Tomson T, Watanabe M, Wiebe S (2014) ILAE

Official Report: A practical clinical definition of epilepsy. Epilepsia 55:475–482.

Fisher RS, Boas W van E, Blume W, Elger C, Genton P, Lee P, Engel J (2005) Epileptic Seizures and Epilepsy: Definitions Proposed by the International League Against Epilepsy (ILAE) and the International Bureau for Epilepsy (IBE). Epilepsia 46:470–472.

Gais S, Mölle M, Helms K, Born J (2002) Learning-dependent increases in sleep spindle density. J Neurosci 22:6830–6834.

Gallentine WB, Mikati MA (2012) Genetic generalized epilepsies. J Clin Neurophysiol 29:408–419.

Gentet LJ, Ulrich D (2003) Strong, reliable and precise synaptic connections between thalamic relay cells and neurones of the nucleus reticularis in juvenile rats. J Physiol 546:801–811.

Gianazza E, Righetti PG (1980) Size and charge distribution of macromolecules in living systems. J Chromotography A 193:1–8.

Gibbs FA, Davis H, Lennox WG (1935) The Electro-encephalogram in epilepsy and in conditions of impaired consciousness. Arch Neurol Psychiatry 34:1133–1148.

Gillen CM, Brill S, Payne JA, Forbush B (1996) Molecular Cloning and Functional Expression of the K-Cl Cotransporter from Rabbit, Rat, and Human. J Biol Chem 271:16237–16244.

Glauser TA, Ben-Menachem E, Bourgeois B, Cnaan A, Guerreiro C, Kälviäinen R, Mattson R, French JA, Perucca E, Tomson T (2013a) Updated ILAE evidence

review of antiepileptic drug efficacy and effectiveness as initial monotherapy for epileptic seizures and syndromes. Epilepsia 54:551–563.

Glauser TA, Cnaan A, Shinnar S, Hirtz DG, Dlugos D, Masur D, Clark PO, Adamson PC (2013b) Ethosuximide, valproic acid, and lamotrigine in childhood absence epilepsy: Initial monotherapy outcomes at 12 months. Epilepsia 54:141–155.

Gloor P (1978) Generalized epilepsy with bilateral synchronous spike and wave discharge. New findings concerning its physiological mechanisms. Electroencephalogr Clin Neurophysiol Suppl 34:245–249.

Glykys J, Dzhala V, Egawa K, Balena T, Saponjian Y, Kuchibhotla K V, Bacskai BJ, Kahle KT, Zeuthen T, Staley KJ (2014) Local impermeant anions establish the neuronal chloride concentration. Science 343:670–675.

Hesdorffer DC, Logroscino G, Benn EKT, Katri N, Cascino G, Hauser WA (2011) Estimating risk for developing epilepsy: A population-based study in Rochester, Minnesota. Neurology 76:23–27.

Hirtz D, Thurman DJ, Gwinn-Hardy K, Mohamed M, Chaudhuri AR, Zalutsky R (2007) How common are the “common” neurologic disorders? Neurology 68:326–337.

Hou G, Smith AG, Zhang Z-W (2016) Lack of Intrinsic GABAergic Connections in the Thalamic Reticular Nucleus of the Mouse. J Neurosci 36:7246–7252.

Houser CR, Vaughn JE, Barber RP, Roberts E (1980) GABA neurons are the major cell type of the nucleus reticularis thalami. Brain Res 200:341–354.

Hughes JR (2009) Absence seizures: a review of recent reports with new

concepts. Epilepsy Behav 15:404–412.

Huguenard JR (1996) Low-threshhold calcium currents in central nervous system neurons. Annu Rev Physiol 58:329–348.

Huguenard JR, McCormick DA (1992) Simulation of the currents involved in rhythmic oscillations in thalamic relay neurons. J Neurophysiol 68:1373–1383.

Huguenard JR, McCormick DA (2007) Thalamic synchrony and dynamic regulation of global forebrain oscillations. Trends Neurosci 30:350–356.

Huguenard JR, Prince DA (1992) A novel T-type current underlies prolonged Ca(2+)-dependent burst firing in GABAergic neurons of rat thalamic reticular nucleus. J Neurosci 12:3804–3817.

Huguenard JR, Prince DA (1994) Intrathalamic rhythmicity studied in vitro: nominal T-current modulation causes robust antioscillatory effects. J Neurosci 14:5485–5502.

Huntsman MM, Huguenard JR (2006) Fast IPSCs in rat thalamic reticular nucleus require the GABAA receptor beta1 subunit. J Physiol 572:459–475.

Huntsman MM, Porcello DM, Homanics GE, DeLorey TM, Huguenard JR (1999) Reciprocal inhibitory connections and network synchrony in the mammalian thalamus. Science 283:541–543.

Jasper HH, Droogleever-Fortuyn J (1947) Experimental studies on the functional anatomy of petit mal epilepsy. Assoc Res Nerv Ment Dis 26:272–298.

Jones EG (1975) Some aspects of the organization of the thalamic reticular complex. J Comp Neurol 162:285–308.

Jones EG (2007) The Thalamus, 2nd ed. Cambridge: Cambridge University Press.

Kaila K, Price TJ, Payne JA, Puskarjov M, Voipio J (2014) Cation-chloride cotransporters in neuronal development, plasticity and disease. Nat Rev Neurosci 15:637–654.

Kanaka C, Ohno K, Okabe A, Kuriyama K, Itoh T, Fukuda A, Sato K (2001) The differential expression patterns of messenger RNAs encoding K-Cl cotransporters (KCC1,2) and Na-K-2Cl cotransporter (NKCC1) in the rat nervous system. Neuroscience 104:933–946.

Kandel A, Buzsáki G (1997) Cellular-synaptic generation of sleep spindles, spike-and-wave discharges, and evoked thalamocortical responses in the neocortex of the rat. J Neurosci 17:6783–6797.

Kaneko T, Mizuno N (1988) Immunohistochemical study of glutaminase-containing neurons in the cerebral cortex and thalamus of the rat. J Comp Neurol 267:590–602.

Kharazia VN, Weinberg RJ (1994) Glutamate in thalamic fibers terminating in layer IV of primary sensory cortex. J Neurosci 14:6021–6032.

Kim D, Song I, Keum S, Lee T, Jeong MJ, Kim SS, McEnery MW, Shin HS (2001) Lack of the burst firing of thalamocortical relay neurons and resistance to absence seizures in mice lacking alpha(1G) T-type Ca(2+) channels. Neuron 31:35–45.

Kim U, McCormick DA (1998) The functional influence of burst and tonic firing mode on synaptic interactions in the thalamus. J Neurosci 18:9500–9516.

Kleiman-Weiner M, Beenhakker MP, Segal WA, Huguenard JR (2009) Synergistic roles of GABAA receptors and SK channels in regulating thalamocortical

oscillations. J Neurophysiol 102:203–213.

Kostopoulos G, Gloor P, Pellegrini A, Gotman J (1981) A study of the transition from spindles to spike and wave discharge in feline generalized penicillin epilepsy: Microphysiological features. Exp Neurol 73:55–77.

Kostopoulos GK (2000) Spike-and-wave discharges of absence seizures as a transformation of sleep spindles: the continuing development of a hypothesis. Clin Neurophysiol 111:S27-38.

Labate A, Briellmann RS, Abbott DF, Waites AB, Jackson GD (2005) Typical childhood absence seizures are associated with thalamic activation. Epileptic Disord 7:373–377.

Land PW, Buffer SA, Yaskosky JD (1995) Barreloids in adult rat thalamus: three-dimensional architecture and relationship to somatosensory cortical barrels. J Comp Neurol 355:573–588.

Landisman CE, Long MA, Beierlein M, Deans MR, Paul DL, Connors BW (2002) Electrical synapses in the thalamic reticular nucleus. J Neurosci 22:1002–1009.

Lee JH, Daud AN, Cribbs LL, Lacerda AE, Pereverzev A, Klöckner U, Schneider T, Perez-Reyes E (1999) Cloning and expression of a novel member of the low voltage-activated T-type calcium channel family. J Neurosci 19:1912–1921.

Leresche N, Lambert RC, Errington AC, Crunelli V (2012) From sleep spindles of natural sleep to spike and wave discharges of typical absence seizures: is the hypothesis still valid? Pflügers Arch Eur J Physiol 463:201–212.

Liao Y-F, Tsai M-L, Chen C-C, Yen C-T (2011) Involvement of the Cav3.2 T-type calcium channel in thalamic neuron discharge patterns. Mol Pain 7:43.

Liu X-B, Murray KD, Jones EG (2011) Low-threshold calcium channel subunit Ca(v) 3.3 is specifically localized in GABAergic neurons of rodent thalamus and cerebral cortex. J Comp Neurol 519:1181–1195.

Llinas R, Jahnsen H (1982) Electrophysiology of mammlian thalamic neurones in vitro. Nature 297:406–408.

Loomis AL, Harvey EN, Hobart G (1935) Potential rhythms of the cerebral cortex during sleep. Science 81:597–598.

MacDonald RL, Barker JL (1977) Pentylenetetrazol and penicillin are selective antagonists of GABA-mediated post-synaptic inhibition in cultured mammalian neurones. Nature 267:720–721.

Makinson CD, Tanaka BS, Sorokin JM, Wong JC, Christian CA, Goldin AL, Escayg A, Huguenard JR (2017) Regulation of Thalamic and Cortical Network Synchrony by Scn8a. Neuron 93:1165–1179.e6.

Marder E, Bucher D (2001) Central pattern generators and the control of rythmic movements. Curr Biol 11:R986–R996.

McCormick DA, Bal T (1997) Sleep and arousal: thalamocortical mechanisms. Annu Rev Neurosci 20:185–215.

Meeren HKM, Pijn JPM, Van Luijtelaar ELJM, Coenen AML, Lopes da Silva FH (2002) Cortical focus drives widespread corticothalamic networks during spontaneous absence seizures in rats. J Neurosci 22:1480–1495.

Moeller F, Siebner HR, Wolff S, Muhle H, Granert O, Jansen O, Stephani U,

Siniatchkin M (2008) Simultaneous EEG-fMRI in drug-naive children with newly diagnosed absence epilepsy. Epilepsia 49:1510–1519.

Morison RS, Bassett DL (1945) Electrical activity of the thalamus and basal ganglia in decorticate cats. J Neurophysiol 8:309–314.

Morison RS, Finley KH, Lothrop GN (1943) Spontaneous electrical activity of the thalamus and other forebrain structures. J Neurophysiol 6:243–254.

Myers VB, Haydon DA (1972) Ion transfer across lipid membranes in the presence of gramicidin A: II. The ion selectivity. Biochim Biophys Acta 274:313–322.

Nauta HJW (1979) Projections of the pallidal complex: An autoradiographic study in the cat. Neuroscience 4:1853–1873.

Ngugi AK, Bottomley C, Kleinschmidt I, Sander JW, Newton CR (2010) Estimation of the burden of active and life-time epilepsy: a meta-analytic approach. Epilepsia 51:883–890.

Oh SW et al. (2014) A mesoscale connectome of the mouse brain. Nature 508:207–214.

Ottersen OP, Fischer BO, Storm-Mathisen J (1983) Retrograde transport of d-[3H]aspartate in thalamocortical neurones. Neurosci Lett 42:19–24.

Panayiotopoulos CP (2008) Typical absence seizures and related epileptic syndromes: Assesment of current state and directions for future research. Epilepsia 49:2131–2139.

Paré D, Hazrati LN, Parent A, Steriade M (1990) Substantia nigra pars reticulata projects to the reticular thalamic nucleus of the cat: a morphological and electrophysiological study. Brain Res 535:139–146.

Parker PRL, Cruikshank SJ, Connors BW (2009) Stability of electrical coupling despite massive developmental changes of intrinsic neuronal physiology. J Neurosci 29:9761–9770.

Payne JA (1997) Functional characterization of the neuronal-specific K-Cl cotransporter: implications for [K+]o regulation. Am J Physiol 273:C1516-25.

Payne JA, Stevenson TJ, Donaldson LF (1996) Molecular characterization of a putative K-Cl cotransporter in rat brain: a neuronal-specific isoform. J Biol Chem 271:16245–16252.

Paz JT, Huguenard JR (2015) Microcircuits and their interactions in epilepsy: is the focus out of focus? Nat Neurosci 18:351–359.

Perez-Reyes E, Cribbs LL, Daud A, Lacerda AE, Barclay J, Williamson MP, Fox M, Rees M, Lee JH (1998) Molecular characterization of a neuronal low-voltage-activated T-type calcium channel. Nature 391:896–900.

Pinault D (2004) The thalamic reticular nucleus: structure, function and concept. Brain Res Rev 46:1–31.

Pinault D, Deschênes M (1998) Projection and innervation patterns of individual thalamic reticular axons in the thalamus of the adult rat: A three-dimensional, graphic, and morphometric analysis. J Comp Neurol 391:180–203.

Pirker S, Schwarzer C, Wieselthaler A, Sieghart W, Sperk G (2000) GABA(A) receptors: immunocytochemical distribution of 13 subunits in the adult rat brain. Neuroscience 101:815–850.

Polack P-O, Guillemain I, Hu E, Deransart C, Depaulis A, Charpier S (2007) Deep layer somatosensory cortical neurons initiate spike-and-wave discharges in a

genetic model of absence seizures. J Neurosci 27:6590–6599.

Prince D, Farrell D (1969) "'Centrencephalic'" spike wave discharges following parenteral penicillin injection in the cat. Neurology 19:309–310.

Rivera C, Voipio J, Payne JA, Ruusuvuori E, Lahtinen H, Lamsa K, Pirvola U, Saarma M, Kaila K (1999) The K+/Cl- co-transporter KCC2 renders GABA hyperpolarizing during neuronal maturation. Nature 397:251–255.

Rose JE, Mountcastle VB (1952) The thalamic tactile region in rabbit and cat. J Comp Neurol 97:441–489.

Sanchez-Vives M V, McCormick DA (1997) Functional properties of perigeniculate inhibition of dorsal lateral geniculate nucleus thalamocortical neurons in vitro. J Neurosci 17:8880–8893.

Scheffer IE, Berkovic S, Capovilla G, Connolly MB, French JA, Guilhoto L, Hirsch E, Jain S, Mathern GW, Moshé SL, Nordli DR, Perucca E, Tomson T, Wiebe S, Zhang YH, Zuberi SM (2017) ILAE classification of the epilepsies: Position paper of the ILAE Commission for Classification and Terminology. Epilepsia 58:512–521.

Seneviratne U, Cook M, D'Souza W (2012) The prognosis of idiopathic generalized epilepsy. Epilepsia 53:2079–2090.

Shosaku A (1986) Cross-correlation analysis of a recurrent inhibitory circuit in the rat thalamus. J Neurophysiol 55:1030–1043.

Sohal VS, Huguenard JR (2003) Inhibitory interconnections control burst pattern and emergent network synchrony in reticular thalamus. J Neurosci 23:8978–8988.

Staley KJ, Mody I (1992) Shunting of excitatory input to dentate gyrus granule cells by a depolarizing GABAA receptor-mediated postsynaptic conductance. J Neurophysiol 68:197–212.

Stein V, Hermans-Borgmeyer I, Jentsch TJ, Hübner CA (2004) Expression of the KCl cotransporter KCC2 parallels neuronal maturation and the emergence of low intracellular chloride. J Comp Neurol 468:57–64.

Steriade M, Deschênes M (1984) The thalamus as a neuronal oscillator. Brain Res Rev 8:1–63.

Steriade M, Deschênes M, Domich L, Mulle C (1985) Abolition of spindle oscillations in thalamic neurons disconnected from nucleus reticularis thalami. J Neurophysiol 54:1473–1497.

Sun Y-G, Wu C-S, Renger JJ, Uebele VN, Lu H-C, Beierlein M (2012) GABAergic synaptic transmission triggers action potentials in thalamic reticular nucleus neurons. J Neurosci 32:7782–7790.

Talley EM, Cribbs LL, Lee JH, Daud A, Perez-Reyes E, Bayliss DA (1999) Differential distribution of three members of a gene family encoding low voltage-activated (T-type) calcium channels. J Neurosci 19:1895–1911.

Tamminen J, Payne JD, Stickgold R, Wamsley EJ, Gaskell MG (2010) Sleep Spindle Activity is Associated with the Integration of New Memories and Existing Knowledge. J Neurosci 30:14356–14360.

Tissot SA (1770) Traité de l’épilepsie: faisant le tome troisième du traité des nerfs et de leurs maladies. Paris: P. F. Didot.

Trinka E, Baumgartner S, Unterberger I, Unterrainer J, Luef G, Haberlandt E,

Bauer G (2004) Long-term prognosis for childhood and juvenile absence epilepsy. J Neurol 251:1235–1241.

Ulrich D, Huguenard JR (1995) Purinergic inhibition of GABA and glutamate release in the thalamus : implications for thalamic network activity. Neuron 15:909–918.

Ulrich D, Huguenard JR (1997) Nucleus-specific chloride homeostasis in rat thalamus. J Neurosci 17:2348–2354.

von Krosigk M, Bal T, McCormick DA (1993) Cellular mechanisms of a synchronized oscillation in the thalamus. Science 261:361–364.

Williams D (1953) A study of thalamic and cortical rhythms in petit mal. Brain 76:50–69.

Wilson DM (1961) The central nervous control of flight in a locust. J Exp Biol 38:471–490.

Yen CT, Conley M, Hendry SHC, Jones EG (1985) The morphology of physiologically identified GABAergic neurons in the somatic sensory part of the thalamic reticular nucleus in the cat. J Neurosci 5:2254–2268.

Zamponi GW, Lory P, Perez-Reyes E (2010) Role of voltage-gated calcium channels in epilepsy. Pflugers Arch 460:395–403.

Zhang L, Jones EG (2004) Corticothalamic inhibition in the thalamic reticular nucleus. J Neurophysiol 91:759–766.

Chapter 2: Tenuous inhibitory GABAergic signaling in the reticular thalamus

Peter M. Klein

Adam C. Lu

Megan E. Harper

Hannah M. McKown

Jessica D. Morgan

Mark P. Beenhakker

Published:

The Journal of Neuroscience

38(5): 1232-1248 (2018)

PMK designed all experiments with the assistance of MPB and ACL (Fig. 8). PMK performed all research except that contributed by ACL (Fig. 8), MEH (Figs. 1 and 3), HMM (Figs. 1 and 3) and JDM (Fig. 4F-H). PMK analyzed all data with guidance from MPB, and assistance from ACL (Fig. 8), MEH (Figs. 1 and 3) and HMM (Figs. 1 and 3). PMK wrote the manuscript in consultation with ACL and MPB.

Abstract

Maintenance of a low intracellular Cl^- concentration (***[Cl⁻]$_i$***) is critical for enabling inhibitory neuronal responses to $GABA_A$ receptor-mediated signaling. Cl^- transporters, including KCC2, and extracellular impermeant anions (***[A]$_o$***) of the extracellular matrix are both proposed to be important regulators of $[Cl^-]_i$. Neurons of the reticular thalamic (***RT***) nucleus express reduced levels of KCC2, indicating that GABAergic signaling may produce excitation in RT neurons. However, by performing perforated patch recordings and calcium imaging experiments in rats (male and female), we find that $[Cl^-]_i$ remains relatively low in RT neurons. While we identify a small contribution of $[A]_o$ to a low $[Cl^-]_i$ in RT neurons, our results also demonstrate that reduced levels of KCC2 remain sufficient to maintain low levels of Cl^-. Reduced KCC2 levels, however, restrict the capacity of RT neurons to rapidly extrude Cl^- following periods of elevated GABAergic signaling. In a computational model of a local RT network featuring slow Cl^- extrusion kinetics, similar to those we found experimentally, model RT neurons are predisposed to an activity-dependent switch from GABA-mediated inhibition to excitation. By decreasing the activity threshold required to produce excitatory GABAergic signaling, weaker stimuli are able to propagate activity within the model RT nucleus. Our results indicate the importance of even diminished levels of KCC2 in maintaining inhibitory signaling within the RT nucleus and suggest how this important activity choke point may be easily overcome in disorders such as epilepsy.

Significance Statement

Precise regulation of intracellular Cl^- levels (***[Cl$^-$]$_i$***) preserves appropriate, often inhibitory, GABAergic signaling within the brain. However, there is disagreement over the relative contribution of various mechanisms that maintain low $[Cl^-]_i$. We found that the Cl^- transporter KCC2 is an important Cl^- extruder in the reticular thalamic (***RT***) nucleus, despite this nucleus having remarkably low KCC2 immunoreactivity relative to other regions of the adult brain. We also identified a smaller contribution of fixed, impermeant anions (***[A]$_o$***) to lowering $[Cl^-]_i$ in RT neurons. Inhibitory signaling among RT neurons is important for preventing excessive activation of RT neurons, which can be responsible for generating seizures. Our work suggests that KCC2 critically restricts the spread of activity within the RT nucleus.

Introduction

Proper inhibitory neurotransmission in the central nervous system is critical for many neural processes (Wong et al., 2003; Kaila et al., 2014) and is primarily mediated by the influx of chloride (***Cl$^-$***) through the $GABA_A$ receptor. However, if the concentration of intracellular Cl^- (***[Cl$^-$]$_i$***) is sufficiently elevated, then $GABA_A$ receptor activation enables Cl^- efflux and neuronal depolarization (Cherubini et al., 1990; Rohrbough and Spitzer, 1996; Staley and Smith, 2001). Thus, depending on the $[Cl^-]_i$, the actions of GABA can be either inhibitory or excitatory.

The low $[Cl^-]_i$ required for GABAergic inhibition is primarily achieved by active Cl^- extrusion driven by the K^+-Cl^- cotransporter KCC2 (Payne et al., 1996; Rivera

et al., 1999). However, negatively charged, fixed macromolecules known as *impermeant anions* can also promote a low $[Cl^-]_i$ (Donnan, 1911), perhaps even more prominently than KCC2 (Delpire and Staley, 2014; Glykys et al., 2014a). To date, the relative contribution of KCC2 and impermeant anions to $[Cl^-]_i$ remains an open debate (Glykys et al., 2014b; Kaila et al., 2014; Luhmann et al., 2014; Voipio et al., 2014; Doyon et al., 2016).

Evaluating the contributions of KCC2 and impermeant anions to GABAergic processes that regulate global brain excitability is particularly pertinent for understanding seizure propagation. The reticular thalamic (***RT***) nucleus envelops and critically regulates the nuclei of the dorsal thalamus (Jones, 2007). Importantly, local circuitry within the RT nucleus operates as an inhibitory choke point that prevents the propagation of seizures (Huntsman et al., 1999; Sohal and Huguenard, 2003; Paz and Huguenard, 2015; Makinson et al., 2017). Notably, the RT nucleus is one of the few adult brain regions with greatly reduced KCC2 expression (Kanaka et al., 2001; Barthó et al., 2004; Sun et al., 2012). Indeed, the paucity of KCC2 in the RT nucleus suggests that GABAergic neurotransmission within the nucleus is excitatory (Sun et al., 2012), thus presenting a conundrum regarding the role of the RT nucleus as an inhibitory seizure choke point.

Reciprocal GABAergic connections among RT neurons form the basis of the thalamic seizure choke point (Ahlsén and Lindström, 1982; Yen et al., 1985; Pinault et al., 1997). Eliminating these connections increases thalamic excitability (Huntsman et al., 1999; Makinson et al., 2017) and possibly causes seizures (Homanics et al., 1997; DeLorey et al., 1998). Computational modeling suggests

that local GABAergic signaling among RT neurons prevents the simultaneous activation of nearby neurons through an activity-vetoing mechanism, thereby restricting seizure generation (Sohal and Huguenard, 2003). This model assumes that GABA is inhibitory, an effect mediated by low $[Cl^-]_i$ (Ulrich and Huguenard, 1997). However, if GABA is excitatory due to low KCC2 expression, it then remains unclear how the RT nucleus can function as a seizure choke point.

In this study, we aim to better understand GABAergic regulation of excitability within the RT nucleus. Using immunohistochemistry, we confirm a reduced KCC2 expression in the RT nucleus and further demonstrate that it remains low throughout development. However, despite low KCC2 immunoreactivity, intracellular, perforated patch clamp recordings of RT neurons indicate that the $[Cl^-]_i$ is low, and that GABAergic signaling inhibits RT neurons. We then show that impermeant anions, abundantly expressed in the RT nucleus, only moderately contribute to a low RT $[Cl^-]_i$. Surprisingly, despite low RT immunoreactivity, KCC2 effectively regulates basal $[Cl^-]_i$ in RT neurons. However, diminished KCC2 leaves RT neurons more susceptible to activity-dependent Cl^- accumulation, likely weakening the capacity of the RT inhibitory choke point to prevent seizures.

Methods

Subjects. Wild type Sprague-Dawley rats (Charles River Laboratories, Wilmington, MA) and wild type C57Bl/6NJ mice (The Jackson Laboratory, Bar Harbor, ME) of either sex were utilized in these experiments. All experiments were approved by the Institutional Care and Use Committee at the University of Virginia

(Charlottesville, VA), in accordance with the National Institutes of Health guidelines.

Intracerebroventricular injections. In some instances, P0-2 rats received an intracerebroventricular (***ICV***) injection of an AAV9.Syn.GCaMP6s.WPRE.SV40 viral vector (Penn Vector Core, Philadelphia, PA, AV-1-PV2824; supplied by the GENIE Project, Janelia Research Campus, HHMI) (Glascock et al., 2011). Sterile microliter calibrated glass pipettes were filled with virus diluted to ~$1x10^{13}$ GC/ml in 0.1% trypan blue dye (Bio-Rad, Raleigh, NC). Rats were cryoanesthetized and the pipette was lowered through the skull, into the lateral ventricle. A picospritzer (Picospritzer III, Parker Hannifin, Hollis, NH) was used to deliver 3 µl of virus solution into each lateral ventricle. Animals were then returned to the dam to allow time for GCaMP6s expression.

Slice preparation. P10-20, animals were deeply anesthetized with pentobarbital and then transcardially perfused with an ice-cold protective recovery solution containing (in mM): 92 NMDG, 26 $NaHCO_3$, 25 glucose, 20 HEPES, 10 $MgSO_4$, 5 Na-ascorbate, 3 Na-pyruvate, 2.5 KCl, 2 thiourea, 1.25 NaH_2PO_4, 0.5 $CaCl_2$, titrated to a pH of 7.3-7.4 with HCl (Ting et al., 2014). Horizontal slices (250 µm) containing the thalamus were cut in ice-cold protective recovery solution using a vibratome (VT1200, Leica Biosystems, Buffalo Grove, IL). Slices were trimmed to remove the hippocampus and cortex, and then transferred to protective recovery solution maintained at 32-34°C for 12 minutes. Brain slices were kept in room

temperature aCSF consisting of (in mM) 126 NaCl, 26 $NaHCO_3$, 10 glucose, 2.5 KCl, 2 $CaCl_2$, 1.25 NaH_2PO_4, 1 $MgSO_4$. All solutions were equilibrated with 95% O_2/5% CO_2.

Electrophysiology. Intracellular recordings were performed in a submerged chamber, with slices situated on nylon netting and perfused with warm (31-33°C) oxygenated aCSF at 2.5 ml/min. All experiments were performed in the presence of kynurenic acid (3 mM) and CGP 55845 (100 nM) to block AMPA, NMDA and $GABA_B$ receptors, and TTX (1 µM) to block sodium channel activation. Cadmium chloride (100 µM) was used to block voltage-dependent calcium channel activation in all Cl^- extrusion experiments. Thalamic neurons were visualized using infrared Dodt gradient contrast illumination on a Zeiss Axio Examiner.A1 microscope (Zeiss Microscopy, Thornwood, NY) and an sCMOS camera (ORCA-Flash4.0, Hamamatsu, Japan). Recording pipettes were pulled from thick-walled borosilicate capillary glass (Sutter Instruments, Novato, CA) using a P1000 puller (Sutter Instruments) and were filled with (in mM): 130 KCl, 1 MgCl2, 0.07 CaCl2, 10 HEPES, 0.1 EGTA (pH-adjusted to 7.3 with KOH, osmolarity 300 mOsm). Pipettes had a 3-4 MΩ tip resistance. Gramicidin (dissolved in DMSO) was added to prefiltered internal solution to produce a final concentration of 5 µg/ml and sonicated for 30 seconds. For one set of experiments (see **Fig. 6**) a CsCl internal pipette solution, containing (in mM): 132 CsCl, 10 HEPES, 0.5 EGTA, 2 $MgCl_2$, 0.16 $CaCl_2$ and 5 QX-314 (pH-adjusted to 7.3 with KOH, osmolarity 295 mOsm) was utilized (Sun et al., 2012).

High resistance (>0.8 GΩ) cell-attached seals were obtained through the application of negative pressure. Changes in access resistance due to gramicidin pore formation were monitored by repeatedly delivering 20 mV hyperpolarizing voltage steps. Access resistance was measured from the transient responses to the applied voltage steps using established methods (Ulrich and Huguenard, 1997). Appropriate pore formation was indicated by access resistance measurements of 50-100 MΩ, typically achieved within 10-40 minutes. Rapid drops in access resistance at any point during these experiments were indicative of a ruptured membrane patch and these recordings were discarded. The $GABA_A$ receptor agonist muscimol (Abcam, Cambridge, MA) was dissolved in aCSF (100 µM) and applied through a patch pipette adjacent to the cell body of the recorded neuron using 10 ms pressure puffs (Picospritzer III). Membrane potentials were all corrected for the voltage drop across the series resistance.

Data were acquired in pClamp software (Molecular Devices, Sunnyvale, CA) using a Multiclamp 700B amplifier (Molecular Devices), low-pass filtered at 2 kHz, and digitized at 10 kHz (Digidata 1440A, Molecular Devices). Data analysis was performed using custom written scripts in MATLAB (MathWorks, Natick, MA).

Calcium imaging. As with the electrophysiology experiments described above, acute brain slices were prepared from P10-20 animals that received an ICV injection of AAV9.Syn.GCaMP6s.WPRE.SV40 at P0-2. Recordings were performed at 31-33°C in aCSF containing: kynurenic acid (3 mM), CGP 55845 (100 nM), and TTX (1 µM). Illumination was provided by a DG-4 arc lamp (Sutter)

using a 470 ± 22 nm bandpass excitation filter. Images were acquired with HCImage software (Hamamatsu) at 10 Hz using a 10x/NA0.2 lens. Chemical stimuli were applied with a custom built local perfusion system, which enabled controlled delivery of aCSF with added 5 µM muscimol or 10mM KCl to the field of imaged RT neurons. Images were analyzed off-line, using custom written scripts in MATLAB to measure changes in image intensity within user defined ROIs.

Drugs and solutions. All drugs used were applied in aCSF. VU0463271 (N-Cyclopropyl-N-(4-methyl-2-thiazolyl)-2-[(6-phenyl-3-pyridazinyl)thio]acetamide, Bio-techne, Minneapolis, MN) was diluted from a 10 mM stock in DMSO to a concentration of 10 µM in aCSF. A 50 U/ml stock of Chondroitinase ABC (ChABC, Sigma Aldrich, St. Louis, MO) was made in 0.1% BSA and diluted down to 0.4 U/ml in aCSF.

Histochemistry. At P5, 10, 15, 20 and 40, animals were deeply anesthetized with pentobarbital and transcardially perfused with PBS, followed by ice-cold 4% PFA in PBS (both pH 7.4). Brains were post-fixed overnight in 4% PFA at 4°C. Horizontal sections (40 µm) containing the thalamus were obtained using a vibratome (VT1000S, Leica Biosystems). Free-floating sections were washed in PBS and then treated with 0.1% sodium borohydride in PBS for 15 minutes to reduce autofluorescence. Sections were washed with PBS, blocked with 2% normal goat serum and Fab fragment of goat anti-mouse IgG (1:500, Jackson ImmunoResearch, West Grove, PA) in PBS for 4 hours at room temperature, and

then washed with PBS. Sections were incubated overnight at 4°C with combined primary antibodies for either KCC2 and parvalbumin (rabbit anti-KCC2, 1:500, EMD Millipore, Billerica, MA; mouse anti-parvalbumin, 1:2000, Sigma Aldrich), or parvalbumin and fluorescein labeled Wisteria floribunda agglutinin (1:2000, Vector Laboratories, Burlingame, CA) in PBS with 1% normal goat serum. Sections were washed in PBS and then incubated overnight at 4°C with appropriate combinations of secondary antibodies (donkey α-mouse AF488 and donkey α-rabbit Cy3 for KCC2 labeling, donkey α-mouse Cy3 for WFA labeling; all 1:200 in PBS with 1% normal goat serum, Jackson ImmunoResearch). Sections were washed in PBS and mounted with Vectashield (Vector Laboratories).

A subset of histochemical experiments were performed in 300 μm sections prepared as described for use in electrophysiological experiments. Horizontal sections were then bisected and one hemisphere was incubated at 37°C in 0.4 U/ml ChABC, while the other hemisphere was incubated in aCSF. These sections were then post-fixed in 4% PFA for 12 hours before being stained for parvalbumin and WFA as described above.

All images were obtained with a Neurolucida system (MicroBrightfield, Colchester, VT) with an Axioskop microscope driven stage and an AxioCam MRc camera (Zeiss Microscopy). All staining and imaging was performed in batches where a set of sections representing all age groups were processed simultaneously. This allowed for us to control for between experiment variability in measured labeling. Images were analyzed using custom written scripts in MATLAB, which allowed for evaluation by two independent, blinded, investigators.

Computational modeling. This model was based on those of Sohal et al. (2003) and Jedlicka et al. (2011). Simulated networks contained 100 RT cells, each of which was modeled as a single compartment. All simulations were run using NEURON (Hines and Carnevale, 1997) at a temperature of 31°C and with a time step of 0.1 ms.

Intrinsic properties. Each RT cell consisted of a cylinder with a length of 20 µm and a diameter of 10 µm, based on the dimensions of neurons observed during our electrophysiological experiments. All cells had the following properties: (1) a specific membrane capacitance of 1 µF/cm^2, (2) an axial resistivity of 100 Ω·cm (Destexhe et al., 1996), (3) a leak current with a reversal potential of -70 mV and a conductance that was randomly selected from a uniform distribution between 45 and 55 µS/cm^2 (Sohal and Huguenard, 2003), (4) Na^+ and K^+ currents underlying action potentials ($\boldsymbol{I_{Na}}$, $\boldsymbol{I_K}$), (5) a low-threshold Ca^{2+} current ($\boldsymbol{I_{Ts}}$), and (6) a Ca^{2+}-dependent K current ($\boldsymbol{I_{KCa}}$), and (7) a $GABA_A$ receptor-mediated current comprising a Cl^- current ($\boldsymbol{I_{Cl}}$) and a nonspecific current that represents HCO_3^- flow ($\boldsymbol{I_{HCO3}}$). Kinetics and details for I_{Na}, I_K, I_{Ts}, I_{KCa} and the kinetics of intracellular Ca^{2+} ($\boldsymbol{[Ca^{2+}]_i}$) were taken from Sohal et al. (2003). The following changes were implemented: (1) the K^+ reversal potential was fixed at -104 mV, (2) the spike threshold was set to -47 mV (Muñoz and Fuentealba, 2012), and (3) I_{Ts} followed the constant field equation with permeability $p_{Ts} = 10^{-4}$ cm/s. Properties of I_{Cl} and I_{HCO3} were taken from Jedlicka et al. (2011), except for the following: (1) extracellular Cl^- concentration was set to 130.5 mM, (2) the conductance ratio g_{Cl}:g_{HCO3} was 4:1,

and (3) the peak $GABA_A$ conductance ($\boldsymbol{g_{peak}}$) per synapse was set to 2.5 nS, or up to 20 nS per cell.

Chloride dynamics. Kinetics of $[Cl^-]_i$ were adapted from Jedlicka et al. (2011). $[Cl^-]_i$ was computed in a submembrane compartment with a depth of 0.5 µm, allowed to diffuse radially with a diffusion coefficient of 2 μm^2/ms, and was actively extruded (representing the action of KCC2) via Michaelis-Menten kinetics. The dissociation constant ($\boldsymbol{K_d}$) of Cl^- extrusion was 15 mM and the maximum flux was computed by: $V_{max} = (Cl_\infty + K_d) / \tau_{KCC2}$. In this equation, Cl_∞ (the steady-state value of $[Cl^-]_i$) was 8 mM. A range of values (4-64 sec) for τ_{KCC2} (the extrusion time constant when $[Cl^-]_i \approx Cl_\infty$) were examined. A constant Cl^- leak current balanced the steady-state extrusion rate.

Network architecture. RT cells were organized in a simple, linear array. All connections were local and topographic, such that each RT cell projected to the eight nearest RT cells (Sohal and Huguenard, 2003). An action potential was counted when the membrane voltage reached 0 mV. Following a synaptic delay of 1 ms, $GABA_A$ receptors were activated according to kinetics described in Jedlicka et al. (2011). The rise and decay time constants of $GABA_A$ currents were 0.1 ms and 50 ms, respectively, and the baseline $GABA_A$ reversal potential was set to -62 mV, based on our data (see **Fig. 2C**).

Simulation protocol. In each simulation, the network was allowed to initially equilibrate for 3 seconds. Following this period, action potential activity was elicited in three central cells (Cells 46, 51 and 56) by applying brief (100 µs, 4 nA) and repetitive current pulses. In stimulated cells p_{Ts} and g_{KCa} (conductance of I_{KCa}) were

set to zero to better control firing behavior. We tested a range of stimulation frequencies (1-60 Hz), delivered for a total duration of 200 seconds. Total simulation duration was 233 seconds.

Experimental design and statistical analysis. Throughout this study, measurements from neurons in the ventrobasal (***VB***) thalamic nuclei were used as controls for observations from RT neurons. All histochemical experiments were performed in brain slices from 4 rats and 4 mice per age group (2 male, 2 female; both hemispheres from ~3 slices per animal were analyzed). The number of recordings for basal measures of E_{GABA} (RT: 7 male, 6 female; VB: 7 male, 7 female) and Cl^- extrusion (RT: 6 male, 5 female; VB: 7 male, 8 female) reflect the number of animals used, with recordings from RT and VB neurons at times occurring within the same subject.

When possible, drug-induced effects were compared against baseline recordings in the same neuron. Each recording of the impact of VU0463271 on basal E_{GABA} (RT: 3 male, 2 female; VB: 1 male, 4 female), basal E_{GABA} when using a Cs-based recording solution (RT: 4 male, 1 female; VB: 3 male, 2 female) and Cl^- extrusion (RT: 2 male, 4 female; VB: 4 male, 4 female) reflects an independent subject, except where recordings from RT and VB neurons occurred within brain slices of the same animal.

The time course of ChABC experiments prohibited pre- and post-treatment recordings from the same neuron, so control recordings were obtained from sham-treated neurons. Each measure of the impact of ChABC treatment on basal E_{GABA}

(RT control: 3 male, 5 female; RT ChABC: 4 male, 3 female; VB control: 3 male, 7 female; VB ChABC: 4 male, 3 female), Cl^- extrusion (RT control: 2 male, 2 female; RT ChABC: 1 male, 2 female; VB control: 4 male, 1 female; VB ChABC: 2 male, 2 female) and basal E_{GABA} when combined with VU0463271 (RT control: 4 male, 4 female; RT ChABC: 2 male, 2 female) reflects the number of animals used, with recordings from RT and VB neurons at times occurring within the same subject. Control and ChABC treated recordings were always performed in different brain slices.

In calcium imaging experiments, muscimol and elevated KCl responses were evaluated in each brain slice, with the KCl treatment being a positive control for the change in fluorescence associated with a mild depolarization. For evaluating the overall distribution of responses, the change in fluorescence of each detected RT neuron was compared (Muscimol: 1772; KCl: 1728). Photobleaching and shifting tissue, among other factors, result in a differing number of detectable cells in experiments performed in the same brain slice. The typical response to muscimol and elevated KCl was evaluated by comparing the median change in fluorescence that a treatment evoked within each subject (5 male, 2 female, average of 1.7 slices per animal). Similar comparisons were made in experiments where brain slices were preincubated in VU0463271 prior to calcium imaging (Muscimol+VU0463271: 1772 cells; KCl+VU0463271: 1728 cells; 3 male, 3 female, average of 1.8 slices per animal).

All statistical tests were performed in MATLAB. Unless otherwise noted, statistical tests to determine the significance of differences between groups were performed

using unpaired or paired Student's t-test. When utilized, ANOVA tests were followed by a *post hoc* Tukey's HSD analysis. Comparisons requiring a nonparametric factorial analysis were calculated using a two-way Aligned Rank Transform ANOVA (Wobbrock et al., 2011). This method independently rank transforms the data to separate the contributions of the main effects and interactions. After the data has been aligned and ranked, a regular parametric ANOVA with Tukey's HSD *post hoc* testing can be used to analyze each individual effect. Group measures are presented as mean ± SEM. The threshold for differences to be considered significant was set at $p<0.05$.

Results

The goal of our study was to resolve how intracellular Cl^- is regulated in the RT nucleus, a structure proposed to serve as an important seizure choke point. We used anatomical and functional approaches to determine the relative contributions of KCC2 and impermeant anions to setting basal $[Cl^-]_i$ in RT neurons. We also assessed the degree to which these two mechanisms define the activity-dependent, Cl^- extrusion capacity of RT neurons. Finally, we incorporated our observations into a computational model of a local RT network to better understand how seizure activity propagation within this network might depend on the properties of Cl^- regulation. Collectively, our experimental and computational results suggest that the weak Cl^- extrusion capacity of RT neurons is sufficient to support basal inhibitory, GABAergic signaling, but that the nucleus is susceptible to an activity-dependent switch from synaptic inhibition to excitation.

KCC2 expression is low, but present in RT neurons

As a major Cl^- transporter in the central nervous system, KCC2 is thought to critically maintain the low $[Cl^-]_i$ that enables inhibitory, $GABA_A$ receptor-mediated signaling in adult neurons (Kaila et al., 2014). Interestingly, the RT nucleus is one of only a small number of regions in the adult rat brain with minimal KCC2 mRNA expression (Kanaka et al., 2001). Reduced expression of KCC2 protein is also observed in the RT nucleus of adult rats (Barthó et al., 2004) and mice (Sun et al., 2012). Anatomical assays primarily served as the basis for these previous measures.

The developmental upregulation of KCC2 in most brain regions is well-established (Kaila et al., 2014). However, to our knowledge, this phenomenon has not been examined in the thalamus. Therefore, we began our study by measuring KCC2 immunoreactivity within the rodent thalamus as a function of age (P5-40) (**Fig. 1**). To control for experimental variability, we concurrently performed immunohistochemistry on sets of brain slices representing all age groups. As in other brain structures, thalamic KCC2 immunoreactivity increased with age in the rats we examined ($F(4,146)=2.60$, $p=0.038$, $n=4$, two-way ANOVA, **Fig. 1B**). Specifically, overall KCC2 immunoreactivity was low throughout the thalamus of P5 rats (21.3±1.3 A.U.), and increased thereafter (P20 rats: 47.4±8.7 A.U., $p=0.049$; P40 rats: 47.4±6.0 A.U., $p=0.033$). While immunoreactivity in both the ventrobasal (***VB***) thalamus and RT nucleus increased with age, the effect was blunted in RT. These results suggest that KCC2 is expressed in the adult rat RT

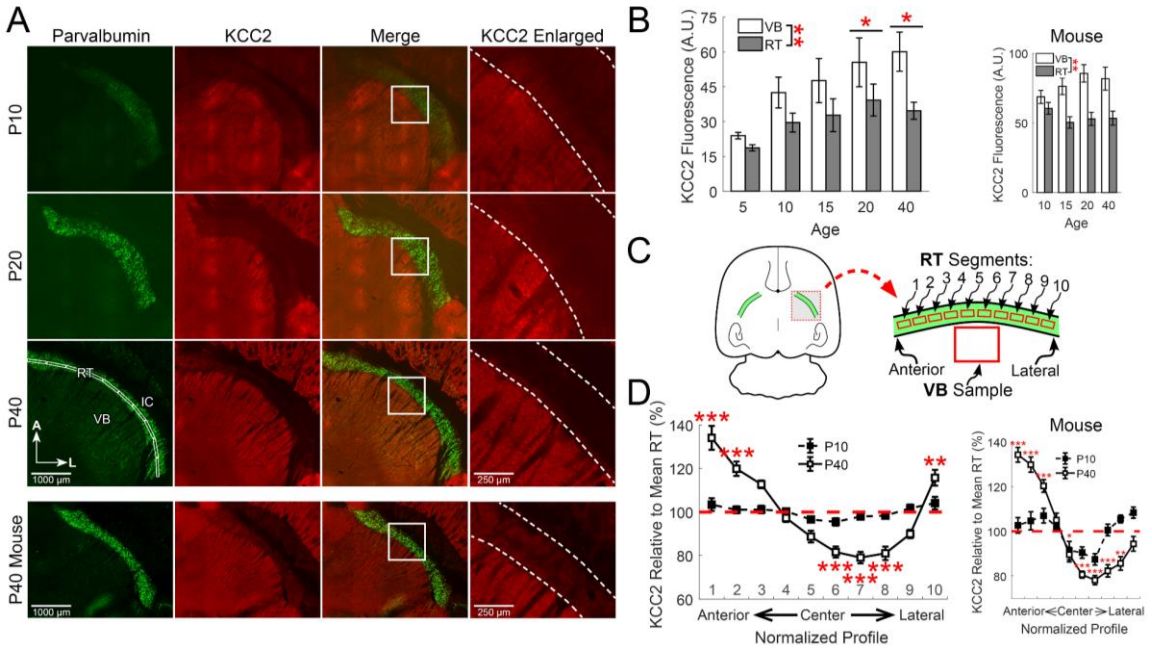

Figure 1. KCC2 expression is low in RT neurons throughout development. ***A***, Immunofluorescence of parvalbumin (green) and KCC2 (red) in horizontal sections of rat thalamus at different developmental time points. All images are oriented with the anterior (A) aspect of the thalamus towards the top, the lateral (L) aspect towards the right and the internal capsule (IC) towards the upper right corner of the image. Dotted lines indicate the boundaries of the RT nucleus in the enlarged images. ***B***, KCC2 immunofluorescence increased across the ages we tested. KCC2 labeling was consistently lower in the RT nucleus, relative to VB, across the ages tested. A similar pattern of KCC2 labeling was observed in mice. ***C***, Schematic of methodology for measuring regional variability in KCC2 intensity across segments of the RT nucleus. Intensity of KCC2 labeling was measured in an ROI, subdivided into 10 segments, that extended from the anterior to the lateral extent of the RT nucleus (see ***A***, lower left) and values were normalized to the mean intensity across this entire span. ***D***, KCC2 labeling was consistent throughout the span of the RT nucleus at P10, but showed significant regional variability in P40 rats and mice. *p<0.05; **p<0.01; ***p<0.001.

nucleus, albeit at relatively lower levels than observed in VB thalamus ($F(1,146)=8.37$, $p=0.0044$, $n=4$, two-way ANOVA). We detected a similar pattern of KCC2 staining in P10-40 mice (**Fig. 1B**).

In addition to gross, age-dependent differences in KCC2 immunoreactivity, we also observed that the distribution of KCC2 expression was not even throughout RT, particularly in adult rats and mice. To quantify KCC2 immunoreactivity, we drew a linear ROI that extended from the anterior-most edge to the lateral-most edge of the RT nucleus (see lower left panel in **Fig. 1A**). This line bisected the RT nucleus, and then automatically expanded to a width of 75 µm. This linear ROI was further subdivided into 10 equal segments that were numbered from 1 (anterior-most) to 10 (lateral-most, see **Fig. 1C**). The mean fluorescence intensity within each segment was calculated.

We quantified KCC2 immunoreactivity in each segment along the anterior-to-lateral axis, relative to the mean intensity level across all RT segments of each slice (**Fig. 1D**), an approach to account for slice-to-slice staining variability. When expression was quantified in this manner in P40 rats, we observed that KCC2 levels were not uniform across segments of the RT nucleus ($F(10,200)=39.4$, $p<0.001$, $n=4$, one-way ANOVA). This finding establishes that KCC2 immunoreactivity varies according to location within the RT nucleus. To discern specific immunoreactive differences among the segments, we compared individual segment means to the overall mean across all RT segments.

Relative to the overall RT mean, KCC2 immunoreactivity was elevated in the two anterior-most segments of the adult rat RT nucleus (segment 1: 134±5.5%,

p<0.001; segment 2: 120±3.3%, p<0.001), as well as in the lateral-most segment (segment 10: 116±3.6%, p=0.004). Centrally-located segments, on the other hand, had much reduced KCC2 immunoreactivity (segment 6: 82±2.5%, p<0.001; segment 7: 79±2.6%, p<0.001, segment 8: 81±3.1%, p<0.001).

Next, we applied the aforementioned approach to younger, P10 rats. Although KCC2 levels varied minimally along the extent of the RT nucleus in P10 rats ($F(10,144)=2.35$, $p=0.013$, $n=4$, one-way ANOVA), no significant differences relative to the overall RT mean were observed. These results suggest that there is greater regional variability in KCC2 immunoreactivity in the RT nucleus of P40 rats than of P10 rats. We observed a broadly similar pattern of KCC2 immunoreactivity in mice (**Fig. 1D**).

Collectively, our results indicate that KCC2 expression is consistently lower in RT neurons than VB neurons throughout the first few postnatal weeks, in agreement with prior reports (Kanaka et al., 2001; Barthó et al., 2004; Sun et al., 2012). However, it remained unclear the extent to which detected immunoreactivity in the RT nucleus was due to KCC2 protein expression or non-specific labeling. Therefore, we decided to use functional measurements to assess whether diminished KCC2 reduces the capacity of RT neurons to maintain a low $[Cl^-]_i$.

$[Cl^-]_i$ is relatively low in RT neurons

Based on our observation that KCC2 immunoreactivity is low in RT neurons, we expected to find elevated $[Cl^-]_i$ in these neurons. If true, then GABAergic signaling in RT neurons would likely be excitatory. To assess $[Cl^-]_i$ in RT neurons without

perturbing the intracellular Cl^- gradient, we performed gramicidin perforated patch recordings in RT neurons of P10-20 rats.

Successful patch perforation was indicated when access resistance measurements reached 50-100 MΩ. Neurons were voltage-clamped at -70 mV and then stepped to a command potential between -110 and -20 mV for 2.5 sec of each 15 sec sweep. These 10 voltage steps were given in a randomized in order to reduce experimentally-induced Cl^- loading. The $GABA_A$ receptor agonist muscimol (100 µM) was pressure-applied to the soma of the voltage-clamped neuron for 10 ms during each voltage step. We adjusted the pressure used for agonist application so that GABA-evoked currents fully decayed within 2 sec from application.

Current-voltage (***I-V***) relationships were plotted for both the leak current and the muscimol-induced current, and the voltage at which these currents was equal indicated the reversal potential for the GABA-induced current ($\boldsymbol{E_{GABA}}$). E_{GABA} is largely determined by E_{Cl}, with E_{HCO} (the reversal potential for bicarbonate ions) providing a smaller contribution (Bormann et al., 1987; Staley et al., 1995). We did not isolate the relative contributions of E_{Cl} and E_{HCO} to E_{GABA} in our recordings, so our calculations may slightly overestimate the $[Cl^-]_i$ of RT neurons (Staley et al., 1995). We corrected all measurements for the voltage drop across the series resistance.

We determined that RT neurons have an E_{GABA} of -62±3.0 mV (n=13, **Fig. 2A,C**). For comparison, E_{GABA} was also measured in VB neurons, where it was found to be significantly more hyperpolarized than in RT neurons (-79±2.7 mV,

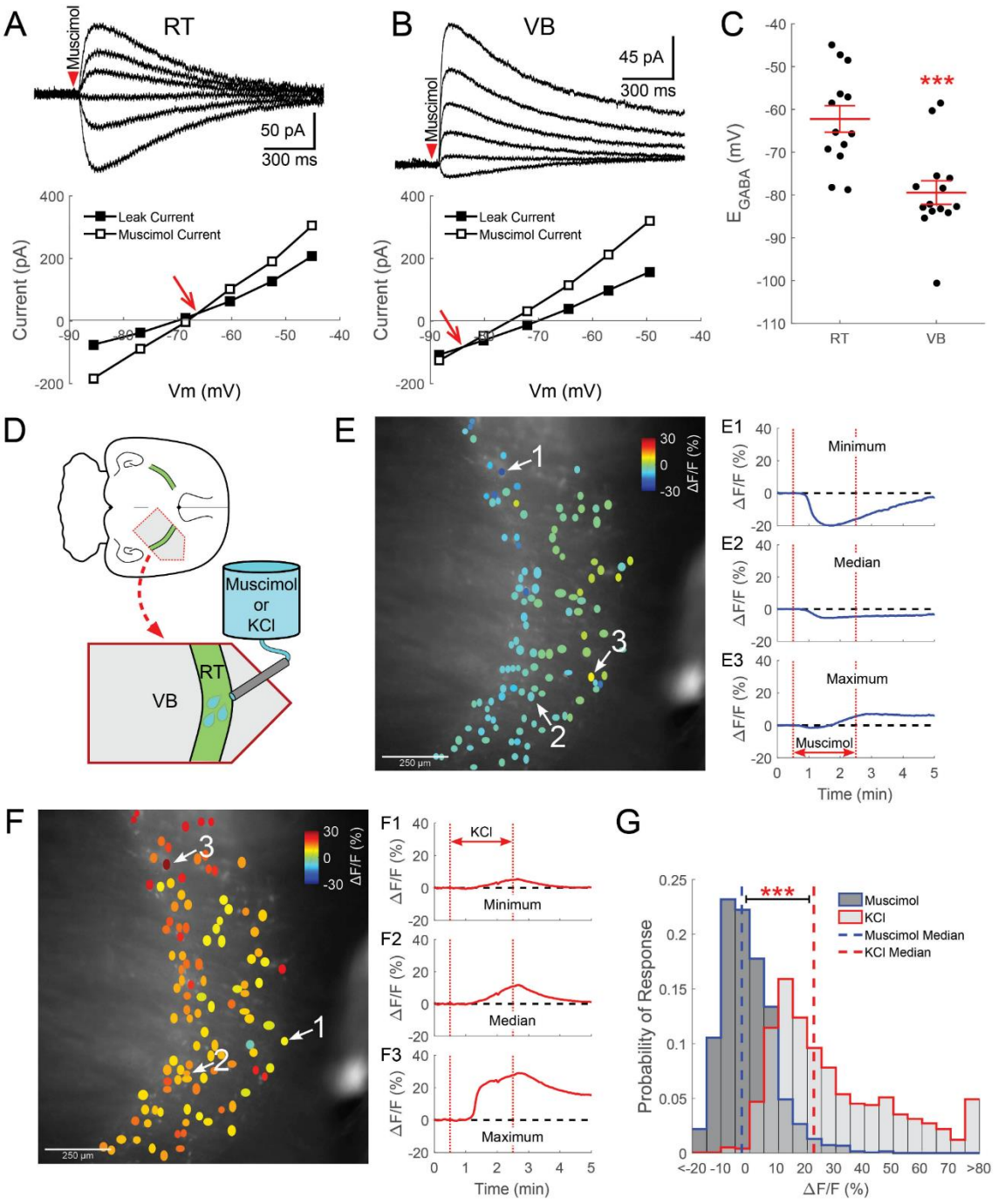

Figure 2. RT neurons maintain a relatively low $[Cl^-]_i$. Gramicidin perforated patch recordings of muscimol-induced (100 µM, 10 ms) currents from RT (***A***) and VB (***B***) neurons at various command potentials. The leak current has been subtracted from the representative traces. The intersection of the pre-stimulation leak current and the

muscimol-induced current was used to determine the $GABA_A$ receptor-mediated equilibrium potential (E_{GABA}, indicated by red arrow). ***C***, The E_{GABA} of RT neurons was more depolarized than in VB neurons, yet remained at levels that likely support inhibitory GABAergic signaling. ***D***, GCaMP6s was expressed in RT neurons for calcium imaging experiments and a local perfusion system provided timed delivery of muscimol (5 µM) or elevated KCl (+10 mM) to the imaged RT nucleus. ***E***, Two minute application of muscimol mostly decreased the fluorescence of RT neurons. ROIs drawn around GCaMP6s expressing RT neurons are colored according to their peak change in fluorescence. Representative examples of neurons displaying the minimum (***E1***), median (***E2***) and maximum (***E3***) fluorescence change in a particular brain slice following muscimol application. ***F***, Two minutes of elevated KCl produced a nearly uniform increase in the fluorescence of RT neurons. Examples of the minimum (***F1***), median (***F2***) and maximum (***F3***) fluorescence changes evoked by elevated KCl application. ***G***, Histograms comparing induced responses in all cells imaged, across multiple animals, shows that the median response (dotted line) to muscimol was a slight decrease in fluorescence. In contrast, mild depolarization with elevated KCl produced a robust increase in fluorescence. Bin size: 5ΔF/F(%). ***p<0.001.

t(25)=4.15, p<0.001, n=14, **Fig. 2B,C**). Based on our recording solutions, $[Cl^-]_i$ was ~12 mM in RT neurons and ~6 mM in VB neurons. Interestingly, while we measured a very consistent E_{GABA} in the majority of VB neurons, this parameter was more variable among RT neurons. The RT nucleus contains a heterogeneous population of neuronal subtypes, associated with distinct functional characteristics (Lee et al., 2007; Halassa et al., 2014; Clemente-Perez et al., 2017), and may provide a source of this variability. Our electrophysiological recordings were targeted to the central section of the RT nucleus, and likely include both parvalbumin- and somatostatin-positive RT neuron subtypes (Clemente-Perez et al., 2017).

While gramicidin perforated patch recordings are designed to maintain physiological $[Cl^-]_i$ in neurons, the low experimental yield afforded by this technique limits the ability to make observations in large populations of neurons. Therefore, we also examined the response of RT neurons to $GABA_A$ receptor stimulation using GCaMP6s-based calcium imaging. Acute brain slices, where GCaMP6s had been virally transfected into RT neurons, were prepared and a local perfusion system was used to deliver test compounds in proximity to the RT nucleus (**Fig. 2D**). Cell-intrinsic responses to muscimol stimulation were isolated by blocking AMPA, NMDA and $GABA_B$ receptors, as well as voltage-gated sodium channels. A two minute application of muscimol (5µM) caused a decrease in the fluorescence of most, but not all, RT neurons (**Fig. 2E,G**). However, subsequently depolarizing the RT neurons with the addition of 10 mM KCl (12.5 mM in total) for two minutes induced a robust increase in fluorescence (**Fig. 2F,G**). Based on E_K measurements

of RT neurons (McCormick and Prince, 1986), the high-K^+ test solution should depolarize neurons to around -45 mV. Compared across animals, 10 mM KCl produced a significantly greater median increase in fluorescence (22.3%, interquartile range 12.1–42.7%, n=1728 cells, n=7 animals, **Fig. 2G**) than the mild decrease following muscimol stimulation (-2.8%, interquartile range -7.1–4.8%, n=1772 cells, n=7 animals, Z=44.86, p<0.001, Wilcoxon rank sum test).

Because KCC2 immunoreactivity is reduced in the RT nucleus, the observation that $[Cl^-]_i$ remained low — and GABAergic signaling remained inhibitory — in most RT neurons was unexpected. Considering that KCC2 immunoreactivity was low in the RT nucleus (see **Fig.** 1), we were motivated to determine if extracellular impermeant anions (***[A]$_o$***) contribute to Cl^- regulation in RT neurons (Glykys et al., 2014a).

While elevated in RT neurons, $[A]_o$ contribute only mildly to setting E_{GABA}

Chondroitin sulfate proteoglycans (***CSPGs***) are major extracellular matrix proteins that contain abundant, negatively charged, sulfate groups, thus making them a significant source of $[A]_o$ (Bandtlow and Zimmermann, 2000; Glykys et al., 2014a). The disaccharide formed by *N*-acetylgalactosamine and glucuronic acid is bound by the plant lectin *Wisteria floribunda* agglutinin (***WFA***), and therefore can be used to label chondroitin sulfate glycosaminoglycan elements of CSPGs (Horii-Hayashi et al., 2015). WFA staining showed that the CSPGs surrounding RT neurons increase during development from P5-40 (**Fig. 3**).

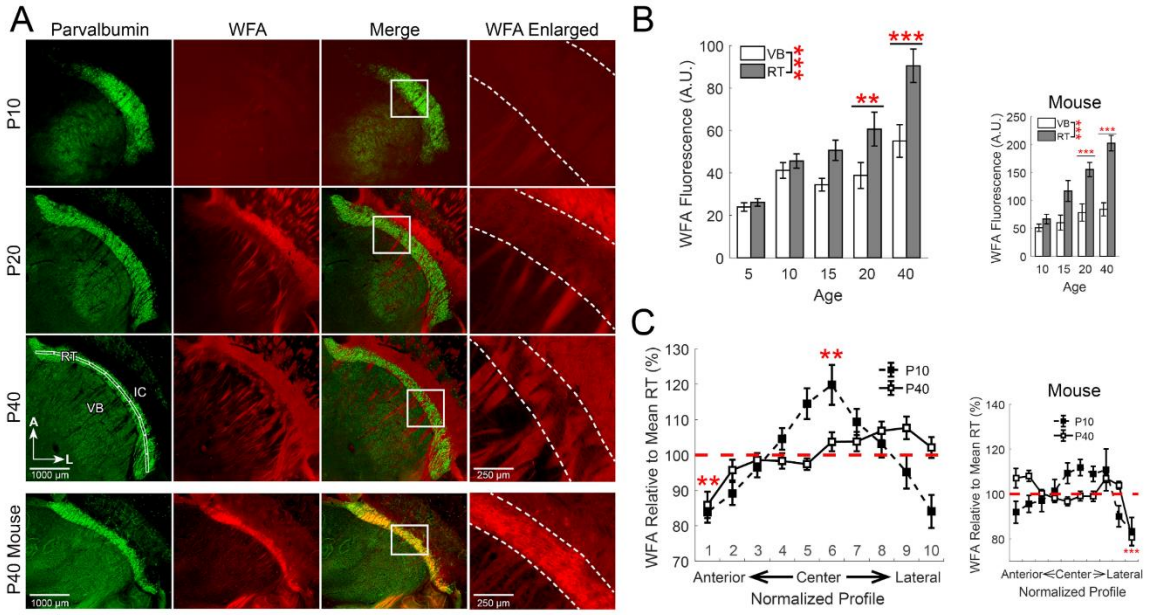

Figure 3. CSPGs are elevated around RT neurons. ***A***, Immunofluorescence of parvalbumin (green) and labeling of CSPGs with WFA (red) in horizontal sections of rat thalamus at different developmental time points. All images are oriented with the anterior (A) aspect of the thalamus towards the top, the lateral (L) aspect towards the right. Dotted lines indicate the boundaries of the RT nucleus in the enlarged images. ***B***, WFA staining increased across the ages we tested and was consistently elevated in the RT nucleus, relative to VB. ***C***, Intensity of WFA labeling was measured in an ROI, subdivided into 10 segments, that extended from the anterior to the lateral extent of the RT nucleus (see ***A***, lower left, **Fig. 1C**) and values were normalized to the mean intensity across this entire span. WFA labeling showed slight regional variability in both P10 and P40 rats. A similar pattern of WFA labeling was observed in mice. **p<0.01; ***p<0.001

We first examined the overall levels of WFA fluorescence in the thalamus across the different ages of rats we tested. As with KCC2 immunoreactivity, WFA stain intensity increased with age ($F(4,218)=14.48$, $p<0.001$, n=4, two-way ANOVA, **Fig. 3B**). While overall WFA levels were initially low throughout the thalamus of P5 rats (25.0±1.8 A.U.), overall WFA staining was elevated in P20 rats (49.7±7.0 A.U., $p=0.0011$) and further increased by P40 (72.7±7.6 A.U., $p<0.001$). This observation is consistent with prior findings showing that WFA staining first appears between P7-14 in many regions of the mouse brain and further increases as the extracellular matrix matures during the next few weeks of development (Horii-Hayashi et al., 2015). Across the ages we evaluated, there was greater mean WFA staining throughout the RT nucleus (57.6±3.4 A.U., n=20), relative to mean levels in VB (39.9±2.6 A.U., n=20, $F(1,218)=16.31$, $p<0.001$, n=4, two-way ANOVA). Intense WFA staining of white matter tracts is likely non-specific as it is not eliminated by enzymatic reduction of CSPGs (Ajmo et al., 2008, see **Fig. 4F**). An overall similar pattern of WFA staining was likewise detected in P10-40 mice (**Fig. 3**).

As with measurements of KCC2 immunoreactivity (see **Fig. 1D**), WFA staining was also evaluated in a linear ROI that extended from the anterior-most edge to the lateral-most edge of the RT nucleus, and was then subdivided into 10 equal segments (see lower left panel in **Fig. 3A**, **Fig. 1C**). We calculated the mean fluorescence intensity within each segment.

When WFA labeling in each segment along the anterior-to-lateral axis was compared to the mean intensity across all of RT, we found that WFA levels were

not uniform across segments of the RT nucleus of P10 rats ($F(10,202)=9.82$, $p<0.001$, n=4, one-way ANOVA, **Fig. 3C**). Relative to the mean WFA intensity within RT, WFA staining was increased in a central segment of RT (segment 6: 119±5.5%, p=0.0047). We also observed that WFA intensity varied along the extent of the RT nucleus in P40 rats ($F(10,254)=5.49$, $p<0.001$, n=4, one-way ANOVA). There was reduced WFA staining in the anterior-most segment of the RT nucleus (segment 1: 86±3.6%, p=0.0046) relative to the mean WFA intensity within RT.

Considering that RT neurons maintain a surprisingly low $[Cl^-]_i$, despite the low expression of KCC2 in the RT nucleus, we next tested the hypothesis that elevated CSPGs surrounding RT neurons (as indicated by our WFA staining) provide a compensatory mechanism of $[Cl^-]_i$ regulation. Therefore, we measured the impact of reducing $[A]_o$ surrounding RT neurons in P10-20 rats. The enzyme chondroitinase ABC (***ChABC***) digests the chondroitin sulfate polysaccharide elements of CSPGs (Yamagata et al., 1968) and releases negatively charged sulfate groups, thereby reducing $[A]_o$ (Glykys et al., 2014a). We measured changes in E_{GABA} between neurons incubated in ChABC (0.4 U/ml, 37°C) for 2 hours and control neurons incubated in the absence of ChABC.

Using perforated patch recordings, we found that the initial E_{GABA} measurement in ChABC-treated RT neurons (-63±3.2 mV, n=7, **Fig. 4A**) was unchanged from control RT neurons (-60±2.9 mV, $t(13)=0.66$, p=0.52, n=8, **Fig. 4C**). Likewise, the initial E_{GABA} measurement in ChABC-treated VB neurons (-

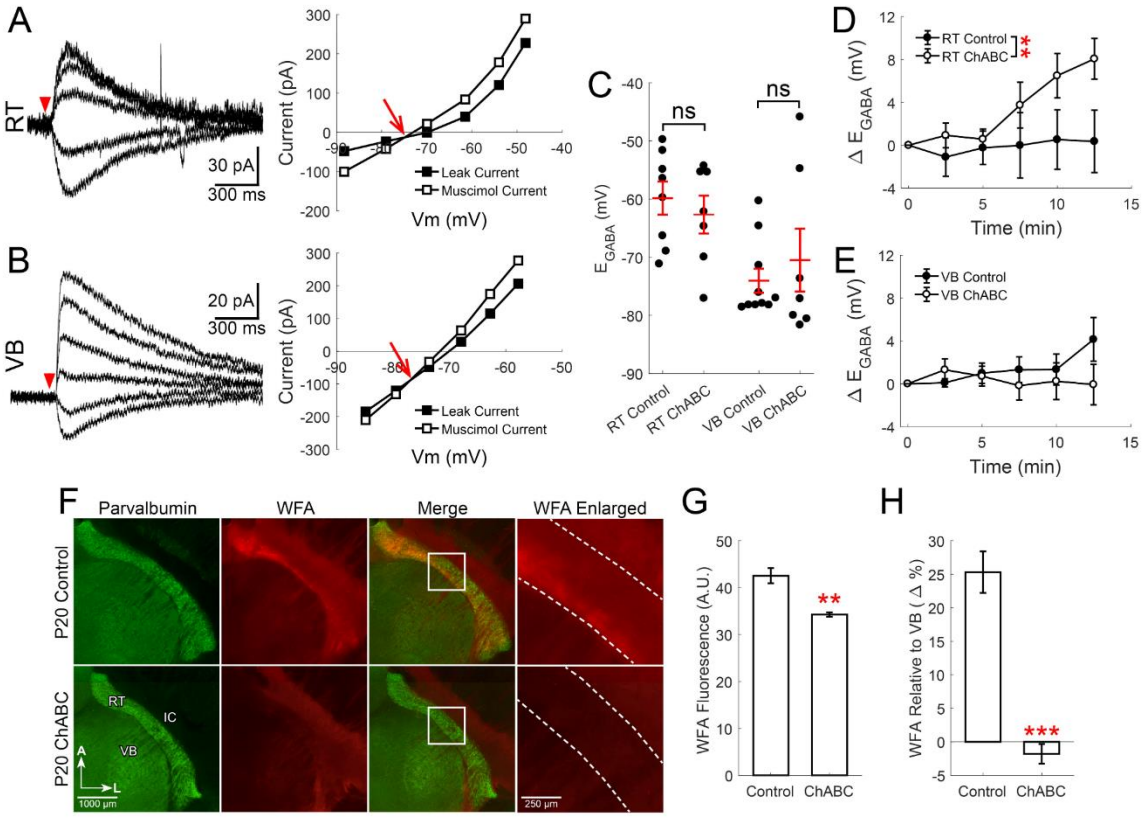

Figure 4. CSPGs mildly contribute to setting E_{GABA} in RT neurons. Gramicidin perforated patch recordings of muscimol-induced (100 µM, 10 ms) currents from RT (***A***) and VB (***B***) neurons at various command potentials, following a 2 hour incubation in ChABC (0.4 U/ml, 37°C). The leak current has been subtracted from the representative traces. E_{GABA} was determined from the intersection of the pre-stimulation leak current and the muscimol-induced current (red arrow). ***C***, ChABC did not alter the initial measurement of E_{GABA} in either RT or VB neurons, relative to control neurons incubated in the absence of ChABC. ***D***, When E_{GABA} measurements were repeated every 2.5 minutes, ChABC treatment produced a small depolarizing shift in E_{GABA} in RT neurons. ***E***, No time dependent shift in E_{GABA} occurred in ChABC-treated VB neurons. ***F***, Immunofluorescence of parvalbumin (green) and labeling of CSPGs with WFA (red) of control and ChABC-treated thalamic slices (300µm) indicates that ChABC (0.4 U/ml, 37°C) effectively reduces

CSPGs surrounding RT neurons. ***G***, WFA labeling in the RT nucleus of ChABC-treated slices was reduced relative to control slices. ***H***, WFA labeling in RT was first normalized to VB levels, thereby revealing a clear effect of ChABC treatment. **p<0.01; ***p<0.001.

70±5.4 mV, n=7, **Fig. 4B**) was no different from control VB neurons, (-74±2.1 mV, t(15)=0.69, p=0.50, n=10, **Fig. 4C**). While the initial measurement of E_{GABA} was not different between ChABC-treated and control RT neurons, we observed an effect of ChABC treatment when E_{GABA} measurements were repeated at 2.5 minute intervals over a 15 minute period ($F(1,68)=8.74$, $p=0.0043$, n=7,7, two-way ANOVA, **Fig. 4D**). Across all time points, ChABC-treated RT neurons underwent a greater, average shift in E_{GABA} (Δ+3.3±0.7 mV, n=7) than control neurons (Δ+0.2±0.8 mV, n=7). The impact of ChABC treatment on the E_{GABA} of RT neurons was particularly evident at 12.5 minutes (control: Δ+0.9±3.4 mV, n=7; ChABC-treated: Δ+8.1±1.9 mV, n=7). There was no effect of either ChABC treatment ($F(1,82)=1.94$, $p=0.17$, n=7,9, two-way ANOVA) or time ($F(5,82)=0.57$, $p=0.72$, n=7,9, two-way ANOVA) on the E_{GABA} of VB neurons (**Fig. 4E**). The modest effect of ChABC treatment on E_{GABA} motivated us to evaluate treatment efficacy in an independent manner. Towards this end, we prepared acute brain slices (300 µm) and then treated them in the same, aforementioned manner. However, rather than performing electrophysiological measurements, we performed WFA labeling protocols on control and ChABC-treated slices to localize CSPGs (**Fig. 4F**). We observed that mean RT WFA fluorescence was lower in ChABC-treated (34.3±0.5 A.U.) versus control slices (42.5±1.6 A.U., $t(15)=4.15$, $p=0.0024$, n=4, **Fig. 4G**), an effect particularly evident when the change was measured by first normalizing RT fluorescence to adjacent, VB fluorescence levels (control: 25.3±3.1%; ChABC: -1.8±1.5%, $t(15)=6.19$, $p<0.0001$, n=4; **Fig. 4H**). This observation confirms that the

ChABC treatment protocol utilized in our perforated patch experiments was indeed associated with a significant reduction in $[A]_o$.

Collectively, these results indicate that although elevated levels of $[A]_o$ surround RT neurons, perturbing CSPGs only affected Cl^- regulation following prolonged periods of stimulation. Considering that $[A]_o$ did not exert a very large impact on the $[Cl^-]_i$ of RT neurons, we next tested the hypothesis that the apparently low level of KCC2 expression in the RT nucleus nonetheless actively contributes to $[Cl^-]_i$ regulation.

KCC2 is a significant regulator of $[Cl^-]_i$ in RT neurons

Due to the generally low Cl^- flux of resting neurons, it has been proposed that even minimal KCC2 might provide sufficient Cl^- extrusion to maintain a hyperpolarizing E_{GABA} (Blaesse et al., 2009). To determine if the apparently reduced level of KCC2 functionally contributes to maintaining a hyperpolarized E_{GABA} in RT neurons, the selective KCC inhibitor VU0463271 (Delpire et al., 2012) was applied during perforated patch recordings in P10-20 rats. While VU0463271 may act on KCCs other than KCC2, brain mRNA levels for KCC1, KCC3 and KCC4 are much lower than for KCC2 (Kaila et al., 2014). There is also no sign that KCC1, KCC3 or KCC4 localize within the thalamus (Rivera et al., 1999; Le Rouzic et al., 2006).

The addition of VU0463271 (10 µM) produced a clear shift to a more depolarized E_{GABA} in perforated patch recordings of RT neurons (**Fig. 5A**). VU0463271 application produced a time-dependent shift in the E_{GABA} of RT neurons ($F(7,32)=24.25$, $p<0.001$, $n=5$, one-way ANOVA), which first became

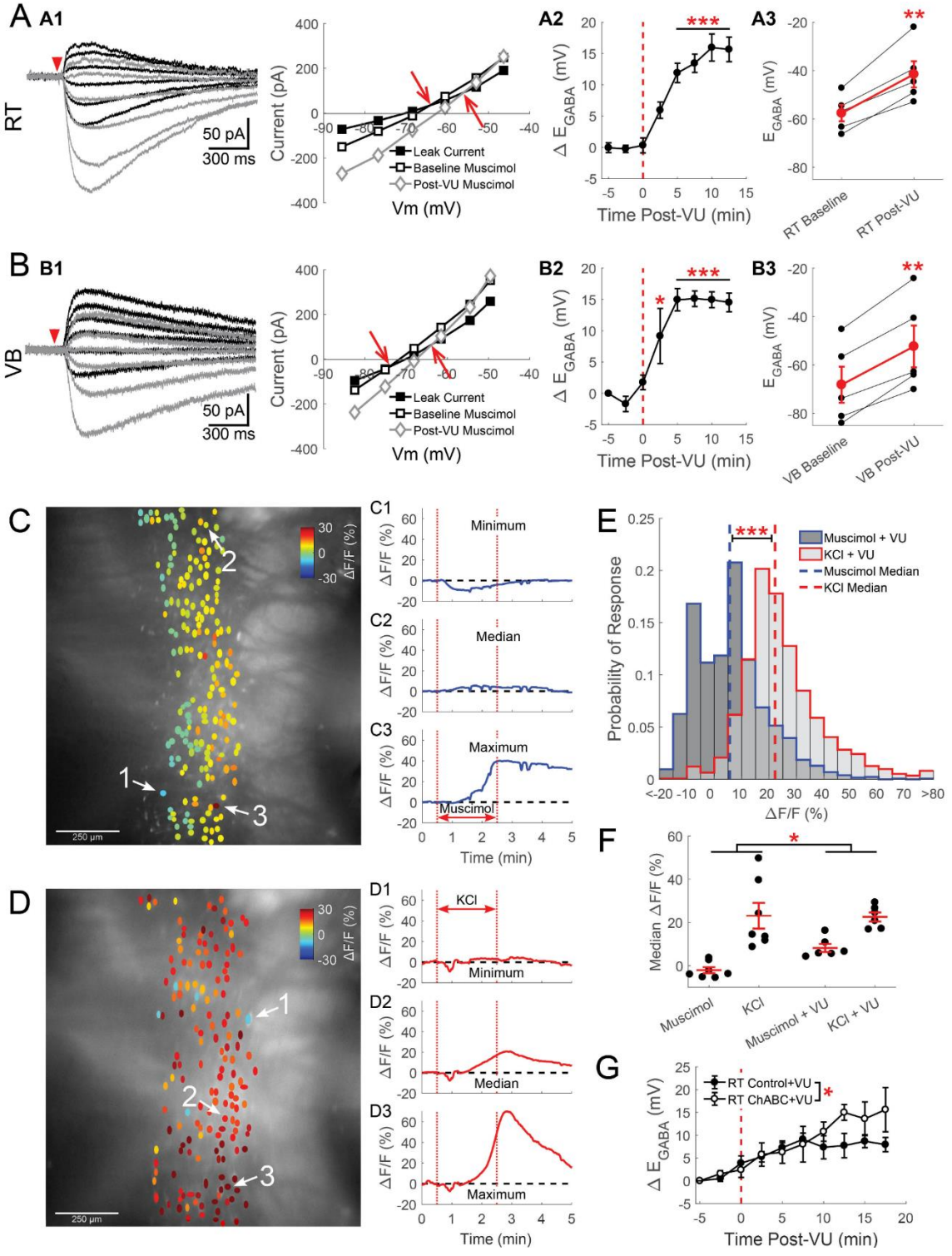

Figure 5. KCC2 regulates E_{GABA} in RT. Gramicidin perforated patch recordings of muscimol-induced (100 μM, 10 ms) currents from RT (***A***) and VB (***B***) neurons at various

command potentials were altered by application of the specific KCC2 antagonist VU0463271 (10 µM). ***A1,B1*** A depolarizing shift in E_{GABA} occurring between baseline (black traces) and after 10 minutes of VU0463271 application (gray traces) was reflected in a shifted intersection between the pre-stimulation leak current and the muscimol-induced current. The leak current has been subtracted from the representative traces. This depolarizing shift was apparent when the time course of the shift in E_{GABA} was measured (***A2,B2***), and when baseline and 10 minutes post VU0463271 E_{GABA} values where compared (***A3,B3***). ***C***, Calcium imaging of GCaMP6s expressing RT neurons, preincubated in VU0463271 (10 µM) for 5 minutes, display a mixed response to a two minute application of muscimol (5 µM) through a local perfusion system. ROIs drawn around GCaMP6s expressing RT neurons are colored according to their peak change in fluorescence. Examples of the minimum (***C1***), median (***C2***) and maximum (***C3***) fluorescence change in a particular brain slice following muscimol application. ***D***, Two minutes of elevated KCl still produced a nearly uniform increase in the fluorescence of RT neurons preincubated in VU0463271. Examples of the minimum (***D1***), median (***D2***) and maximum (***D3***) fluorescence changes evoked by elevated KCl application. ***E***, Histograms comparing induced responses in all cells imaged, across multiple animals. Muscimol produced a slight increase in the median response. In contrast, mild depolarization with elevated KCl produced a robust increase in fluorescence. Bin size: 5ΔF/F(%). ***F***, In a comparison of the median GCaMP6s response, per brain slice, pretreatment with VU0463271 produced a greater increase in fluorescence, across the stimuli tested. ***G***, Gramicidin perforated patch recordings of muscimol-induced (100 µM, 10 ms) currents in RT neurons pretreated with ChABC (0.4 U/ml, 2 hours at 37°C) displayed a greater depolarizing shift in E_{GABA} following VU0463271 application (10 µM) than did control treated neurons. *p<0.05; **p<0.01; ***p<0.001.

clear following 5 minutes of treatment with VU0463271 (Δ+12±1.5 mV, p<0.001, **Fig. 5A2**). Overall, the baseline E_{GABA} (-58±3.4 mV) became more depolarized following 10 minutes of VU0463271 application (-42±5.4 mV, t(4)=6.24, p=0.0034, n=5, paired t-test, **Fig. 5A3**).

As in RT neurons, there was a time-dependent shift in the E_{GABA} of VB neurons following VU0463271 application (F(7,32)=14.38, p<0.001, n=5, one-way ANOVA, **Fig. 5B**). This shift in E_{GABA} first became clear following 2.5 minutes of treatment with VU0463271 (Δ+9±4.4 mV, p=0.04, **Fig. 5B2**). Overall, VU0463271 also depolarized the E_{GABA} of VB neurons (baseline: -69±5.6 mV; post-VU0463271: -52±8.7 mV, t(4)=7.47, p=0.0017, n=5, paired t-test, **Fig. 5B3**). In control experiments, no similar time-dependent shift in E_{GABA} was observed (data not shown), comparable to the minimal change of E_{GABA} observed in control recordings from our ChABC experiments (c.f. **Fig. 4D,E**).

As with our initial measurements of E_{GABA} in RT neurons, we again used calcium imaging to examine responses of larger populations of neurons, now preincubated with VU0463271 (10 μM) for 5 minutes prior to the start of recording. Preincubation was necessary because responses evoked by local muscimol perfusion attenuated following multiple rounds of application (data not shown). A two-minute application of muscimol now produced a more varied response, with an increase in fluorescence occurring in most RT neurons (**Fig. 5C**). In aggregate, muscimol stimulation evoked a small, but now positive, 5.5% change in median fluorescence (Interquartile range -4.9–12.4%, n=1722 cells, n=6 animals, **Fig. 5E**).

As before, mildly depolarizing VU0463271-preincubated, RT neurons with the addition of 10 mM KCl for two minutes produced a robust increase in fluorescence (22.2%, Interquartile range 16.0–31.1%, n=1732 cells, n=6 animals, Z=35.92, p<0.001, Wilcoxon rank sum test, **Fig. 5D**).

When the median calcium imaging response per animal was compared across the four conditions tested (c.f. **Figs. 2E-G** and **5C-E**), larger changes in fluorescence occurred in VU0463271-treated brain slices (15.4±2.5%, n=12) than in controls (10.5±4.6%, n=14, F(1,22)=4.76, p=0.040, two-way Aligned Rank Transform ANOVA, **Fig. 5F**). The response to a mild depolarization with KCl was very similar between control (23.1±5.9%, n=7) and VU0463271 pretreated brain slices (22.6±2.1%, n=6). Therefore, the observed treatment effect is likely due to the difference in the muscimol-induced change in fluorescence between control (-2.0±1.4%, n=7) and VU0463171 pretreated brain slices (8.2±1.9%, n=6). The impact of VU0463271 on muscimol-induced responses is consistent with the depolarizing E_{GABA} shift we observed in VU0463271-treated RT neurons.

As we have found that either inhibiting KCC2 or reducing $[A]_o$ depolarizes the E_{GABA} of RT neurons, we now sought to assess the interaction of these two mechanisms in regulating $[Cl^-]_i$. Similar to prior experiments, we applied VU0463271 during perforated patch recordings from P10-20 rats in brain slices that were either incubated in ChABC (0.4 U/ml, 37°C) for 2 hours or control slices incubated in the absence of ChABC (**Fig. 5G**). We found that the average change in E_{GABA} measured in ChABC-treated neurons (Δ+7.7±1.2 mV), across all times of

VU0463271 exposure, was larger than in control-treated neurons (Δ+5.4±0.6 mV, F(1,100)=5.66, p=0.020, n=4,8, two-way ANOVA). This observation suggests that VU0463271 and ChABC treatment act through distinct molecular mechanisms.

While VU0463271 is thought to specifically antagonize the KCCs, we sought to validate the role of KCC2 in RT neurons using an additional method. Intracellular Cs^+ is known to effectively reduce the ability of KCC2 to extrude Cl^- (Williams and Payne, 2004). Therefore, rather than the KCl-based recording pipette solution we used in prior experiments, we now utilized a CsCl-based solution. Recordings from RT neurons using the aforementioned CsCl internal solution revealed a more depolarized E_{GABA} during the five minutes of baseline recording (-54±2.9 mV, **Fig. 6A**) than found when using a KCl pipette solution (c.f. Figure 2C). The depolarized reversal potential observed using a Cs-based internal solution appears to result from the blockade of KCC2, because subsequent application of VU0463271 (10 μM) produced no significant, time-dependent shift in E_{GABA} ($F(7,31)=0.62$, $p=0.74$, n=5, one-way ANOVA, **Fig. 6A2**). Thus, VU0463271 had little overall effect on the E_{GABA} of RT neurons (-45±4.5 mV, n=5, $t(4)=1.72$, $p=0.16$, paired t-test, **Fig. 6A3**).

Similar to RT neurons, the baseline E_{GABA} of VB neurons was less hyperpolarized when recorded with a CsCl internal solution (**Fig. 6B**). Nonetheless, we observed a small, time-dependent shift in E_{GABA} in response to application of VU0463271 ($F(7,31)=16.92$, $p=0.0025$, n=5, one-way ANOVA) following 7.5 minutes of treatment (Δ+5±1.1 mV, $p=0.011$, **Fig. 6B2**). Overall, the baseline E_{GABA} (-69±1.4 mV) became more depolarized following 10 minutes of

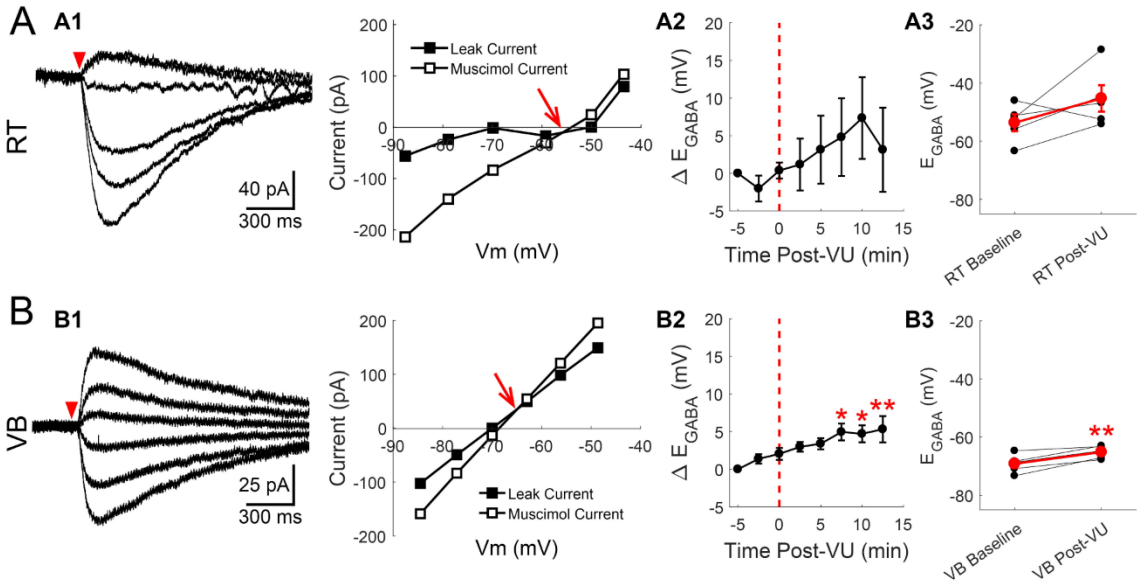

Figure 6. Cs alters $[Cl^-]_i$ homeostasis in RT neurons. Gramicidin perforated patch recordings of muscimol-induced currents from RT (***A***) and VB (***B***) neurons at various command potentials, using a CsCl-based internal solution. The leak current has been subtracted from the representative traces. ***A1***, Baseline E_{GABA} was more depolarized than in prior recordings with a KCl-based internal solution. Representative recording and current-voltage plot are shown. ***A2***, Time series revealing that CsCl-based solutions mitigated the effect of VU0463271 application in E_{GABA}, relative to KCl-based recordings (**Fig. 5**). ***A3***, Average change in E_{GABA} before and after 10 minutes of VU0463271 application. ***B1-3***. Similar measures examined in VB neurons, as described in A1-3. VU0463271 application still shifted E_{GABA} in VB neurons, although the responses were blunted. *p<0.05; **p<0.01.

VU0463271 application (-65±1.0 mV, t(4)=4.74, p=0.009, n=5, paired t-test, **Fig. 6B3**). The ability to still detect VU0463271 sensitivity may reflect a greater resiliency of VB neurons to the impact of a Cs-based internal solution on KCC2 function.

Together, these findings suggest that the KCC2 expressed in the RT nucleus still contributes significantly to maintaining a relatively low baseline $[Cl^-]_i$, which in turn supports inhibitory responses to GABAergic signaling in RT neurons. However, it remains possible that reduced KCC2 expression diminishes the capacity of RT neurons to maintain a low $[Cl^-]_i$ during intense periods of GABAergic signaling.

RT neurons have a diminished ability to recover from Cl^- loading

While RT neurons express sufficient levels of KCC2 to maintain a low basal $[Cl^-]_i$, it remains unclear how relatively limited KCC2 expression impacts the responses of RT neurons to more intense periods of GABAergic signaling. In the cortical undercut model, a reduction in KCC2 expression is not accompanied by a shift in basal E_{GABA}, although Cl^- accumulates faster in these neurons during stimulation (Jin et al., 2005). Therefore, we tested the capacity of RT neurons to resist Cl^- loading during repetitive GABAergic signaling, and the rate at which Cl^- extrusion returns E_{GABA} to basal levels once stimulation has ceased.

Cl^- loading and recovery was measured using perforated patch recordings where the membrane potential of the neuron was held at -30 mV for 500 ms, and then ramped from -100 to -10 mV over a duration of 500 ms (**Fig. 7A**). This voltage-

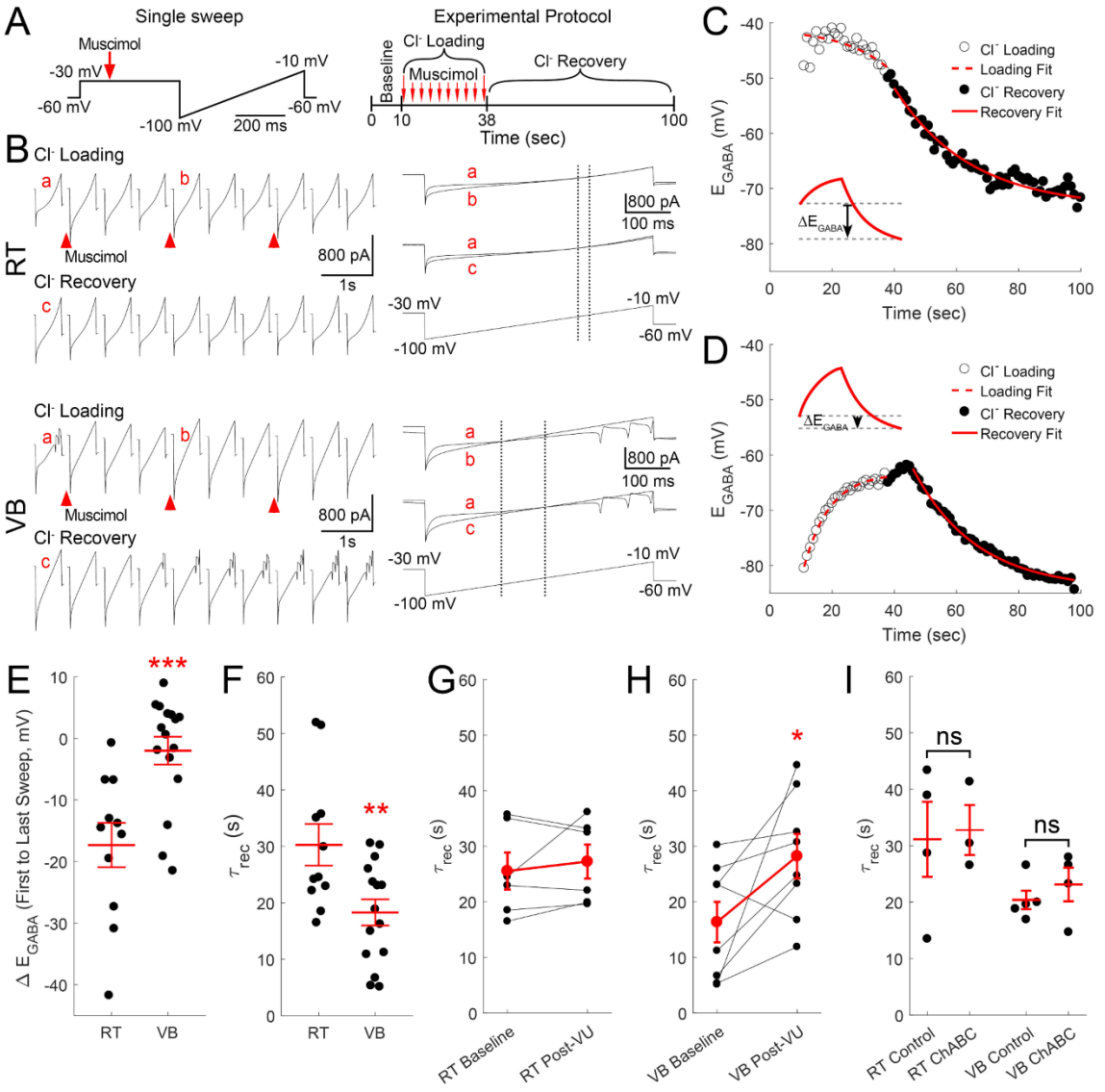

Figure 7. Recovery from Cl⁻ loading is limited in RT neurons. ***A***, Schematics of protocol for Cl⁻ loading experiments. Neurons were voltage clamped at -30 mV for 500 ms and then ramped from -100 to -10 mV over a duration of 500 ms (left). This protocol lasted one second and was repeated 100 times per cell (right). After 10 sec of baseline recording, Cl⁻ was loaded by applying 10 puffs of muscimol (20 ms, 100 µM), once every three seconds, while the neuron was held at -30 mV. ***B***, Gramicidin perforated patch recordings of RT and VB neurons during measurement of Cl⁻ loading and recovery. E_{GABA} was measured by finding the point in the voltage ramp where the membrane current responses

from before (a) and during (b) muscimol application intersected (marked by dotted line). Cl^- recovery was measured by tracking the change in E_{GABA} following the last application of muscimol (a vs. c). Single-exponential functions were fit to the shifting E_{GABA} occurring in RT (***C***) and VB (***D***) neurons to determine time constants for Cl^- loading and recovery. ***E***, The change in E_{GABA} (ΔE_{GABA}) was measured between the start of Cl^- loading and the final reading during Cl^- recovery (see inset in ***C***). This measurement indicates that chloride loading occurs rapidly in RT neurons. ***F***, The basal Cl^- recovery rate (τ_{rec}) was slower in RT than in VB neurons. The τ_{rec} in RT neurons was unaffected by a 10 minute application of VU0463271 (***G***, 10 µM), but became slower in VB neurons (***H***). ***I***, A two hour incubation in ChABC (0.4 U/ml, 37°C) did not alter the τ_{rec} of either RT or VB neurons. *p<0.05; **p<0.01; ***p<0.001.

clamp protocol was repeated once per second for 100 seconds. Following a 10 sec period of baseline recording, Cl^- loading was induced with 10, 20 ms puffs of 100 µM muscimol, occurring once every three seconds (**Fig. 7A**). Muscimol was applied while the neuron was voltage-clamped at -30 mV to promote Cl^- entry. E_{GABA} was determined by finding the voltage at which the baseline and Cl^- loading current traces intersected, following correction for the voltage drop across the series resistance (**Fig. 7B,** a vs. b). Changes in E_{GABA} associated with Cl^- recovery, also determined according to the intersection with baseline current traces (**Fig. 7B**, a vs. c), were measured for 62 sec following the end of Cl^- loading. For each neuron, the time constants for Cl^- loading (τ_{load}) and recovery (τ_{rec}) were determined by fitting the measured E_{GABA} values during the rising and falling phases, respectively, with single-exponential functions (**Fig. 7C,D**).

Our experiments revealed a clear difference in τ_{load} between RT and VB neurons, and indicated that RT neurons are particularly susceptible to Cl^- loading. In general, VB neurons displayed Cl^- loading profiles similar to those previously described (Jin et al., 2005), where the initial E_{GABA} measurement at the start of loading was comparable to the final E_{GABA} at the end of recovery (ΔE_{GABA}: -2.0±2.0 mV, n=16, **Fig. 7D,E**). The insets in **Fig. 7C-D** illustrate how this measurement was calculated. In contrast to VB neurons, RT neurons displayed a flat Cl^- loading profile and the E_{GABA} measured at the end of recovery was substantially below the initial measurement (ΔE_{GABA}: -17.3±3.3 mV, n=11, $t(25)=3.81$, $p<0.001$, **Fig. 7C,E**). This near-instantaneous τ_{load} is likely due to the initial application of muscimol

producing a rapid shift in the E_{GABA} of RT neurons, which then only returns to basal levels following a prolonged recovery; our experimental paradigm promotes large Cl^- influxes by applying muscimol while neurons are highly depolarized (see **Fig. 7A**). While we measured a τ_{load} of 8.5 ± 0.6 sec in VB neurons (data not shown), such measurements were obscured in RT neurons by the rapid dynamics of Cl^- loading.

Consistent with the limited Cl^- extrusion capacity of RT neurons revealed by our Cl^- loading measurements, the τ_{rec} for RT neurons (30.3±3.7 sec, n=11) was significantly slower than in VB neurons (18.3±2.3 sec, n=15, t(24)=2.89, p=0.008, **Fig. 7F**). As with our earlier measurements of basal E_{GABA}, we next investigated if limited KCC2 nonetheless contributes to Cl^- loading and recovery in RT neurons. Unlike in our basal E_{GABA} measurements, application of the KCC2 antagonist VU0463271 did not produce a shift in the τ_{rec} of RT neurons between baseline (25.5±3.3 sec) and 10 minute post-VU0463271 (10 µM) measurements (27.2±3.1 sec, n=6, t(5)=0.77, p=0.47, paired t-test, **Fig. 7G**). In contrast, we observed that the τ_{rec} for VB neurons became slower following 10 minutes of VU0463271 treatment (16.4±3.6 sec vs. 28.2±4.0 sec, n=8, t(7)=2.44, p=0.045, paired t-test, **Fig. 7H**).

We also assessed the impact of reducing $[A]_o$ on the speed of recovery from Cl^- loading. The τ_{rec} for RT neurons incubated in ChABC (0.4 U/ml, 37°C) for 2 hours (32.8±4.4 sec, n=3) was unchanged from control RT neurons that were incubated in the absence of ChABC (31.1±6.6 sec, n=4, t(5)=0.19, p=0.86, **Fig.**

7I). We also detected no impact of ChABC incubation on the τ_{rec} of VB neurons (20.4±3.0 sec, n=4), as compared to control VB neurons (23.1±1.6 sec, n=5, t(7)=0.86, p=0.42, **Fig. 7I**).

Collectively, these extrusion experiments indicate that RT neurons have a reduced capacity to resist activity-dependent shifts in $[Cl^-]_i$. While VU0463271 was effective in slowing the rate of Cl^- extrusion in VB neurons, we observed no VU0463271 effect on Cl^- extrusion in RT neurons. The lack of VU0463271 sensitivity on Cl^- extrusion in RT may result from low KCC2 expression; that is, KCC2 is likely overwhelmed during substantial chloride loading, thereby mitigating the effects of pharmacological blockade. Due to their lack of efficient Cl^- extrusion mechanisms, RT neurons may be more susceptible to undergoing a shift from inhibitory to excitatory GABAergic signaling during periods of repeated stimulation, such as during a seizure.

Low Cl^- extrusion may promote the spread of activity between RT neurons

Although RT neurons maintain a basal $[Cl^-]_i$ that appears to be sufficiently low to support inhibitory GABAergic signaling, reduced levels of KCC2 compromise rapid recovery from Cl^- loading in these neurons. Previous computational models have examined activity-dependent Cl^-accumulation in neurons (Jedlicka et al., 2011), and how even mildly reduced KCC2-mediated Cl^- extrusion disrupts neural coding (Doyon et al., 2015). We expanded upon this prior work by modeling the impact of reduced Cl^- extrusion on signaling within a network of RT neurons. We developed

this model primarily to understand how the RT seizure choke point behaves during low and moderate activity bouts.

Based on prior models used to study seizure activity within the RT nucleus (Sohal and Huguenard, 2003), we designed a linear network of 100 RT neurons, in which each cell projected GABAergic synapses to the eight nearest neurons (**Fig. 8A**). To approximate excitatory input to this network, we delivered repetitive, simulated depolarizing current injections to three centrally located neurons in the array (Cells 46, 51 and 56) to evoke action potentials (**Fig. 8B,C1**; e.g., Cell 51). In the example shown here, the three stimulated RT neurons generated action potentials at 30 Hz, and all RT neurons extruded Cl^- with a τ_{rec} of 32 seconds, a value comparable to our experimental results. Evoked action potentials immediately produced GABAergic currents in neurons postsynaptic to the stimulated cell (**Fig. 8C1**; e.g., Cell 53 inset). While each individual postsynaptic potential only generated a transient increase in $[Cl^-]_i$, the slow decay kinetics of IPSCs in RT neurons (Huntsman and Huguenard, 2006), coupled with slow Cl^- extrusion mechanisms in RT neurons, resulted in a fairly steady, activity-dependent, elevation in $[Cl^-]_i$. Once $[Cl^-]_i$ became sufficiently elevated, postsynaptic potentials became suprathreshold and evoked action potentials (**Fig. 8C2**; e.g., cell 53). Thus, as glutamatergic signaling was not present in our model, excitatory GABAergic signaling was sufficient to propagate activity within this simplified network.

Next, we examined how varying the τ_{rec} within our model altered the spread of activation. When the τ_{rec} was equal to 32 seconds, 30 Hz stimulation was sufficient

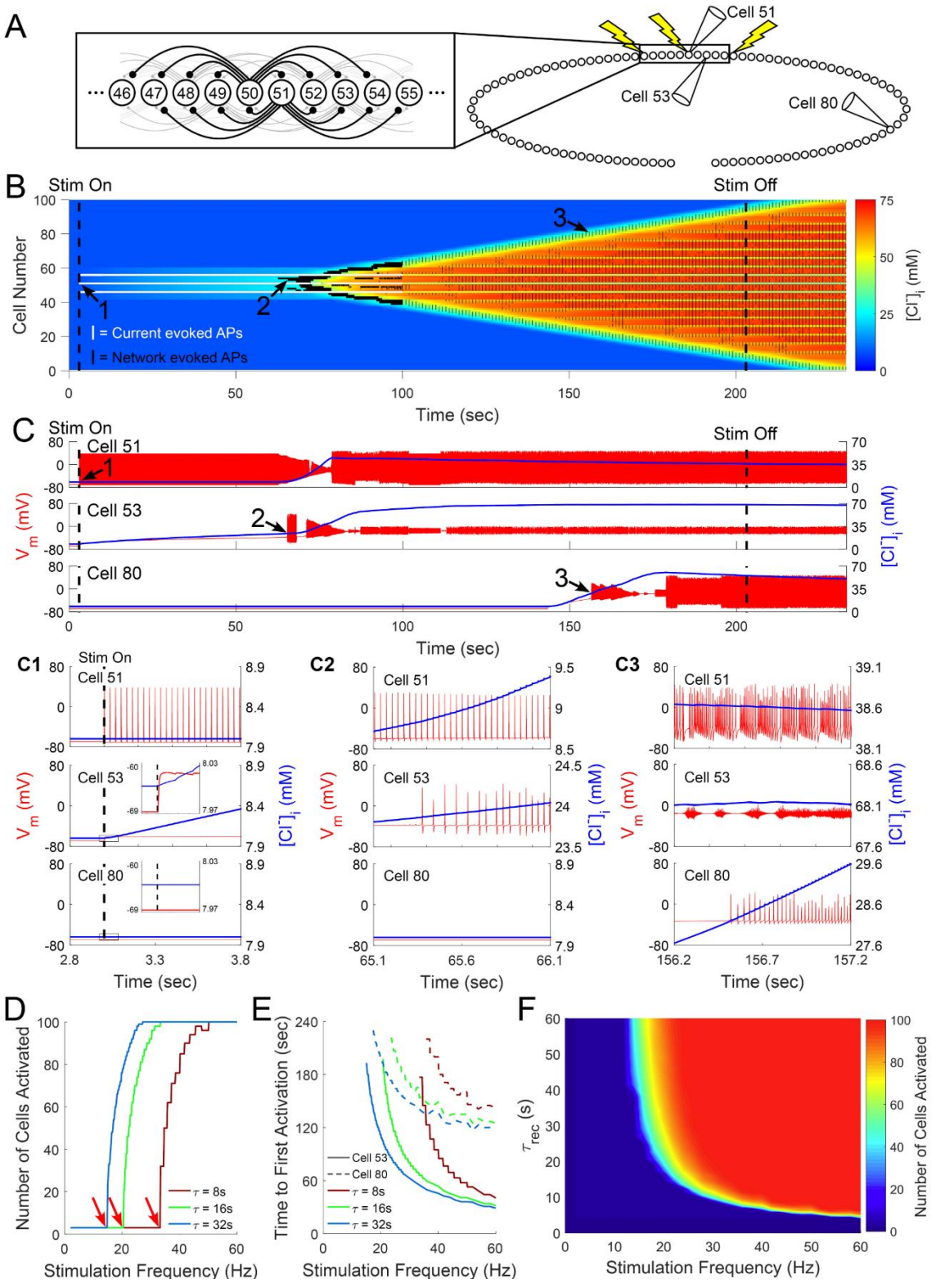
A
46
47
48
49
50
51
52
53
54
55
Cell 51
Cell 53
Cell 80
B
Stim On
Stim Off
Cell Number
1
2
3
= Current evoked APs
= Network evoked APs
Time (sec)
[Cl⁻]i (mM)
C
Stim On
Stim Off
Cell 51
Cell 53
Cell 80
Vm (mV)
[Cl⁻]i (mM)
Time (sec)
C1
C2
C3
D
Number of Cells Activated
Stimulation Frequency (Hz)
τ = 8s
τ = 16s
τ = 32s
E
Time to First Activation (sec)
Cell 53
Cell 80
F
τrec (s)
Number of Cells Activated

Figure 8. Computational modeling of $[Cl^-]_i$ dynamics in a network of RT neurons. ***A***, Network composed of a linear array of 100 RT neurons, each projecting GABAergic synapses to the eight nearest neurons. Current injections to Cells 46, 51 and 56 simulated excitatory inputs to this network. ***B***, Graphical representation of evolving $[Cl^-]_i$ within all model RT neurons over time. Action potential activity generated by individual model RT neurons is overlaid. White vertical lines indicate action potentials in neurons directly receiving current injection, while black vertical lines indicate synaptically-evoked action potentials. In a network wherein Cells 46, 51 and 56 received 30 Hz stimulation and all cells were characterized by a Cl^- recovery rate (τ_{rec}) of 32 sec, $[Cl^-]_i$ initially increased only in the neurons receiving direct GABAergic projections from the stimulated cells. Over time, however, activity propagated throughout the entire network. ***C***, Example V_m (red) and $[Cl^-]_i$ (blue) traces from Cells 51, 53 and 80 from ***B***. Cell 51 received direct, current stimulation. Cell 53 received monosynaptic input from a stimulated cell. Cell 80 was more distant from the site of stimulation. Expanded insets show the shifts in V_m and $[Cl^-]_I$ at various time points during the propagation of activity within the RT network (***C1-3***). When $[Cl^-]_i$ became sufficiently elevated for GABAergic signaling to evoke action potentials in these neurons (***C2***), the rise in $[Cl^-]_i$ began to spread throughout the network, along with an increase in the number of cells firing action potentials (***C3***). ***D***, Higher frequency stimulation increased the number of activated neurons (arrows indicate the inflection point where activation first occurs) and (***E***) decreased the time required to first evoke action potentials (Cell 53, solid lines; Cell 80, dashed lines). ***F***, Both slower τ_{rec} and more frequent stimulation were correlated with an increased likelihood of activity spreading within the RT nucleus.

to produce activation throughout the network, including neurons more distant from the sites of direct stimulation (**Fig. 8C3**; e.g., Cell 80). When we accelerated τ_{rec}, higher frequency stimulation was required to recruit activity within our network (**Fig. 8D**), as KCC2 more effectively offset Cl^- accumulation between postsynaptic potentials. In aggregate, we observed a rapid, τ_{rec}-dependent, inflection point between stimulation frequencies unable to recruit network activity and stimulation frequencies that triggered activity throughout the entire RT network (**Fig. 8D**). Increasing the stimulation frequency also effectively reduced the latency for distant neurons to begin firing action potentials (**Fig. 8E**). We examined the interplay between τ_{rec} and stimulation frequency on global RT network activity across a range of parameters (**Fig. 8F**). Across this range of parameters, only a narrow band separated conditions that activated zero neurons and all neurons in our network, suggesting a tenuous boundary between normal activity and hyperactivity. Finally, we also observed that slightly increasing the initial $[Cl^-]_i$ of the neurons in our model, comparable to the shift we observed following the reduction of $[A]_o$ with ChABC, slightly promoted the spread of activity throughout our network (data not shown).

Our model demonstrates that the limited Cl^- extrusion capability of RT neurons, largely dictated by expression of KCC2, has a considerable impact on the response of this nucleus to excitatory drive. Specifically, the model predicts that RT neurons with a τ_{rec} of 32 seconds, similar to what we measured experimentally, are more susceptible to an activity-dependent shift towards GABA-mediated

excitation than neurons with a faster τ_{rec}. This propensity for undergoing a shift from inhibitory to excitatory GABAergic signaling allows weaker stimuli to produce activation that spreads throughout the RT nucleus.

Discussion

We demonstrate that RT neurons maintain a low $[Cl^-]_i$ despite showing reduced immunoreactivity for the Cl^- transporter KCC2. The limited KCC2 in RT neurons nonetheless sustains a hyperpolarized E_{GABA}, but restricts Cl^- extrusion in response to prolonged GABAergic signaling. RT neurons are therefore susceptible to an activity-dependent shift from inhibitory to excitatory GABAergic signaling. Elevated impermeant anions surrounding RT neurons contribute modestly to E_{GABA}. Overall, these findings support the importance of Cl^- transporters and impermeant anions in regulating $[Cl^-]_i$ in the thalamus and enabling inhibitory GABAergic signaling among RT neurons.

The RT nucleus is a gatekeeper of signaling between cortical and subcortical structures (Jones, 1975; Pinault, 2004; McAlonan et al., 2008). Inhibition among RT neurons is hypothesized to prevent seizures and suppress extraneous sensory input. Regarding the former function, intra-RT inhibition is proposed to establish a seizure choke point that constrains the widespread thalamic synchrony underlying generalized seizures (Sohal and Huguenard, 2003; Paz and Huguenard, 2015; Makinson et al., 2017). Regarding the latter function, inhibitory RT signaling is proposed to focus attention by filtering extraneous sensory stimuli (Crick, 1984; McAlonan et al., 2008; Halassa et al., 2014; Wimmer et al., 2015; Wells et al.,

2016). Comprising this focusing mechanism produces sensory gating deficits. Indeed, hallucinations and delusions associated with schizophrenia are hypothesized to result from RT neuron dysfunction (Krause et al., 2003; Egerton et al., 2005; Ferrarelli and Tononi, 2011; Ahrens et al., 2015). If seizure regulation and attention gating require inhibition within the RT nucleus, then we show that they do so under tenuous circumstances.

GABAergic signaling inhibits RT neurons

Utilizing electrophysiological and calcium imaging techniques, we find that RT neuron activity is, in aggregate, inhibited by GABA. Our measured E_{GABA} for RT neurons (-62±3.0 mV) is substantially more hyperpolarized than RT action potential threshold (~-47 mV; Dreyfus et al., 2010; Muñoz and Fuentealba, 2012). As *in vivo* recordings reveal that RT neurons rest at -62 mV (Bazhenov et al., 1999), our results indicate that $GABA_A$ receptor activation clamps RT neurons at their resting membrane potential. Indeed, our calcium imaging reveals that most RT neurons respond to muscimol with minimal change in fluorescence (median $\Delta F/F$ = -2.8%, interquartile range -7.1–4.8%, see **Fig. 2G**), suggesting that $GABA_A$ receptor activation does not alter resting membrane potential. Even if RT neurons rest at -69 mV, as reported *in vitro* (Gentet and Ulrich, 2003), then $GABA_A$ receptor activation would nonetheless promote shunting inhibition (Edwards, 1990; Staley and Mody, 1992; Blaesse et al., 2009).

It remains possible that a subthreshold membrane depolarization resulting from $GABA_A$-receptor activation evokes action potentials in RT neurons. Modest

GABA-induced depolarizations may recruit low voltage-activated, T-type Ca^{2+} channels that further depolarize RT neurons towards firing threshold (Sun et al., 2012). If true, then a widespread increase in muscimol-induced GCaMP fluorescence would likely result. However, muscimol only intensified fluorescence in a few RT neurons, possibly reflecting cells initially resting at relatively hyperpolarized membrane potentials with more available T-type channels (Perez-Reyes, 2003; Dreyfus et al., 2010). Alternatively, brighter cells may have corresponded to the small subpopulation of RT neurons with a more depolarized basal E_{GABA}, reflecting the heterogeneity of distinct subpopulations known to exist within RT (Lee et al., 2007; Clemente-Perez et al., 2017).

KCC2 is an important regulator of $[Cl^-]_i$ in RT neurons

Reduced KCC2 mRNA (Kanaka et al., 2001) and protein (Barthó et al., 2004; Sun et al., 2012) in RT neurons of adult rodents predict that GABAergic signaling is excitatory. However, anatomical experiments are unable to evaluate KCC2 function. Recording E_{GABA} with the selective KCC antagonist VU0463271 reveals that even limited KCC2 in RT neurons contributes to Cl^- homeostasis. While VU0463271 has minimal off-target interactions, it does inhibit α_{1B} adrenergic receptors (Delpire et al., 2012; Sivakumaran et al., 2015). As adrenergic signaling may alter KCC2 surface stability and transporter efficacy (Mahadevan and Woodin, 2016), VU0463271 may alter $[Cl^-]_i$ via an indirect, albeit still KCC2-dependent mechanism. While VU0463271 analogues antagonize other KCCs beyond KCC2

(Delpire and Weaver, 2016), the thalamus appears to only express KCC2 (Rivera et al., 1999; Le Rouzic et al., 2006).

To validate VU0463271, we performed a subset of perforated patch recordings with a Cs-based pipette solution. While this approach prevents anionic contamination of recorded neurons, cations still diffuse through gramicidin pores and alter intracellular ionic concentrations (Myers and Haydon, 1972). While K^+ and Cs^+ ions are both substrates for Cl^- transport by KCC2, Cs^+ translocation occurs at a significantly slower rate, restricting Cl^- extrusion and effectively inhibiting KCC2 (Williams and Payne, 2004). The occlusion of a VU0463271 effect by Cs^+ indicates that both compounds impact E_{GABA} by blocking the action of KCC2. Cs-based recording solutions have previously yielded noticeably higher measurements of $[Cl^-]_i$ in RT neurons (Sun et al., 2012).

$[A]_o$ only mildly impact $[Cl^-]_i$ regulation in RT neurons

Our anatomical staining shows that CSPGs, a major source of $[A]_o$, are elevated in the RT nucleus by the second postnatal week, consistent with past investigations (Vitellaro-Zuccarello et al., 2001; Gáti et al., 2010). Regional and cell-type specific heterogeneity exists in CSPG localization (Matthews et al., 2002), and WFA preferentially labels CSPGs surrounding parvalbumin-positive interneurons (Gáti et al., 2010). Heightened WFA labeling surrounding RT neurons matches the nearly homogenous population of parvalbumin-positive interneurons in this nucleus. In contrast, the limited WFA labeling of VB neurons is attributed to

a sparse localization of CSPGs around the preterminal compartments of axons (Gáti et al., 2010).

While ChABC treatment increases $[Cl^-]_i$ in hippocampal neurons (Glykys et al., 2014a), we observed no change in the basal E_{GABA} of RT or VB neurons following a two hour incubation in ChABC. However, the E_{GABA} of ChABC treated RT neurons became more depolarized following repeated measurement. This observation is consistent with the hypothesis that $[A]_o$ can define a set point for E_{GABA}, but that other mechanisms likely provide the Cl^- flux required for the neuron to equilibrate to this new level (Delpire and Staley, 2014). Our repeated measurements of E_{GABA} involved repetitive $GABA_A$ receptor activation, which may have provided a sufficient Cl^- flux to unmask the impact of ChABC treatment. Nevertheless, while Glykys et al. (2014a) found ChABC treatment of hippocampal neurons produced a 16 mM increase in $[Cl^-]_i$, the greatest change in E_{GABA} we observed in RT neurons was only equivalent to a 4 mM increase in $[Cl^-]_i$. Utilizing a more intense ChABC treatment or a higher throughput technique to measure changes in $[Cl^-]_i$, such as Clomeleon imaging (Dzhala et al., 2012; Wimmer et al., 2015), may permit the unmasking of a greater contribution of $[A]_o$ to Cl^- homeostasis in thalamic neurons.

Slow Cl^- extrusion enhances spreading activation among RT neurons

While the steady-state E_{GABA} value measured in RT neurons supports inhibition, low KCC2 expression significantly slows Cl^- extrusion in RT neurons. Repeated $GABA_A$ receptor activation produces rapid $[Cl^-]_i$ accumulation and an associated

depolarizing GABAergic response (Staley et al., 1995; Kuner and Augustine, 2000; Jedlicka et al., 2011). Having both weaker initial GABAergic inhibition and a diminished capacity to recover from activity-dependent Cl^- influx, RT neurons appear predisposed to shift towards excitatory GABAergic signaling when repeatedly stimulated. Indeed, our computational model suggests that slow Cl^- extrusion leaves RT neurons susceptible to undergoing an inhibitory-to-excitatory shift after receiving a train of GABAergic inputs. Slower RT neuron Cl^- extrusion rates also correlate with a reduced threshold to evoke excitatory signaling and accelerate the spread of excitatory GABAergic signaling throughout the network. We hypothesize that this recapitulates the characteristic sudden onset of absence seizures (Lüttjohann and Van Luijtelaar, 2015), occurring once the inhibitory choke point formed by the RT nucleus is overwhelmed.

Years of anatomical evidence reveal the presence of GABAergic synapses onto RT neurons (Ahlsén and Lindström, 1982; Yen et al., 1985; Ohara, 1988; Cox et al., 1996), and electrophysiological studies suggest that RT neurons are functionally connected via GABAergic synapses (Zhang and Jones, 2004; Deleuze and Huguenard, 2006; Makinson et al., 2017). However, the existence of intra-RT connectivity remains debated (Landisman et al., 2002; Cruikshank et al., 2010; Hou et al., 2016). Nevertheless, the substantia nigra pars reticulata (Paré et al., 1990), globus pallidus (Nauta, 1979) and basal forebrain (Asanuma and Porter, 1990) also provide GABAergic input to RT neurons. These inputs will likewise inhibit RT neuron activity, due to the low $[Cl^-]_i$ we have measured. Regardless of the source, $GABA_A$ receptor-mediated signaling onto RT neurons modulates

rhythmic thalamic oscillations. Both local application of the $GABA_A$ antagonist bicuculline (Sanchez-Vives and McCormick, 1997) and targeted knockdown of the $GABA_A$ subunit β_3 (Huntsman et al., 1999) selectively block GABAergic signaling in the RT nucleus, without impacting other thalamic neurons. In both cases, reducing $GABA_A$ receptor-mediated inputs to RT neurons promotes absence seizure-like hypersynchronous oscillations.

Conclusions

In sum, the findings of this study demonstrate that GABAergic inhibition is tenuous within the reticular thalamic (***RT***) nucleus. Weak chloride extrusion mechanisms render RT neurons susceptible to an activity-dependent switch to GABAergic excitation. These findings have important implications for RT's proposed role as a seizure choke point for generalized epilepsies.

References

Ahlsén G, Lindström S (1982) Mutal inhibition between perigeniculate neurones. Brain Res 236:482–486.

Ahrens S, Jaramillo S, Yu K, Ghosh S, Hwang G-R, Paik R, Lai C, He M, Huang ZJ, Li B (2015) ErbB4 regulation of a thalamic reticular nucleus circuit for sensory selection. Nat Neurosci 18:104–111.

Ajmo JM, Eakin AK, Hamel MG, Gottschall PE (2008) Discordant localization of WFA reactivity and brevican/ADAMTS-derived fragment in rodent brain. BMC Neurosci 9:14.

Asanuma C, Porter LL (1990) Light and electron microscopic evidence for a GABAergic projection from the caudal basal forebrain to the thalamic reticular nucleus in rats. J Comp Neurol 302:159–172.

Bandtlow CE, Zimmermann DR (2000) Proteoglycans in the developing brain: new conceptual insights for old proteins. Physiol Rev 80:1267–1290.

Barthó P, Payne JA, Freund TF, Acsády L (2004) Differential distribution of the KCl cotransporter KCC2 in thalamic relay and reticular nuclei. Eur J Neurosci 20:965–975.

Bazhenov M, Timofeev I, Steriade M, Sejnowski TJ (1999) Self-sustained rhythmic activity in the thalamic reticular nucleus mediated by depolarizing GABA A receptor potentials. Nat Neurosci 2:168–174.

Blaesse P, Airaksinen MS, Rivera C, Kaila K (2009) Cation-chloride cotransporters and neuronal function. Neuron 61:820–838.

Bormann J, Hamill OP, Sakmann B (1987) Mechanism of anion permeation

through channels gated by glycine and gamma-aminobutyric acid in mouse cultured spinal neurones. J Physiol 385:243–286.

Cherubini E, Rovira C, Gaiarsa JL, Corradetti R, Ari Y Ben (1990) GABA mediated excitation in immature rat CA3 hippocampal neurons. Int J Dev Neurosci 8:481–490.

Clemente-Perez A, Makinson SR, Higashikubo B, Brovarney S, Cho FS, Urry A, Holden SS, Wimer M, Dávid C, Fenno LE, Acsády L, Deisseroth K, Paz JT (2017) Distinct Thalamic Reticular Cell Types Differentially Modulate Normal and Pathological Cortical Rhythms. Cell Rep 19:2130–2142.

Cox CL, Huguenard JR, Prince DA (1996) Heterogeneous axonal arborizations of rat thalamic reticular neurons in the ventrobasal nucleus. J Comp Neurol 366:416–430.

Crick F (1984) Function of the thalamic reticular complex: the searchlight hypothesis. Proc Natl Acad Sci 81:4586–4590.

Cruikshank SJ, Urabe H, Nurmikko A V, Connors BW (2010) Pathway-specific feedforward circuits between thalamus and neocortex revealed by selective optical stimulation of axons. Neuron 65:230–245.

Deleuze C, Huguenard JR (2006) Distinct electrical and chemical connectivity maps in the thalamic reticular nucleus: potential roles in synchronization and sensation. J Neurosci 26:8633–8645.

DeLorey TM, Handforth A, Anagnostaras SG, Homanics GE, Minassian BA, Asatourian A, Fanselow MS, Delgado-Escueta A, Ellison GD, Olsen RW (1998) Mice lacking the β3 subunit of the GABAA receptor have the epilepsy

phenotype and many of the behavioral characteristics of Angelman syndrome. J Neurosci 18:8505–8514.

Delpire E, Baranczak A, Waterson AG, Kim K, Kett N, Morrison RD, Daniels JS, Weaver CD, Lindsley CW (2012) Further optimization of the K-Cl cotransporter KCC2 antagonist ML077 : development of a highly selective and more potent in vitro probe. Bioorg Med Chem Lett 22:4532–4535.

Delpire E, Staley KJ (2014) Novel determinants of the neuronal Cl- concentration. J Physiol 592:4099–4114.

Delpire E, Weaver CD (2016) Challenges of Finding Novel Drugs Targeting the K-Cl Cotransporter. ACS Chem Neurosci 7:1624–1627.

Destexhe A, Bal T, Mccormick DA, Sejnowski TJ (1996) Ionic mechanisms underlying synchronized oscillations and propagating waves in a model of ferret thalamic slices. J Neurophysiol 76:2049–2070.

Donnan FG (1911) Theorie der membran gleichgewichte und membran potentiale bei vorhandernsein von nicht dialysierenden elektrolyten. Zeitschrift für Elektrochimie und Angewandlte Phys Chemie 17:572–581.

Doyon N, Prescott SA, De Koninck Y (2015) Mild KCC2 hypofunction causes inconspicuous chloride dysregulation that degrades neural coding. Front Cell Neurosci 9:1–16.

Doyon N, Vinay L, Prescott SA, De Koninck Y (2016) Chloride Regulation: A Dynamic Equilibrium Crucial for Synaptic Inhibition. Neuron 89:1157–1172.

Dreyfus FM, Tscherter A, Errington AC, Renger JJ, Shin H-S, Uebele VN, Crunelli V, Lambert RC, Leresche N (2010) Selective T-Type Calcium Channel Block

in Thalamic Neurons Reveals Channel Redundancy and Physiological Impact of ITwindow. J Neurosci 30:99–109.

Dzhala V, Valeeva G, Glykys J, Khazipov R, Staley K (2012) Traumatic Alterations in GABA Signaling Disrupt Hippocampal Network Activity in the Developing Brain. J Neurosci 32:4017–4031.

Edwards DH (1990) Mechanisms of depolarizing inhibition at the crayfish giant motor synapse. I. Electrophysiology. J Neurophysiol 64:541–550.

Egerton A, Reid L, McKerchar CE, Morris BJ, Pratt JA (2005) Impairment in perceptual attentional set-shifting following PCP administration: A rodent model of set-shifting deficits in schizophrenia. Psychopharmacology (Berl) 179:77–84.

Ferrarelli F, Tononi G (2011) The thalamic reticular nucleus and schizophrenia. Schizophr Bull 37:306–315.

Gáti G, Morawski M, Lendvai D, Jäger C, Négyessy L, Arendt T, Alpár A (2010) Distribution and classification of aggrecan-based extracellular matrix in the thalamus of the rat. J Neurosci Res 88:3257–3266.

Gentet LJ, Ulrich D (2003) Strong, reliable and precise synaptic connections between thalamic relay cells and neurones of the nucleus reticularis in juvenile rats. J Physiol 546:801–811.

Glascock JJ, Osman EY, Coady TH, Rose FF, Shababi M, Lorson CL (2011) Delivery of Therapeutic Agents Through Intracerebroventricular (ICV) and Intravenous (IV) Injection in Mice. J Vis Exp:1–4.

Glykys J, Dzhala V, Egawa K, Balena T, Saponjian Y, Kuchibhotla K V, Bacskai

BJ, Kahle KT, Zeuthen T, Staley KJ (2014a) Local impermeant anions establish the neuronal chloride concentration. Science 343:670–675.

Glykys J, Dzhala VI, Egawa K, Balena T, Saponjian Y, Kuchibhotla K V, Bacskai BJ, Kahle KT, Zeuthen T, Staley KJ (2014b) Response to Comments on “Local impermeant anions establish the neuronal chloride concentration.” Science 345:1130–d.

Halassa MM, Chen Z, Wimmer RD, Brunetti PM, Zhao S, Zikopoulos B, Wang F, Brown EN, Wilson MA (2014) State-dependent architecture of thalamic reticular subnetworks. Cell 158:808–821.

Hines ML, Carnevale NT (1997) The NEURON simulation environment. Neural Comput 9:1179–1209.

Homanics GE, DeLorey TM, Firestone LL, Quinlan JJ, Handforth A, Harrison NL, Krasowski MD, Rick CEM, Korpi ER, Mäkelä R, Brilliant MH, Hagiwara N, Ferguson C, Snyder K, Olsen RW (1997) Mice devoid of γ-aminobutyrate type A receptor β3 subunit have epilepsy, cleft palate, and hypersensitive behavior. Proc Natl Acad Sci 94:4143–4148.

Horii-Hayashi N, Sasagawa T, Matsunaga W, Nishi M (2015) Development and Structural Variety of the Chondroitin Sulfate Proteoglycans-Contained Extracellular Matrix in the Mouse Brain. Neural Plast 2015.

Hou G, Smith AG, Zhang Z-W (2016) Lack of Intrinsic GABAergic Connections in the Thalamic Reticular Nucleus of the Mouse. J Neurosci 36:7246–7252.

Huntsman MM, Huguenard JR (2006) Fast IPSCs in rat thalamic reticular nucleus require the GABAA receptor beta1 subunit. J Physiol 572:459–475.

Huntsman MM, Porcello DM, Homanics GE, DeLorey TM, Huguenard JR (1999) Reciprocal inhibitory connections and network synchrony in the mammalian thalamus. Science 283:541–543.

Jedlicka P, Deller T, Gutkin BS, Backus KH (2011) Activity-dependent intracellular chloride accumulation and diffusion controls GABA(A) receptor-mediated synaptic transmission. Hippocampus 21:885–898.

Jin X, Huguenard JR, Prince DA (2005) Impaired Cl- Extrusion in Layer V Pyramidal Neurons of Chronically Injured Epileptogenic Neocortex. J Neurophysiol 93:2117–2126.

Jones EG (1975) Some aspects of the organization of the thalamic reticular complex. J Comp Neurol 162:285–308.

Jones EG (2007) The Thalamus, 2nd ed. Cambridge: Cambridge University Press.

Kaila K, Price TJ, Payne JA, Puskarjov M, Voipio J (2014) Cation-chloride cotransporters in neuronal development, plasticity and disease. Nat Rev Neurosci 15:637–654.

Kanaka C, Ohno K, Okabe A, Kuriyama K, Itoh T, Fukuda A, Sato K (2001) The differential expression patterns of messenger RNAs encoding K-Cl cotransporters (KCC1,2) and Na-K-2Cl cotransporter (NKCC1) in the rat nervous system. Neuroscience 104:933–946.

Krause M, Hoffmann WE, Hajós M (2003) Auditory sensory gating in hippocampus and reticular thalamic neurons in anesthetized rats. Biol Psychiatry 53:244–253.

Kuner T, Augustine GJ (2000) A genetically encoded ratiometric indicator for

chloride: capturing chloride transients in cultured hippocampal neurons. Neuron 27:447–459.

Landisman CE, Long MA, Beierlein M, Deans MR, Paul DL, Connors BW (2002) Electrical synapses in the thalamic reticular nucleus. J Neurosci 22:1002–1009.

Le Rouzic P, Ivanov TR, Stanley PJ, Baudoin FMH, Chan F, Pinteaux E, Brown PD, Luckman SM (2006) KCC3 and KCC4 expression in rat adult forebrain. Brain Res 1110:39–45.

Lee S-H, Govindaiah G, Cox CL (2007) Heterogeneity of firing properties among rat thalamic reticular nucleus neurons. J Physiol 582:195–208.

Luhmann HJ, Kirischuk S, Kilb W (2014) Comment on “Local impermeant anions establish the neuronal chloride concentration.” Science 345:1130–c.

Lüttjohann A, Van Luijtelaar G (2015) Dynamics of networks during absence seizure’s on- and offset in rodents and man. Front Physiol 6:1–17.

Mahadevan V, Woodin MA (2016) Regulation of neuronal chloride homeostasis by neuromodulators. J Physiol 10:1–13.

Makinson CD, Tanaka BS, Sorokin JM, Wong JC, Christian CA, Goldin AL, Escayg A, Huguenard JR (2017) Regulation of Thalamic and Cortical Network Synchrony by Scn8a. Neuron 93:1165–1179.e6.

Matthews RT, Kelly GM, Zerillo CA, Gray G, Tiemeyer M, Hockfield S (2002) Aggrecan glycoforms contribute to the molecular heterogeneity of perineuronal nets. J Neurosci 22:7536–7547.

McAlonan K, Cavanaugh J, Wurtz RH (2008) Guarding the gateway to cortex with

attention in visual thalamus. Nature 456:391–394.

McCormick DA, Prince DA (1986) Acetylcholine induces burst firing in thalamic reticular neurones by activating a potassium conductance. Nature 319:402–405.

Muñoz F, Fuentealba P (2012) Dynamics of action potential initiation in the GABAergic thalamic reticular nucleus in vivo. PLoS One 7:e30154.

Myers VB, Haydon DA (1972) Ion transfer across lipid membranes in the presence of gramicidin A: II. The ion selectivity. Biochim Biophys Acta 274:313–322.

Nauta HJW (1979) Projections of the pallidal complex: An autoradiographic study in the cat. Neuroscience 4:1853–1873.

Ohara PT (1988) Synaptic organization of the thalamic reticular nucleus. J Electron Microsc Tech 10:283–292.

Paré D, Hazrati LN, Parent A, Steriade M (1990) Substantia nigra pars reticulata projects to the reticular thalamic nucleus of the cat: a morphological and electrophysiological study. Brain Res 535:139–146.

Payne JA, Stevenson TJ, Donaldson LF (1996) Molecular characterization of a putative K-Cl cotransporter in rat brain: a neuronal-specific isoform. J Biol Chem 271:16245–16252.

Paz JT, Huguenard JR (2015) Microcircuits and their interactions in epilepsy: is the focus out of focus? Nat Neurosci 18:351–359.

Perez-Reyes E (2003) Molecular Physiology of Low-Voltage-Activated T-type Calcium Channels. Physiol Rev 83:117–161.

Pinault D (2004) The thalamic reticular nucleus: structure, function and concept.

Brain Res Rev 46:1–31.

Pinault D, Smith Y, Deschênes M (1997) Dendrodendritic and axoaxonic synapses in the thalamic reticular nucleus of the adult rat. J Neurosci 17:3215–3233.

Rivera C, Voipio J, Payne JA, Ruusuvuori E, Lahtinen H, Lamsa K, Pirvola U, Saarma M, Kaila K (1999) The K+/Cl- co-transporter KCC2 renders GABA hyperpolarizing during neuronal maturation. Nature 397:251–255.

Rohrbough J, Spitzer NC (1996) Regulation of intracellular Cl- levels by Na(+)-dependent Cl- cotransport distinguishes depolarizing from hyperpolarizing GABAA receptor-mediated responses in spinal neurons. J Neurosci 16:82–91.

Sanchez-Vives M V, McCormick DA (1997) Functional properties of perigeniculate inhibition of dorsal lateral geniculate nucleus thalamocortical neurons in vitro. J Neurosci 17:8880–8893.

Sivakumaran S, Cardarelli RA, Maguire J, Kelley MR, Silayeva L, Morrow DH, Mukherjee J, Moore YE, Mather RJ, Duggan ME, Brandon NJ, Dunlop J, Zicha S, Moss SJ, Deeb TZ (2015) Selective Inhibition of KCC2 Leads to Hyperexcitability and Epileptiform Discharges in Hippocampal Slices and In Vivo. J Neurosci 35:8291–8296.

Sohal VS, Huguenard JR (2003) Inhibitory interconnections control burst pattern and emergent network synchrony in reticular thalamus. J Neurosci 23:8978–8988.

Staley K, Smith R (2001) A new form of feedback at the GABA(A) receptor. Nat Neurosci 4:674–676.

Staley KJ, Mody I (1992) Shunting of excitatory input to dentate gyrus granule cells by a depolarizing GABAA receptor-mediated postsynaptic conductance. J Neurophysiol 68:197–212.

Staley KJ, Soldo BL, Proctor WR (1995) Ionic Mechanisms of Neuronal Excitation by Inhibitory GABAA Receptors. Science 269:977–981.

Sun Y-G, Wu C-S, Renger JJ, Uebele VN, Lu H-C, Beierlein M (2012) GABAergic synaptic transmission triggers action potentials in thalamic reticular nucleus neurons. J Neurosci 32:7782–7790.

Ting JT, Daigle TL, Chen Q, Feng G (2014) Acute brain slice methods for adult and aging animals: application of targeted patch clamp analysis and optogenetics. In: Patch-Clamp Methods and Protocols, 2nd ed. (Martina M, Taverna S, eds), pp 221–242 Methods in Molecular Biology. New York, NY: Springer New York.

Ulrich D, Huguenard JR (1997) Nucleus-specific chloride homeostasis in rat thalamus. J Neurosci 17:2348–2354.

Vitellaro-Zuccarello L, Meroni A, Amadeo A, De Biasi S (2001) Chondroitin sulfate proteoglycans in the rat thalamus: Expression during postnatal development and correlation with calcium-binding proteins in adults. Cell Tissue Res 306:15–26.

Voipio J, Boron WF, Jones SW, Hopfer U, Payne JA, Kaila K (2014) Comment on “Local impermeant anions establish the neuronal chloride concentration.” Science 345:1130–b.

Wells MF, Wimmer RD, Schmitt LI, Feng G, Halassa MM (2016) Thalamic reticular

impairment underlies attention deficit in Ptchd1(Y/-) mice. Nature 532:58–63.

Williams JR, Payne JA (2004) Cation transport by the neuronal K(+)-Cl(-) cotransporter KCC2: thermodynamics and kinetics of alternate transport modes. Am J Physiol Cell Physiol 287:C919–C931.

Wimmer RD, Schmitt LI, Davidson TJ, Nakajima M, Deisseroth K, Halassa MM (2015) Thalamic control of sensory selection in divided attention. Nature 526:705–709.

Wobbrock JO, Findlater L, Gergle D, Higgins JJ (2011) The aligned rank transform for nonparametric factorial analyses using only ANOVA procedures. In: Proceedings of the ACM Conference on Human Factors in Computing Systems (CHI ‘11). Vancouver, British Columbia (May 7-12, 2011), pp 143–146. New York: ACM.

Wong CGT, Bottiglieri T, Snead OC (2003) GABA, gamma-hydroxybutyric acid, and neurological disease. Ann Neurol 54:S3–S12.

Yamagata T, Saito H, Habuchi O, Suzuki S (1968) Purification and Properties and Chondrosulfatases ” of Bacterial Chondroitinases. J Biol Chem 243:1523–1535.

Yen CT, Conley M, Hendry SHC, Jones EG (1985) The morphology of physiologically identified GABAergic neurons in the somatic sensory part of the thalamic reticular nucleus in the cat. J Neurosci 5:2254–2268.

Zhang L, Jones EG (2004) Corticothalamic inhibition in the thalamic reticular nucleus. J Neurophysiol 91:759–766.

Chapter 3: Chloride regulation in the thalamus of WAG/Rij rats

Peter M. Klein

Ashley J. Mason

Mark P. Beenhakker

PMK designed all experiments with the assistance of MPB. PMK performed all research except that contributed by AJM (Figs. 1 and 2). PMK analyzed all data with guidance from MPB, and assistance from AJM (Figs. 1 and 2). PMK wrote the manuscript in consultation with MPB.

Abstract

Absence seizures are thought to occur when the seizure choke point formed by inhibitory GABAergic signaling among reticular thalamic (***RT***) neurons is disrupted. The Cl^- transporter KCC2 and extracellular impermeant anions ($[A]_o$) present in the extracellular matrix allow RT neurons to maintain sufficiently low intracellular Cl^- concentrations ($[Cl^-]_i$) to maintain inhibitory responses to GABAergic signaling under basal conditions. We find that expression of both KCC2 and $[A]_o$ is reduced in RT neurons of the seizure-prone WAG/Rij strain of rats relative to wild-type animals. We examine the possibility of modulating spontaneous seizure frequency in WAG/Rij rats by pharmacologically altering Cl^- handling in RT neurons, but we do not observe any impact with our current experimental paradigm. We also validate the use of chloride imaging to observe shifting $[Cl^-]_i$ in RT neurons, which could be applied to future *in vivo* measurements of the Cl^- dynamics that accompany absence seizures. Our results suggest that absence seizures in WAG/Rij rats may be facilitated by a diminished capacity of RT neurons to maintain low $[Cl^-]_i$ relative in wild-type animals.

Introduction

Inhibitory GABAergic signaling among reticular thalamic (***RT***) neurons is thought to form a critical seizure choke point that normally prevents the propagation of seizures by the thalamus (Sohal and Huguenard, 2003; Paz and Huguenard, 2015). Disrupting $GABA_A$ receptor-mediated connectivity among RT neurons is sufficient to increase thalamic excitability (Huntsman et al., 1999; Makinson et al.,

2017) and increase the occurrence of spontaneous seizures (Homanics et al., 1997; DeLorey et al., 1998).

The influx of chloride (***Cl***$^-$) through $GABA_A$ receptors typically mediates inhibitory neurotransmission, yet sufficiently elevated intracellular Cl^- concentrations (***[Cl$^-$]$_i$***) can promote Cl^- efflux and neuronal depolarization (Cherubini et al., 1990; Rohrbough and Spitzer, 1996). Low $[Cl^-]_i$ in adult neurons is maintained both through active extrusion by the K^+-Cl^- cotransporter KCC2 (Payne et al., 1996; Rivera et al., 1999) and through the forces exerted by negatively charged, fixed macromolecules known as *impermeant anions* (Delpire and Staley, 2014; Glykys et al., 2014a).

We have previously observed that although KCC2 expression is low in the RT nucleus throughout development, RT neurons nonetheless maintain a low basal $[Cl^-]_i$ that supports inhibitory responses to GABAergic signaling (Klein et al., 2018). The reduced levels of KCC2 expressed in RT neurons, and to a lesser extent the presence of elevated levels of extracellular impermeant anions (***[A]$_o$***), enable RT neurons to keep $[Cl^-]_i$ low during periods of moderate activity. However, the reduced KCC2-mediated Cl^- extrusion capacity of RT neurons is easily overwhelmed during repeated activation, weakening the capacity of inhibitory signaling within the RT choke point to prevent seizures.

Our prior findings relating the tenuous nature of inhibitory GABAergic signaling among RT neurons to the susceptibility of the RT seizure choke point to breakdown are largely based on single cell electrophysiology and computational

modeling. What remains unknown is how ineffectual Cl^- regulation in RT neurons impacts the generation of seizures in intact animals.

The WAG/Rij inbreed strain of rats has long been used as a genetic model of absence epilepsy (van Luijtelaar and Coenen, 1986; Coenen and Van Luijtelaar, 1987). While absence seizures in WAG/Rij rats are likely initiated in the perioral region of the somatosensory cortex, activity rapidly spreads throughout the brain by recruiting the rhythm-generating circuitry of the thalamus (Meeren et al., 2002). The exact mechanisms by which such activity rapidly spreads in WAG/Rij rats remains unclear.

In the present study, we investigate $[Cl^-]_i$ regulation in RT neurons of WAG/Rij rats and whether altering Cl^- handling in RT neurons is sufficient to modify the rate at which seizures occur. Using immunohistochemistry, we find that KCC2 expression in the RT nucleus of adult WAG/Rij is lower than wild-type Sprague Dawley rats. Expression of $[A]_o$ is also diminished in some regions of the RT nucleus in adult WAG/Rij rats. However, we did not observe any impact of pharmacologically altering thalamic $[A]_o$ levels or KCC2 function on the frequency of absence seizures in WAG/Rij rats. We also demonstrate that chloride imaging can be used to observe shifts in the $[Cl^-]_i$ of RT neurons, which could potentially be applied to *in vivo* measurements of the Cl^- dynamics that accompany absence seizures.

Methods

Subjects. WAG/Rij rats were obtained from a breeding colony established at the University of Virginia from two original breeding pairs imported from the Netherlands. Wild type Sprague-Dawley rats (***SD***, Charles River Laboratories) were used as a control strain and rats of either sex were utilized in these experiments. Floxed SuperClomeleon mice (*Superclm1-loxP*; a gift obtained from Kevin Staley, Massachusetts General Hospital, Boston, MA) were mated with *Vgat-cre* mice (The Jackson Laboratory) to produce conditional expression of SuperClomeleon in GABAergic neurons. All experiments were approved by the Institutional Care and Use Committee at the University of Virginia (Charlottesville, VA), in accordance with the National Institutes of Health guidelines.

Slice preparation. P10-20 SuperClomeleon mice were deeply anesthetized with pentobarbital and then transcardially perfused with an ice-cold protective recovery solution containing (in mM): 92 NMDG, 26 $NaHCO_3$, 25 glucose, 20 HEPES, 10 $MgSO_4$, 5 Na-ascorbate, 3 Na-pyruvate, 2.5 KCl, 2 thiourea, 1.25 NaH_2PO_4, 0.5 $CaCl_2$, titrated to a pH of 7.3-7.4 with HCl (Ting et al., 2014). Horizontal slices (250 µm) containing the thalamus were cut in ice-cold protective recovery solution using a vibratome (VT1200, Leica Biosystems). Slices were trimmed to remove the hippocampus and cortex, and then transferred to protective recovery solution maintained at 32-34°C for 12 minutes. Brain slices were kept in room temperature aCSF consisting of (in mM) 126 NaCl, 26 $NaHCO_3$, 10 glucose, 2.5 KCl, 2 $CaCl_2$, 1.25 NaH_2PO_4, 1 $MgSO_4$. All solutions were equilibrated with 95% O_2/5% CO_2.

Chloride imaging. Chloride imaging of acute brain slices from P10-20 SuperClomeleon mice was performed in a submerged chamber, with slices situated on nylon netting and perfused with warm (31-33°C) oxygenated aCSF at 2.5 ml/min. All experiments were performed in the presence of kynurenic acid (3 mM) and CGP 55845 (100 nM) to block AMPA, NMDA and $GABA_B$ receptors, and TTX (1 µM) to block sodium channel activation. Thalamic neurons were visualized using a Zeiss Axio Examiner.A1 microscope (Zeiss Microscopy) and an sCMOS camera (ORCA-Flash4.0, Hamamatsu). Illumination was provided by a DG-4 arc lamp (Sutter) using a 440 ± 20 nm bandpass excitation filter. A dichroic mirror (458 nm cutoff) passed emitted light that was bandpass filtered at 485 ± 10 nm for CFP or 535 ± 11 nm for YFP emission. Emission filters were housed in a filter wheel (LB10, Sutter) to allow for rapid switching. Images were acquired with HCImage software (Hamamatsu) using a 400 ms exposure for both CFP and YFP signal, with each composite frame captured at 0.1 Hz using a 40x/NA1.0 lens. Background signal was individually subtracted from both the CFP and YFP images, and the ratio of YFP/CFP fluorescence intensity (***R***) was calculated within regions of interest that were drawn around identifiable cell bodies. Following a 10 minute period of baseline recording, the KCC2 antagonist VU0463271 (10 µM) was bath applied to a portion of SuperClomeleon brain slices. Images were analyzed off-line, using custom written scripts in MATLAB to measure changes over time in the YFP/CFP ratio within the user defined ROIs.

EEG recordings. P160-200 WAG/Rij rats were stereotaxically implanted with three stainless-steel, supradural electrodes. Two electrodes recorded bilateral cortical activity and the third was a cerebellar reference electrode. A 22-gauge guide cannula (Plastics One) was placed above the right RT nucleus (-2.6 mm anteroposterior, 3.4 mm mediolateral, -5.0 mm dorsoventral of bregma). Following at least one week of recovery from electrode implantation surgery, video-EEG recordings commenced using a differential amplifier (A-M Systems) with the signal digitized (AD Instruments) at 200 Hz. Rats were connected to the amplifier via a flexible electrical cable containing a 4-channel unity gain operational-amplification head stage to eliminate noise from cable movement, which then passed through an electrical commutator (Dragonfly). During EEG recordings a 28-gauge infusion cannula was placed into the guide cannula, where it extended an additional 1 mm ventrally into the RT nucleus. Tubing connected to the infusion cannula passed through a fluid swivel (Instech) prior to reaching a CMA 4004 syringe pump (Harvard Apparatus). On each day of a seven day series of experiments, EEG recording began an hour prior to the start of the 12 hour dark cycle. After four hours of baseline recording, 2 µl of either drug or vehicle solution was injected into the RT nucleus via the infusion cannula at 500 nl/min. EEG recordings were restarted every 24 hours after all infusion tubing was flushed with water and then loaded with a different solution. The order in which drug or vehicle injections occurred was randomized and performed by double-blinded experimenters. EEG recordings were scored prior to unblinding for spontaneous seizures, characterized by 5-9 Hz

spike-wave discharges lasting longer than 3 seconds and with amplitudes at least two times greater than baseline activity.

Drugs and solutions. 10 mM stock of VU0463271 (N-Cyclopropyl-N-(4-methyl-2-thiazolyl)-2-[(6-phenyl-3-pyridazinyl)thio]acetamide, Bio-techne) and 40 mM stock of CLP257 ((5Z)-5-[(4-Fluoro-2-hydroxyphenyl)methylene]-2-(tetrahydro-1-(2H)-pyridazinyl)-4(5H)-thiazolone, Bio-techne) were prepared in DMSO. Bumetanide (3-butylamino-4-phenoxy-5-sulfamoylbenzoic acid, Sigma Aldrich) was dissolved to 25 mM in ethanol. A 50 U/ml stock of Chondroitinase ABC (***ChABC***, Sigma Aldrich) was made in 0.1% BSA. For SuperClomeleon imaging, VU0463271 was diluted to 10 µM in aCSF. Compounds for EEG experiments were dissolved to a final concentration in either 0.9% NaCl (VU0463271, 25 µM; CLP257, 100 µM; bumetanide, 25 µM) or ChABC buffer (50 mM Tris, 60 mM sodium acetate 0.02% BSA, pH 8.0; ChABC, 25 U/ml). Vehicle injections consisted of buffer and solvent pairings matched to those used in drug infusions.

Histochemistry. At P20 and 150, SD and WAG/Rij rats were deeply anesthetized with pentobarbital prior to being transcardially perfused with PBS, followed by ice-cold 4% PFA in PBS (both pH 7.4). Brains were post-fixed overnight in 4% PFA at 4°C. Horizontal sections (40 µm) containing the thalamus were obtained using a vibratome (VT1000S, Leica Biosystems). Free-floating sections were washed in PBS and then treated with 0.1% sodium borohydride in PBS for 15 minutes to reduce autofluorescence. Sections were washed with PBS, blocked with 2%

normal goat serum and Fab fragment of goat anti-mouse IgG (1:500, Jackson ImmunoResearch) in PBS for 4 hours at room temperature, and then washed with PBS. Sections were incubated overnight at 4°C with combined primary antibodies for either KCC2 and parvalbumin (rabbit anti-KCC2, 1:500, EMD Millipore; mouse anti-parvalbumin, 1:2000, Sigma Aldrich), or parvalbumin and fluorescein labeled Wisteria floribunda agglutinin (1:2000, Vector Laboratories) in PBS with 1% normal goat serum. Sections were washed in PBS and then incubated overnight at 4°C with appropriate combinations of secondary antibodies (donkey α-mouse AF488 and donkey α-rabbit Cy3 for KCC2 labeling, donkey α-mouse Cy3 for WFA labeling; all 1:200 in PBS with 1% normal goat serum, Jackson ImmunoResearch). Sections were washed in PBS and mounted with Vectashield (Vector Laboratories).

Previous studies have evaluated the specificity of the KCC2 antibody (rabbit anti-KCC2, EMD Millipore, 07-432) we utilized for immunohistochemistry experiments (Williams et al., 1999; Stil et al., 2011; Wang and Sun, 2012). Western blots of rat brain lysates with the same antibody produce a strong band as expected at ~140 kDa and an unexpected weak band at ~250 kDa, which are eliminated by preabsorption with a control peptide (Williams et al., 1999; Wang and Sun, 2012). Complete knock-out of KCC2 expression is lethal at birth, limiting the ability to validate antibody specificity in negative controls. However, the KCC2b isoform of KCC2 accounts for >80% of all neuron-specific expression, and mice expressing only KCC2a display a corresponding reduction of KCC2 labeling in western blot and immunohistochemistry assays (Stil et al., 2011). Additionally, the

general brain expression pattern of KCC2 we observe is consistent with prior reports (Kanaka et al., 2001; Barthó et al., 2004; Sun et al., 2012).

All images were obtained with a Neurolucida system (MicroBrightfield) with an Axioskop microscope driven stage and an AxioCam MRc camera (Zeiss Microscopy). All staining and imaging was performed in batches where a set of sections representing all age/sex/strain groups were processed simultaneously. This allowed for us to control for between experiment variability in measured labeling. Images were analyzed using custom written scripts in MATLAB, which allowed for evaluation by two independent, blinded, investigators.

Experimental design and statistical analysis. Where possible in this study, measurements of the ventrobasal (***VB***) thalamic nuclei were used as controls for observations from RT neurons. All histochemical experiments were performed in brain slices from 4 rats (2 male, 2 female; both hemispheres from ~3 slices per animal were analyzed). For EEG experiments, drug-induced effects were always compared against baseline recordings in the same animal. Each recording of the impact of a drug infusion on seizure activity represents a trial in a unique subject (2 male, 2 female). Individual rats received drug or vehicle infusions in a randomized order determined by a blinded investigator. For SuperClomeleon imaging experiments, brain slices from the same subject (2 male, 1 female) were in some instances utilized for both control and drug application recordings. All changes in SuperClomeleon signal were compared against the initial baseline activity within each recorded brain slice.

All statistical tests were performed in MATLAB. Unless noted, statistical tests to determine the significance of differences between groups were performed using unpaired Student's t-tests. When utilized, ANOVA tests were followed by a *post hoc* Tukey's HSD analysis. Group measures are presented as mean ± SEM. The threshold for differences to be considered significant was set at $p<0.05$.

Results

The aim of our study was to determine if altering the regulation of $[Cl^-]_i$ in RT neurons is sufficient to modulate the occurrence of spontaneous absence seizures. We have used the WAG/Rij rat genetic model of absence epilepsy to explore the link between RT neuron Cl^- regulation and absence seizure generation. We used anatomical approaches to determine if KCC2 and extracellular impermeant anion expression differs between WAG/Rij and wild-type Sprague Dawley rats. We also combined EEG recordings from WAG/Rij rats with direct thalamic infusion of modulators of $[Cl^-]_i$ to observe whether seizure occurrence was altered. Finally, we validated the use of chloride imaging to observe alterations in the $[Cl^-]_i$ of RT neurons. Altogether, our results provide insight into the ability of GABAergic signaling among RT neurons to form a critical seizure choke point.

KCC2 expression is similarly low in the RT nucleus of SD and WAG/Rij rats

We have previously demonstrated that while expression of the Cl^- transporter KCC2 is low in the thalamus of neonatal (i.e. P5) SD rats, KCC2 expression increases as the rats continue to age towards adolescence (i.e. P40) (Klein et al.,

2018). However, KCC2 expression is consistently lower in RT neurons than in VB neurons throughout early development. In the current study, we investigate the interaction between thalamic Cl^- regulation and seizure activity using the WAG/Rij genetic model of absence epilepsy. As WAG/Rij rats do not regularly experience absence seizures until after P100 (Coenen and Van Luijtelaar, 1987), we now examine KCC2 expression in P150 rats. We additionally measure KCC2 expression in P20 WAG/Rij rats, which corresponds to our prior electrophysiological studies on KCC2 function in RT neurons of SD rats (Klein et al., 2018).

We observed a broadly similar pattern of KCC2 expression in the brains of WAG/Rij and SD rats at P20 and P150, with noticeably reduced levels of KCC2 in the RT nucleus relative to surrounding structures (**Fig. 1A**). To control for experimental variability, we concurrently performed immunohistochemistry on sets of brain slices representing both ages and strains. Across both strains and regions of the thalamus, KCC2 increased with age from P20 (38.8±1.9 A.U.) to P150 (43.6±1.6 A.U.; $F(1,1,151)=4.72$, $p=0.031$, $n=4$, three-way ANOVA; **Fig. 1B**). However, we found that across both ages and strains KCC2 expression was consistently lower in the RT nucleus (35.7±1.1 A.U.) than in VB neurons (46.8±1.4 A.U.; $F(1,1,151)=40.34$, $p<0.0001$, $n=4$, three-way ANOVA). Interestingly, at P150 KCC2 expression throughout the thalamus was lower in WAG/Rij rats (39.3±1.6 A.U.) than in SD rats (48.6±2.6 A.U.; $F(1,1,151)=27.0$, $p=0.0006$, $n=4$, three-way ANOVA). Our prior research indicates that even low levels of KCC2 can

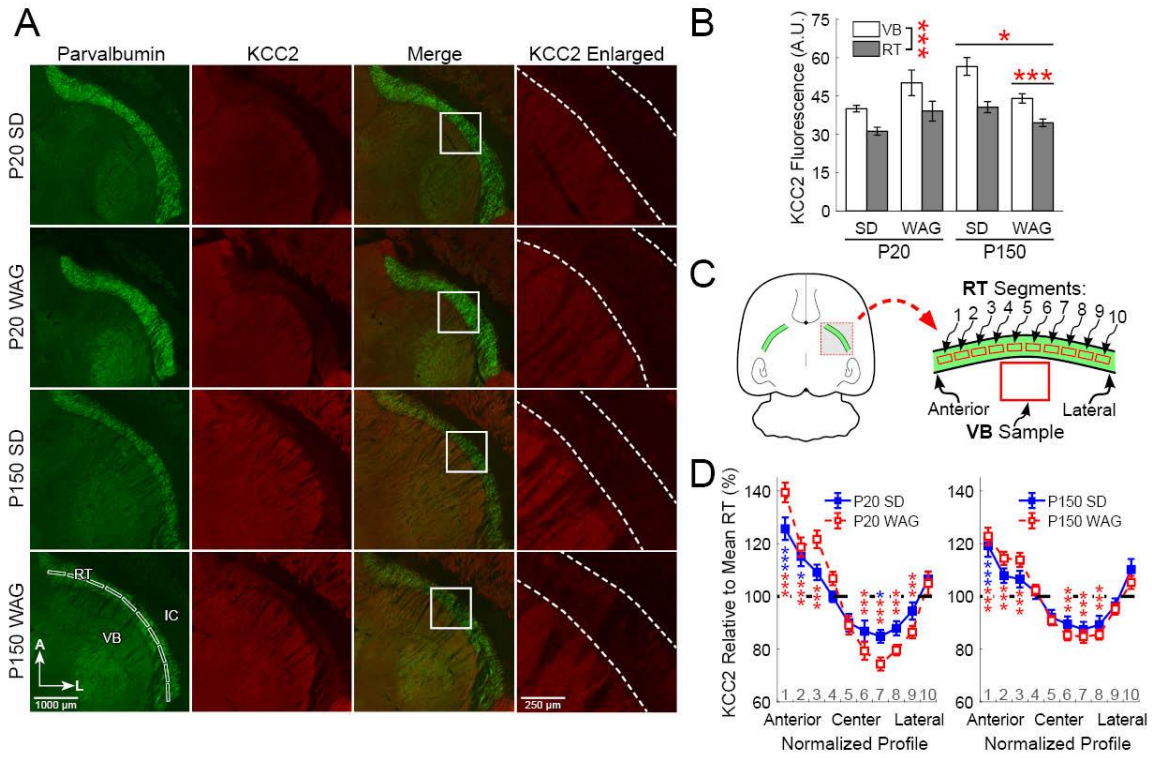

Figure 1. KCC2 expression is low in RT neurons of WAG/Rij and SD rats. ***A***, Immunofluorescence of parvalbumin (green) and KCC2 (red) in horizontal sections of WAG/Rij and SD rat thalamus at different time points. All images are oriented with the anterior (A) aspect of the thalamus towards the top, the lateral (L) aspect towards the right and the internal capsule (IC) towards the upper right corner of the image. Dotted lines indicate the boundaries of the RT nucleus in the enlarged images. ***B***, KCC2 immunofluorescence increased with age in both strains. KCC2 labeling was consistently lower in the RT nucleus, relative to VB, across all groups. ***C***, Schematic of methodology for measuring regional variability in KCC2 intensity across segments of the RT nucleus. Intensity of KCC2 labeling was measured in an ROI, subdivided into 10 segments, that extended from the anterior to the lateral extent of the RT nucleus (see ***A***, lower left) and values were normalized to the mean intensity across this entire span. ***D***, KCC2 labeling showed significant regional variability in all groups. *p<0.05; **p<0.01; ***p<0.001.

nonetheless substantially contribute to maintaining a low basal $[Cl^-]_i$ and support inhibitory responses to GABAergic signaling (Klein et al., 2018).

Consistent with previous observations in SD rats, KCC2 expression was not evenly expressed throughout the RT nucleus (Barthó et al., 2004; Klein et al., 2018). As in our prior report, we quantified differential KCC2 immunoreactivity within the RT nucleus by drawing a linear ROI that extended from the anterior-most edge to the lateral-most edge of the RT nucleus (see lower left panel in **Fig. 1A**). This line bisected the RT nucleus and had a width of 75 µm. This linear ROI was further subdivided into 10 equal segments that were numbered from 1 (anterior-most) to 10 (lateral-most, see **Fig. 1C**). The mean fluorescence intensity within each segment was calculated.

We quantified how KCC2 immunoreactivity varied within each segment along the anterior-to-lateral axis, relative to the mean intensity level across all RT segments of each slice (**Fig. 1D**), to account for slice-to-slice staining variability. We observed that KCC2 levels were not uniform across segments of the RT nucleus at P20 in either SD ($F(10,263)=17.97$, $p<0.001$, $n=4$, one-way ANOVA) or WAG/Rij rats ($F(10,202)=46.89$, $p<0.001$, $n=4$, one-way ANOVA). Relative to the overall RT mean in P20 SD rats, KCC2 immunoreactivity was elevated in the two anterior-most segments of the RT nucleus (segment 1: 126±4.2%, $p<0.001$; segment 2: 115±3.7%, $p=0.021$). One centrally-located segment, on the other hand, had much reduced KCC2 immunoreactivity (segment 7: 84±2.4%, $p=0.020$). Similarly, in P20 WAG/Rij rats KCC2 expression was elevated in the three anterior-most segments of the RT nucleus (segment 1: 139±3.8%, $p<0.001$; segment 2:

119±4.1%, p<0.001; segment 3: 122±3.2%, p<0.001) and reduced in more centrally-located segments (segment 6: 79±3.7%, p<0.001; segment 7: 74±2.5%, p<0.001, segment 8: 79±1.9%, p<0.001; segment 9: 86±2.4%, p=0.017).

We also applied the approach described above to observe differences in expression of KCC2 across the span of RT in P150 rats (**Fig. 1D**). As at P20, levels of KCC2 varied among segments of the RT nucleus at P150 in both SD ($F(10,143)=11.29$, $p<0.001$, n=4, one-way ANOVA) and WAG/Rij rats ($F(10,231)=35.19$, $p<0.001$, n=4, one-way ANOVA). While in P150 SD rats KCC2 expression was only elevated in the anterior-most segment of the RT nucleus (segment 1: 119±4.3%, p<0.001), in P150 WAG/Rij rats both the three anterior-most (segment 1: 123±3.2%, p<0.001; segment 2: 114±2.5%, p<0.001; segment 3: 114±2.7%, p<0.001) and three centrally-located segments (segment 6: 85±1.9%, p<0.001; segment 7: 85±2.4%, p<0.001, segment 8: 85±1.9%, p<0.001) of the RT nucleus varied from the overall mean expression level.

Altogether, our results suggest that KCC2 expression is broadly similar in the thalamus of SD and WAG/Rij rats. While KCC2 expression is consistently reduced in the RT nucleus relative to VB neurons of both the ages and stains we studied, we have previously determined that even low levels of KCC2 are sufficient to maintain a low $[Cl^-]_i$ under basal conditions (Klein et al., 2018). However, we also determined that reduced KCC2 expression weakened the ability of RT neurons to maintain inhibitory responses to GABAergic signaling and potentially limited the effectiveness of the RT nucleus to prevent seizures. The observation

that KCC2 expression is lower in the thalamus of P150 WAG/Rij rats than in P150 SD rats may be linked to the propensity of adult WAG/Rij rats to experience spontaneous absence seizures.

$[A]_o$ are highly expressed surrounding RT neurons in SD and WAG/Rij rats

There is also evidence that extracellular impermeant anions (***$[A]_o$***), predominantly the highly sulfated chondroitin sulfate proteoglycans (***CSPGs***) of the extracellular matrix, may be important regulators of $[Cl^-]_i$ in neurons (Glykys et al., 2014a). While I previously observed that CSPGs become elevated in the RT nucleus of SD rats beginning around P20, these impermeant anions do not appear to contribute considerably to maintaining inhibitory GABAergic responses between P10-20 (Klein et al., 2018). However, the extracellular matrix is still developing beyond the third postnatal week (Vitellaro-Zuccarello et al., 2001; Wang and Fawcett, 2012; Horii-Hayashi et al., 2015), so the importance of $[A]_o$ for maintaining low $[Cl^-]_i$ in RT neurons may be greater in adult animals. Here we use *Wisteria floribunda* agglutinin (***WFA***) labeling of CSPGs to examine differences in thalamic $[A]_o$ between SD and WAG/Rij rats at P20 and P150 (**Fig. 2A**).

As with KCC2, WFA staining was elevated in the RT nucleus (23.1±1.1 A.U.) relative to VB nucleus (15.7±0.6 A.U.; $F(1,1,177)=44.83$, $p<0.0001$, n=4, three-way ANOVA) across the strains and ages tested (**Fig. 2A-B**). There was also a substantial increase in CSGPs within the thalamus across the strains tested between P20 (15.5±0.5 A.U.) and P150 (23.4±1.4 A.U.; $F(1,1,177)=49.65$, $p<0.0001$, n=4, three-way ANOVA). While the CSPGs expressed in the RT

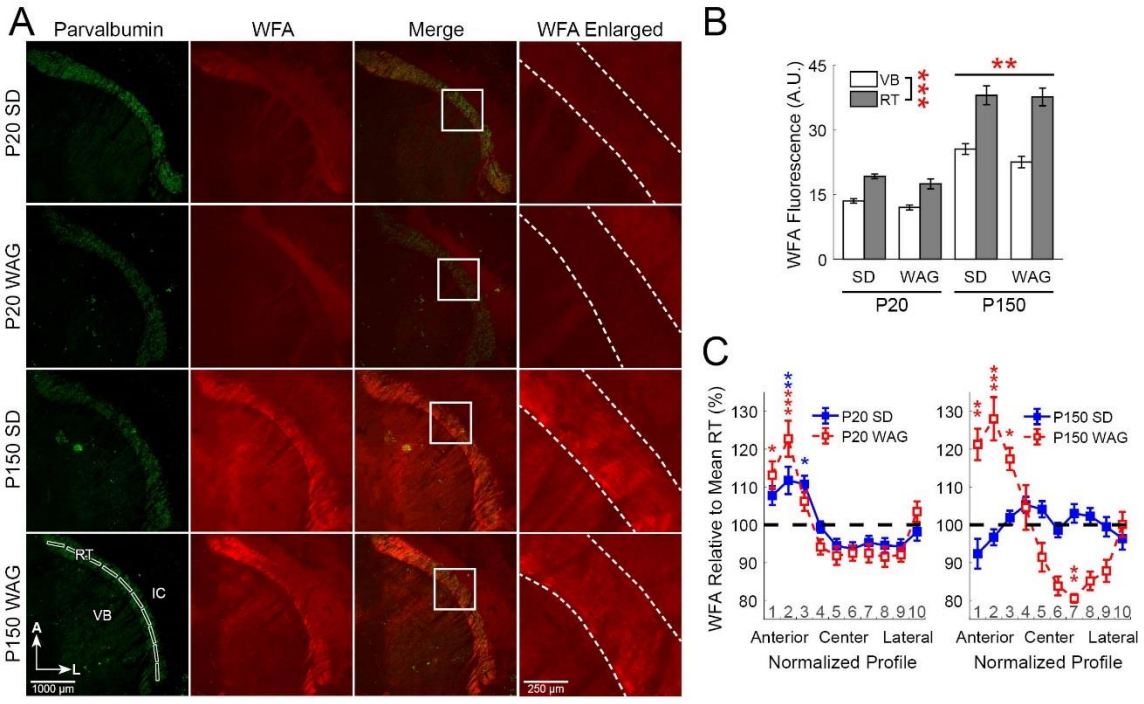

Figure 2. CSPGs are elevated around RT neurons of WAG/Rij and SD rats. *A*, Immunofluorescence of parvalbumin (green) and labeling of CSPGs with WFA (red) in horizontal sections of WAG/Rij and SD rat thalamus at different time points. All images are oriented with the anterior (A) aspect of the thalamus towards the top, the lateral (L) aspect towards the right and the internal capsule (IC) towards the upper right corner of the image. Dotted lines indicate the boundaries of the RT nucleus in the enlarged images. ***B***, WFA labeling increased with age in both strains. WFA labeling was consistently elevated in the RT nucleus, relative to VB, across all groups. ***C***, WFA labeling showed significant regional variability, including at P20 and P150 for WAG/Rij rats. *p<0.05; **p<0.01; ***p<0.001.

nucleus at P20 did not exert a large influence on $[Cl^-]_i$, the larger pool on $[A]_o$ present at P150 may be more critically involved in regulating inhibitory GABAergic signaling among RT neurons.

Using the methodology described above (see **Fig. 1C**), we now examined if there were regional differences in CSPG expression across the span of the RT nucleus. We observed that WFA labeling varied among segments of the RT nucleus at P20 in both SD ($F(10,253)=11.26$, $p<0.001$, $n=4$, one-way ANOVA) and WAG/Rij rats ($F(10,241)=20.32$, $p<0.001$, $n=4$, one-way ANOVA; **Fig. 2C**). Relative to the overall RT mean in P20 SD rats, WFA labeling was elevated in two anterior segments of the RT nucleus (segment 2: 112±3.6%, $p<0.001$; segment 3: 111±2.1%, $p=0.0083$). CSPG expression was similarly elevated in the two anterior-most segments of the RT nucleus of P20 WAG/Rij rats (segment 1: 112±2.5%, $p<0.001$; segment 2: 116±3.1%, $p<0.001$). Interestingly, while WFA labeling was not uniform throughout the RT nucleus of P150 SD rats ($F(10,243)=2.67$, $p=0.0041$, $n=4$, one-way ANOVA), there were no individual segments that varied from the average overall intensity. The pattern of WFA labeling was much different from in the RT nucleus of P150 WAG/Rij rats, where it was also not uniform ($F(10,243)=6.71$, $p<0.001$, $n=4$, one-way ANOVA). In P150 WAG/Rij rats, CSPG expression was elevated in one of the anterior segments of the RT nucleus (segment 2: 114±4.8%, $p=0.025$).

Although CSPGs did not impart much influence on the $[Cl^-]_i$ of RT neurons in P20 SD rats (Klein et al., 2018), more extensive expression of CSPGs in P150

rats may increase the relative contribution of $[A]_o$ to maintaining inhibitory responses to GABAergic signaling within the RT nucleus. The distribution of CSPGs is fairly even throughout the RT nucleus of P20 SD, P20 WAG/Rij and P150 SD rats, with the exception of a slight elevation in the anterior-most segments of RT for some groups. Developmental upregulation of CSPGs in the central segments of the RT nucleus could counteract the consistently low expression of KCC2 in the same segments. Perhaps more noteworthy is the sizeable reduction in CSPG expression in the center of the RT nucleus of P150 WAG/Rij rats. With limited KCC2 and lower $[A]_o$ expression, centrally located RT neurons in P150 WAG/Rij rats may have a compromised ability to maintain a low $[Cl^-]_i$ and function as a critical seizure choke point. We therefore decided to measure the impact of modulating various $[Cl^-]_i$ regulatory mechanisms in RT neurons, including KCC2 and $[A]_o$, on the occurrence of spontaneous absence seizures in WAG/Rij rats.

Briefly altering thalamic $[Cl^-]_i$ regulation does not alter spontaneous seizures

We have previously observed that inhibiting KCC2 function, or to a lesser extent reducing $[A]_o$, leads to an increase in the $[Cl^-]_i$ of RT neurons (Klein et al., 2018). Through computational modeling, we find that conditions that increase $[Cl^-]_i$ or disrupt the ability of RT neurons to effectively extrude Cl^- may lower the activity threshold required for GABAergic signaling to become excitatory among RT neurons. In doing so, seizure-like activity may more easily spread through networks of RT neurons. Previous studies has observed that brief infusions of the KCC2 antagonist VU0463271 (Sivakumaran et al., 2015) or the $[A]_o$ digesting

enzyme ChABC (Rankin-Gee et al., 2015) into the hippocampus were capable of increasing seizure susceptibility. We now sought to examine if modulating thalamic $[Cl^-]_i$ regulation was sufficient to alter the frequency of spontaneous seizures in WAG/Rij rats.

Adult WAG/Rij rats were implanted with EEG electrodes and a unilateral infusion cannula was placed adjacent to the right RT nucleus of each rat. Following several days of recovery from electrode and cannula placement, EEG activity was recorded from each rat over the course of a week (all recordings occurred between P183-224). Spontaneous absence seizures were recorded from cortical electrodes of all WAG/Rij rats (2/2 male and 2/2 female) and matched prior descriptions (van Luijtelaar and Coenen, 1986; Coenen and Van Luijtelaar, 1987), with 5-8 Hz spike-and-wave discharges lasting only a few seconds (**Fig. 3A**). We observed that seizures occurred more frequently in male (5.3±0.68 seizures/hour) than female WAG/Rij rats (1.2±0.24 seizures/hour, $t(26)=5.62$, $p<0.001$, n=2 per sex, t-test; **Fig. 3B**). Sex differences were not previously observed in the seizure frequency of WAG/Rij rats (Coenen and Van Luijtelaar, 1987; Van Luijtelaar et al., 1996), but may have occurred due to genetic drift from the originally characterized inbreed strain. On each day of EEG recording, following a four-hour baseline period, a four minute infusion (500 nl/min) of either a drug or vehicle solution was performed via the implanted cannula. Infusions always occurred within the first four hours of the lights-off period and investigators were blinded to the solution identity.

We examined the impact of altering thalamic KCC2 activity on the occurrence of spontaneous seizures (**Fig. 3C**) through either inhibiting KCC2 with

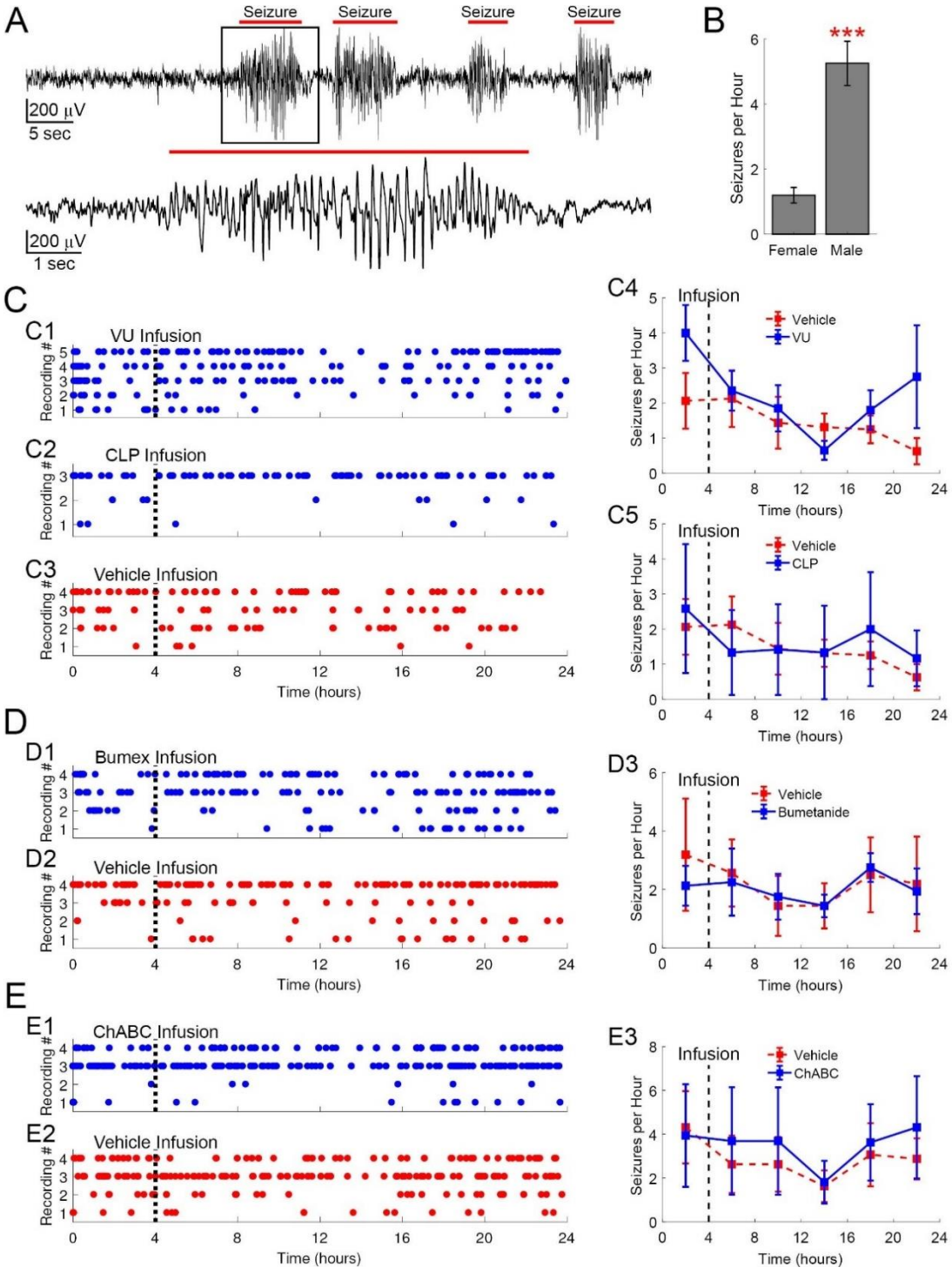

Figure 3. Absence seizures in WAG/Rij rats are unaltered by limited modulation of $[Cl^-]_i$ in thalamic neurons. ***A***, Example of a cortical EEG recording from a P187 male WAG/Rij rat, displaying multiple examples of spontaneous absence seizures. ***B***, The

frequency of absence seizures was substantially higher in male versus female WAG/Rij rats. All rats were unilaterally implanted with an infusion cannula adjacent to the right RT nucleus. Brief (4 min) infusions of various compounds were performed 4 hours after the start of each recording and the occurrence of absence seizures was scored throughout the duration of the recording (***C-E***). Raster plots depict the time each seizure occurred across recordings performed in multiple rats. ***C***, Altering the function of KCC2 with the antagonist VU0463271 (25 µM, ***C1***) or activator CLP257 (100 µM, ***C2***) did not alter seizure occurrence in WAG/Rij rats relative to vehicle infusions (***C3***). There was no difference in seizure frequency between VU0463271 and vehicle recordings (***C4***) or CLP257 and vehicle recordings (***C5***). ***D***, Disrupting NKCC1 function with the antagonist bumetanide (25 µM, ***D1***) did not impact seizure occurrence in WAG/Rij rats relative to vehicle infusions (***D2***). Seizure frequency was similar between bumetanide and vehicle recordings (***D3***). ***E***, Reducing $[A]_o$ with the enzyme ChABC (25 U/ml, ***E1***) did not alter seizure occurrence in WAG/Rij rats relative to vehicle infusions (***E2***). Seizure frequency was unchanged between ChABC and vehicle recordings (***E3***). All vehicle infusions matched the buffer and solvent composition used for corresponding drug infusions. ***p<0.001.

VU0463271 (25 µM, **Fig. 3C1**) or using CLP 257 (100 µM, **Fig. 3C2**) to increase membrane expression of KCC2 (Gagnon et al., 2013). There was no clear change in seizure incidence in response to VU0463271, CLP257 or vehicle infusions (**Fig. 3C1-3**). Seizure frequency was unchanged between recordings that included VU0463271 (2.2±1.12 seizures/hour) or vehicle infusions (1.5±0.56 seizures/hour; $F(1,53)=3.09$, $p=0.086$, n=4, two-way ANOVA; **Fig. 3C4**). Similarly, infusion of CLP257 did not alter seizure frequency (1.6±0.54 seizures/hour) from levels recorded during vehicle infusions (1.5±0.56 seizures/hour; $F(1,41)=0.09$, $p=0.76$, n=4, two-way ANOVA; **Fig. 3C5**). Our results indicate that a brief infusion of compounds to modulate KCC2 activity was insufficient to alter spontaneous seizure frequency in WAG/Rij rats.

Unlike KCC2, which under normal physiological conditions transports Cl^- out of neurons, the Cl^- transporter NKCC1 accumulates Cl^- in neurons and produces a higher $[Cl^-]_i$ (Yamada et al., 2004). The NKCC1 antagonist bumetanide can reduce seizures by promoting a lower $[Cl^-]_i$ in neurons and thus enhancing GABAergic inhibition (Dzhala et al., 2005; Sivakumaran and Maguire, 2016). We therefore examined whether infusion of bumetanide into the thalamus of WAG/Rij rats altered seizure incidence (25 µM, **Fig. 3D1**), relative to vehicle infusions (**Fig. 3D2**). There was no difference in seizure frequency between recordings that included bumetanide (2.2±0.69 seizures/hour) or vehicle infusions (2.0±0.45 seizures/hour; $F(1,47)=0.08$, $p=0.78$, n=4, two-way ANOVA; **Fig. 3D3**). Thus, a short disruption of NKCC1 transporter activity in the thalamus of adult WAG/Rij rats was not sufficient to alter the occurrence of spontaneous seizures.

We also investigated whether reducing the pool of $[A]_o$ surrounding RT neurons with the enzyme ChABC could alter the ability of the thalamus to generate absence seizures. Reducing $[A]_o$ can produce an elevated $[Cl^-]_i$ in neurons (Glykys et al., 2014a; Klein et al., 2018), which could weaken the ability of inhibitory GABAergic signaling within the RT nucleus to serve as a seizure choke point. However, seizure incidence was similar between recordings following ChABC (25 U/ml, **Fig. 3E1**) and vehicle infusions (**Fig. 3E2**). Seizure frequency was unchanged between recordings involving ChABC (3.5±0.87 seizures/hour) or vehicle infusions (2.9±0.87 seizures/hour; $F(1,47)=0.43$, $p=0.52$, $n=4$, two-way ANOVA; **Fig. 3E3**). Therefore, a small application of ChABC was insufficient to modify the capacity of the thalamus to generate absence seizures.

Overall, we found little correlation between altering mechanisms that regulate $[Cl^-]_i$ in RT neurons with changes in WAG/Rij rat seizure occurrence. While similarly brief infusions of VU0463271 (Sivakumaran et al., 2015) or ChABC (Rankin-Gee et al., 2015) into the hippocampus were sufficient to increase seizure susceptibility, more prolonged drug infusions may be required to disrupt $[Cl^-]$ in RT neurons to a point where seizure activity is altered. The highly variable baseline seizure activity between WAG/Rij rats also suggests that these experiments need to be repeated in a larger cohort of animals.

Chloride imaging of changes in RT neuron $[Cl^-]_i$

Experiments combining manipulations of thalamic $[Cl^-]_i$ regulation with EEG recordings provide a macroscopic view of the link between inhibitory GABAergic

signaling among RT neurons and absence seizures, yet do not capture the specific changes in the $[Cl^-]_i$ of individual RT neurons that may enable seizures to occur. The ratiometric, FRET-based Cl^- indicator SuperClomeleon has the potential to be used *in vivo* to record the changes in RT neuron $[Cl^-]_i$ that may accompany seizure onset. Prior to using this approach, we began by validating whether SuperClomeleon could detect pharmacologically-induced changes in the $[Cl^-]_i$ of RT neurons, as previously reported with gramicidin perforated patch recordings (Klein et al., 2018).

In acute brain slices from *Superclm1-loxP*;*Vgat-cre* mice, we observed expression of SuperClomeleon in RT neurons that displayed a fairly stable baseline YFP/CFP FRET ratio (**Fig. 4A**). Bath application of the KCC2 antagonist VU0463271 (10 µM) produced a noticeable decrease in the YFP/CFP ratio, indicative of increased quenching of YFP fluorescence by increased $[Cl^-]_i$ (Grimley et al., 2013). When VU0463271-induced changes in YFP/CFP ratio were normalized to the initial 10-minute baseline period and compared across different slices, there was a clear trend for VU0463271 to increase the $[Cl^-]_i$ of RT neurons (**Fig. 4B**). Examining the effect of VU0563271 at five minute intervals adjacent to the time of drug application (**Fig. 4C**), VU0463271-treated RT neurons displayed a reduced baseline-normalized YFP/CFP ratio across the sampled time points (93.6±2.3%, n=3 slices, 76 neurons) relative to control neurons (100.9±0.9%, n=2 slices, 30 neurons; $F(1,34)=25.25$, $p=0.0001$, two-way ANOVA). The impact of VU0463271 treatment was particularly noticeable at 15 minutes (control: 101.9±6.8%, VU0463271-treated: 87.2±1.8%, $p=0.043$) and 20 minutes (control:

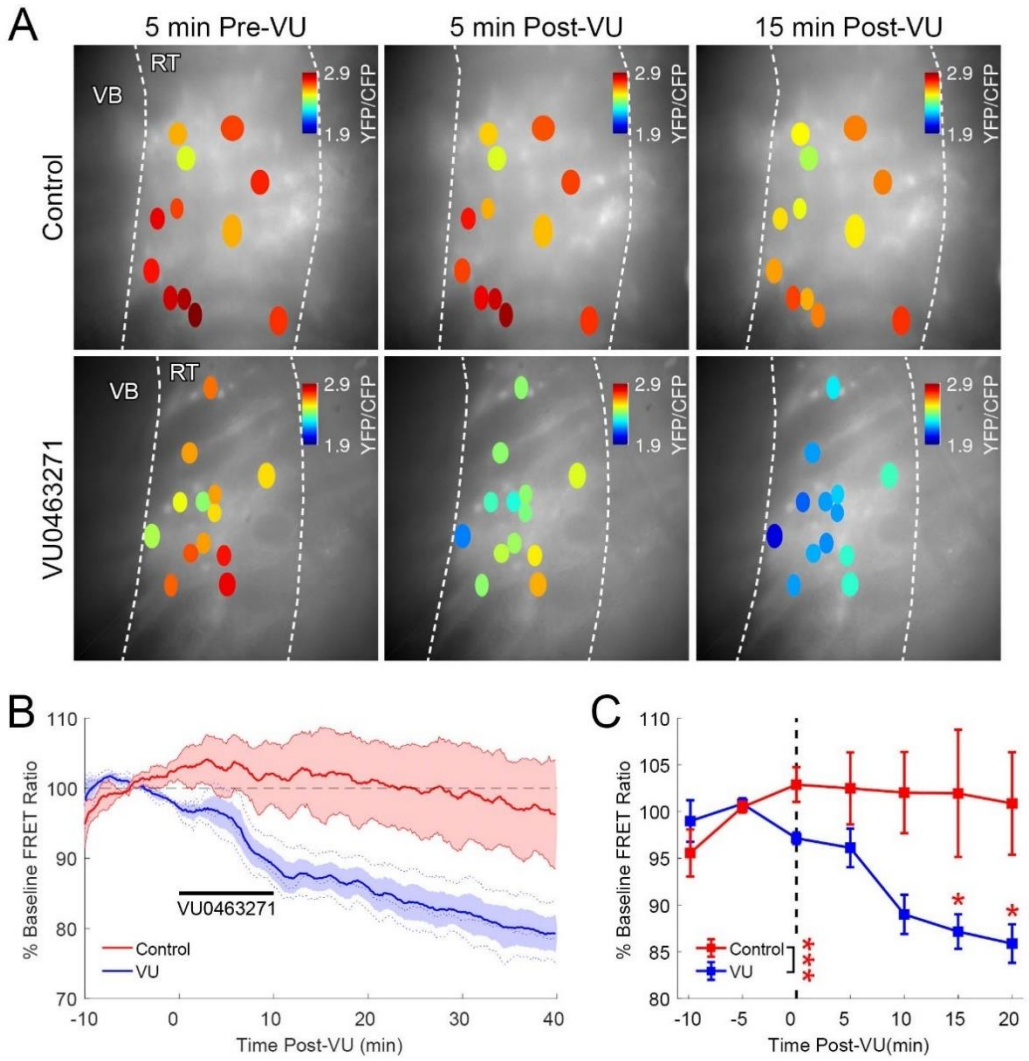

Figure 4. SuperClomeleon detects VU0463271-induced changes in RT neuron $[Cl^-]_i$. ***A***, SuperClomeleon was expressed in RT neurons for chloride imaging experiments. ROIs drawn around SuperClomeleon expressing RT neurons are colored according to their YFP/CFP fluorescence ratio. Representative images show examples of SuperClomeleon signal at various times relative to bath application of VU0463271 (10 µM) at 10 minutes. ***B***, Changes in YFP/CFP FRET ratio were averaged across all ROIs in individual slices (dotted lines) and normalized to the mean ratio during the initial 10 minute baseline period before being averaged across slices (solid line). ***C***, VU-induced changes in FRET ratio were compared at various time points relative to drug application. *p<0.05, ***p<0.001.

100.9±5.5%, VU0463271-treated: 85.9±2.1%, p=0.038) from the start of the VU0463271 application. The ability to observe physiologically relevant changes in the $[Cl^-]_i$ of RT neurons using SuperClomeleon suggests that *in vivo* recordings pairing chloride imaging in the thalamus with EEG monitoring of seizure activity are plausible.

Discussion

We demonstrate that expression of KCC2 and $[A]_o$ is reduced in the RT nucleus of adult WAG/Rij rats relative to levels in SD rats. A deficit in KCC2 and $[A]_o$ expression could compromise the ability of RT neurons to maintain a sufficiently low $[Cl^-]_i$ to enable inhibitory responses to GABAergic signaling and weaken the thalamic seizure choke point. Brief pharmacological modulation of $[Cl^-]_i$ regulation in thalamic neurons was insufficient to alter the frequency of spontaneous seizures in WAG/Rij rats. We also determined that the chloride indicator SuperClomeleon can detect shifts in $[Cl^-]_i$ that accompany the inhibition of KCC2 in RT neurons. SuperClomeleon therefore appears well suited for use in future *in vivo* studies that evaluate potential shifts in RT $[Cl^-]_i$ that correspond to the onset of electrographic seizures.

KCC2 and $[A]_o$ expression is reduced in RT neurons of adult WAG/Rij Rats

KCC2 expression was mostly comparable between SD and WAG/Rij rats, with reduced levels of KCC2 in the RT nucleus of both strains. However, we also observed at P150 that KCC2 expression throughout the thalamus was lower in

WAG/Rij than SD rats. Even small deficits in KCC2 expression can alter responses to GABAergic signaling among networks of neurons (Doyon et al., 2016; Klein et al., 2018).

Overall staining for CSPGs, a major source of $[A]_o$, was elevated in the RT nucleus of both SD and WAG/Rij rats at P150. However, $[A]_o$ levels are highly skewed within the RT nucleus of P150 WAG/Rij rats, with elevated expression in the most anterior end of RT and lower expression in the central portion of RT. Therefore, the central region of the RT nucleus in P150 WAG/Rij rats has low expression of both KCC2 and $[A]_o$. Our prior study on Cl^- regulation in the RT nucleus (Klein et al., 2018) suggests that reduced levels of both KCC2 and $[A]_o$ would allow Cl^- to more rapidly accumulate in the RT nucleus of WAG/Rij rats.

While gramicidin perforated patch recordings show that $[Cl^-]_i$ in paracentral thalamic neurons of WAG/Rij rats is unaltered from control animals (Brockhaus and Pape, 2011), future studies should examine basal $[Cl^-]_i$ and Cl^- extrusion in RT and VB neurons of WAG/Rij animals. Chloride imaging in WAG/Rij rats using SuperClomeleon would also provide valuable insight into how low expression of KCC2 and $[A]_o$ relates to the occurrence of spontaneous absence seizures.

Briefly altering thalamic $[Cl^-]_i$ regulation does not alter spontaneous seizures

In the present study, we did not observe any shift in the spontaneous seizure frequency of WAG/Rij rats following a brief infusion of VU0463271, CLP257, bumetanide or ChABC into the thalamus. We were surprised by the lack of any effect on seizure activity, as VU0463271 and ChABC are both capable of

increasing RT neuron $[Cl^-]_i$ in acute slice experiments (Klein et al., 2018). Limited VU0463271 (Sivakumaran et al., 2015) or ChABC (Rankin-Gee et al., 2015) infusions into the hippocampus lasting under five minutes were both sufficient to increase seizure susceptibility. However, longer drug infusions may be needed to produce sufficiently large alterations in thalamic $[Cl^-]_i$ regulation to alter the seizure frequency of WAG/Rij rats.

The large discrepancy in seizure frequency between male and female WAG/Rij rats also likely reduced our ability to resolve any subtle changes in produced by drug infusion. We did not anticipate such a large effect of sex on seizure frequency as male and female WAG/Rij rats were previously observed to display very similar seizure characteristics (Coenen and Van Luijtelaar, 1987; Van Luijtelaar et al., 1996). The low baseline seizure frequency in female rats could enhance our ability to detect treatments that increase the rate of seizures, whereas drugs that produce fewer seizures may be more noticeable against the high baseline seizure activity of male WAG/Rij rats.

Chloride imaging can reveal changes in RT neuron $[Cl^-]_i$

In acute brain slices from mice expressing the chloride indicator SuperClomeleon in RT neurons, we observed that inhibiting KCC2 with VU0463271 increased $[Cl^-]_i$. We have previously observed the same impact of VU0463271 on $[Cl^-]_i$ in RT neurons using perforated patch recordings (Klein et al., 2018). The concordance of these results suggest that chloride imaging can be used to study $[Cl^-]_i$ regulation in thalamic neurons.

A significant advantage of SuperClomeleon imaging over perforated patch recordings is the relative ease with which $[Cl^-]_i$ can be measured across a large number of neurons either *in vitro*, or potentially even *in vivo*. SuperClomeleon has previously been virally transfected into the lateral geniculate nucleus of the thalamus and then used to image changes in $[Cl^-]_i$ in awake and behaving mice using fiber photometry (Wimmer et al., 2015; Wells et al., 2016). *In vivo* SuperClomeleon imaging could potentially be combined with EEG recordings to monitor the changes in RT $[Cl^-]_i$ that correspond with the onset of absence seizures.

Conclusions

The present study demonstrates that expression of KCC2 and $[A]_o$ is reduced in the RT nucleus of seizure-prone WAG/Rij rats relative to adult SD rats. Combining EEG recordings from WAG/Rij rats with pharmacological modulation of thalamic $[Cl^-]_i$ regulation and *in vivo* chloride imaging offers the possibility to better understand the ability of inhibitory GABAergic signaling among RT neurons to produce a critical seizure choke point.

References

Barthó P, Payne JA, Freund TF, Acsády L (2004) Differential distribution of the KCl cotransporter KCC2 in thalamic relay and reticular nuclei. Eur J Neurosci 20:965–975.

Brockhaus J, Pape HC (2011) Abnormalities in GABAergic synaptic transmission of intralaminar thalamic neurons in a genetic rat model of absence epilepsy. Mol Cell Neurosci 46:444–451.

Cherubini E, Rovira C, Gaiarsa JL, Corradetti R, Ari Y Ben (1990) GABA mediated excitation in immature rat CA3 hippocampal neurons. Int J Dev Neurosci 8:481–490.

Coenen AML, Van Luijtelaar ELJM (1987) The WAG/Rij rat model for absence epilepsy: age and sex factors. Epilepsy Res 1:297–301.

DeLorey TM, Handforth A, Anagnostaras SG, Homanics GE, Minassian BA, Asatourian A, Fanselow MS, Delgado-Escueta A, Ellison GD, Olsen RW (1998) Mice lacking the β3 subunit of the GABAA receptor have the epilepsy phenotype and many of the behavioral characteristics of Angelman syndrome. J Neurosci 18:8505–8514.

Delpire E, Staley KJ (2014) Novel determinants of the neuronal Cl- concentration. J Physiol 592:4099–4114.

Doyon N, Vinay L, Prescott SA, De Koninck Y (2016) Chloride Regulation: A Dynamic Equilibrium Crucial for Synaptic Inhibition. Neuron 89:1157–1172.

Dzhala VI, Talos DM, Sdrulla DA, Brumback AC, Mathews GC, Benke TA, Delpire E, Jensen FE, Staley KJ (2005) NKCC1 transporter facilitates seizures in the

developing brain. Nat Med 11:1205–1213.

Gagnon M, Bergeron MJ, Lavertu G, Castonguay A, Tripathy S, Bonin RP, Perez-Sanchez J, Boudreau D, Wang B, Dumas L, Valade I, Bachand K, Jacob-Wagner M, Tardif C, Kianicka I, Isenring P, Attardo G, Coull J a M, De Koninck Y (2013) Chloride extrusion enhancers as novel therapeutics for neurological diseases. Nat Med 19:1524–1528.

Glykys J, Dzhala V, Egawa K, Balena T, Saponjian Y, Kuchibhotla K V, Bacskai BJ, Kahle KT, Zeuthen T, Staley KJ (2014) Local impermeant anions establish the neuronal chloride concentration. Science 343:670–675.

Grimley JS, Li L, Wang W, Wen L, Beese LS, Hellinga HW, Augustine GJ (2013) Visualization of Synaptic Inhibition with an Optogenetic Sensor Developed by Cell-Free Protein Engineering Automation. J Neurosci 33:16297–16309.

Homanics GE, DeLorey TM, Firestone LL, Quinlan JJ, Handforth A, Harrison NL, Krasowski MD, Rick CEM, Korpi ER, Mäkelä R, Brilliant MH, Hagiwara N, Ferguson C, Snyder K, Olsen RW (1997) Mice devoid of γ-aminobutyrate type A receptor β3 subunit have epilepsy, cleft palate, and hypersensitive behavior. Proc Natl Acad Sci 94:4143–4148.

Horii-Hayashi N, Sasagawa T, Matsunaga W, Nishi M (2015) Development and Structural Variety of the Chondroitin Sulfate Proteoglycans-Contained Extracellular Matrix in the Mouse Brain. Neural Plast 2015.

Huntsman MM, Porcello DM, Homanics GE, DeLorey TM, Huguenard JR (1999) Reciprocal inhibitory connections and network synchrony in the mammalian thalamus. Science 283:541–543.

Kanaka C, Ohno K, Okabe A, Kuriyama K, Itoh T, Fukuda A, Sato K (2001) The differential expression patterns of messenger RNAs encoding K-Cl cotransporters (KCC1,2) and Na-K-2Cl cotransporter (NKCC1) in the rat nervous system. Neuroscience 104:933–946.

Klein PM, Lu AC, Harper ME, McKown HM, Morgan JD, Beenhakker MP (2018) Tenuous Inhibitory GABAergic Signaling in the Reticular Thalamus. J Neurosci 38:1232–1248.

Makinson CD, Tanaka BS, Sorokin JM, Wong JC, Christian CA, Goldin AL, Escayg A, Huguenard JR (2017) Regulation of Thalamic and Cortical Network Synchrony by Scn8a. Neuron 93:1165–1179.e6.

Meeren HKM, Pijn JPM, Van Luijtelaar ELJM, Coenen AML, Lopes da Silva FH (2002) Cortical focus drives widespread corticothalamic networks during spontaneous absence seizures in rats. J Neurosci 22:1480–1495.

Payne JA, Stevenson TJ, Donaldson LF (1996) Molecular characterization of a putative K-Cl cotransporter in rat brain: a neuronal-specific isoform. J Biol Chem 271:16245–16252.

Paz JT, Huguenard JR (2015) Microcircuits and their interactions in epilepsy: is the focus out of focus? Nat Neurosci 18:351–359.

Rankin-Gee EK, McRae PA, Baranov E, Rogers S, Wandrey L, Porter BE (2015) Perineuronal net degradation in epilepsy. Epilepsia 56:1124–1133.

Rivera C, Voipio J, Payne JA, Ruusuvuori E, Lahtinen H, Lamsa K, Pirvola U, Saarma M, Kaila K (1999) The K+/Cl- co-transporter KCC2 renders GABA hyperpolarizing during neuronal maturation. Nature 397:251–255.

Rohrbough J, Spitzer NC (1996) Regulation of intracellular Cl- levels by Na(+)-dependent Cl- cotransport distinguishes depolarizing from hyperpolarizing GABAA receptor-mediated responses in spinal neurons. J Neurosci 16:82–91.

Sivakumaran S, Cardarelli RA, Maguire J, Kelley MR, Silayeva L, Morrow DH, Mukherjee J, Moore YE, Mather RJ, Duggan ME, Brandon NJ, Dunlop J, Zicha S, Moss SJ, Deeb TZ (2015) Selective Inhibition of KCC2 Leads to Hyperexcitability and Epileptiform Discharges in Hippocampal Slices and In Vivo. J Neurosci 35:8291–8296.

Sivakumaran S, Maguire J (2016) Bumetanide reduces seizure progression and the development of pharmacoresistant status epilepticus. Epilepsia 57:222–232.

Sohal VS, Huguenard JR (2003) Inhibitory interconnections control burst pattern and emergent network synchrony in reticular thalamus. J Neurosci 23:8978–8988.

Stil A, Jean-Xavier C, Liabeuf S, Brocard C, Delpire E, Vinay L, Viemari JC (2011) Contribution of the potassium-chloride co-transporter KCC2 to the modulation of lumbar spinal networks in mice. Eur J Neurosci 33:1212–1222.

Sun Y-G, Wu C-S, Renger JJ, Uebele VN, Lu H-C, Beierlein M (2012) GABAergic synaptic transmission triggers action potentials in thalamic reticular nucleus neurons. J Neurosci 32:7782–7790.

Ting JT, Daigle TL, Chen Q, Feng G (2014) Acute brain slice methods for adult and aging animals: application of targeted patch clamp analysis and

optogenetics. In: Patch-Clamp Methods and Protocols, 2nd ed. (Martina M, Taverna S, eds), pp 221–242 Methods in Molecular Biology. New York, NY: Springer New York.

van Luijtelaar ELJM, Coenen AML (1986) Two types of electrocortical paroxysms in an inbred strain of rats. Neurosci Lett 70:393–397.

Van Luijtelaar ELJM, Dirksen R, Vree TB, Van Haaren F (1996) Effects of acute and chronic cocaine administration on EEG and behaviour in intact and castrated male and intact and ovariectomized female rats. Brain Res Bull 40:43–50.

Vitellaro-Zuccarello L, Meroni A, Amadeo A, De Biasi S (2001) Chondroitin sulfate proteoglycans in the rat thalamus: Expression during postnatal development and correlation with calcium-binding proteins in adults. Cell Tissue Res 306:15–26.

Wang D, Fawcett J (2012) The perineuronal net and the control of CNS plasticity. Cell Tissue Res 349:147–160.

Wang X, Sun QQ (2012) Characterization of axo-axonic synapses in the piriform cortex of Mus musculus. J Comp Neurol 520:832–847.

Wells MF, Wimmer RD, Schmitt LI, Feng G, Halassa MM (2016) Thalamic reticular impairment underlies attention deficit in Ptchd1(Y/-) mice. Nature 532:58–63.

Williams JR, Sharp JW, Kumari VG, Wilson M, Payne JA (1999) The neuron-specific K-Cl cotransporter, KCC2. Antibody development and initial characterization of the protein. J Biol Chem 274:12656–12664.

Wimmer RD, Schmitt LI, Davidson TJ, Nakajima M, Deisseroth K, Halassa MM

(2015) Thalamic control of sensory selection in divided attention. Nature 526:705–709.

Yamada J, Okabe A, Toyoda H, Kilb W, Luhmann HJ, Fukuda A (2004) Cl- uptake promoting depolarizing GABA actions in immature rat neocortical neurones is mediated by NKCC1. J Physiol 557:829–841.

Chapter 4: Conclusions

Implications

In my dissertation, I have sought to utilize multifaceted approaches to address the question of which underlying mechanisms enable GABAergic signaling among RT neurons to form a critical seizure choke point. I find that despite RT neurons expressing substantially less of the Cl^- extruding cotransporter KCC2 than other thalamic neurons, RT neurons still maintain a relatively low $[Cl^-]_i$. The $[Cl^-]_i$ of RT neurons appears to be sufficiently low to support inhibitory responses to GABAergic signaling under basal conditions. By employing pharmacological manipulations, I have determined that the reduced levels of KCC2 expressed in RT neurons nonetheless contribute substantially to sustaining a low basal $[Cl^-]_i$. However, low expression of KCC2 leaves RT neurons more vulnerable to undergoing a rapid accumulation of $[Cl^-]_i$ during more intense periods of GABAergic stimulation. Computational modeling of GABAergic signaling among a network of RT neurons indicates that a reduced ability to rapidly extrude Cl^-, associated with low KCC2 expression, makes the network more susceptible to undergoing a shift to excitatory responses to GABAergic signaling. The weakened ability of RT neurons to maintain inhibitory responses to GABAergic signaling undermines the thalamic seizure chokepoint and facilitates a seizure-like spread of synchronized neuronal firing via GABAergic excitation. I have now established an *in vivo* paradigm to assess whether $[Cl^-]_i$-regulatory mechanisms in RT neurons control absence seizures. Overall, my findings further inform our understanding of the mechanisms within the RT nucleus that form a critical seizure choke point.

Understanding the underlying neurological mechanisms that generate seizures is critical for informing the development of improved therapies for patients with epilepsy. There is currently a clear need for the development of more effective and better tolerated treatments for absence seizures. Although ethosuximide, valproate and lamotrigine reduce absence seizures in a portion of patients, over half of all patients using these therapies will either continue to experience seizures or will discontinue treatment due to the intolerability of side effects (Glauser et al., 2013a, 2013b). The lack of effective antiepileptic drugs with minimal side effects is not limited to absence epilepsy, with 38% of patients with adult onset epilepsy failing to achieve seizure freedom using current treatments (Mohanraj and Brodie, 2005). Shockingly, despite the development of dozens of new antiepileptic drugs in the last hundred years, there has been only limited progress from the 57% of patients who became seizure-free using treatments, mainly potassium bromide, that were available in the 1880s (Gowers, 1881). The failure of preclinical research to successfully develop more effective antiepileptic drugs, suggests a need to test compounds in diverse animal models (Galanopoulou and Mowrey, 2016; Löscher, 2017) and to examine additional mechanisms, such as the those that underlie seizure choke points (Paz and Huguenard, 2015).

My research into the underlying mechanisms of the RT seizure choke point suggests that improving the Cl^- extrusion capability of RT neurons could increase the threshold of activity required to initiate an absence seizure. KCC2 hypofunction, resulting from loss-of-function mutations, is linked to several forms of epilepsy in humans (Kahle et al., 2014; Moore et al., 2017). Hippocampal slices

from mice expressing point mutations in KCC2 also display an enhanced capacity to generate seizure-like events (Kelley et al., 2016). Thus, there is wide interest in developing therapies that can restore or enhance the Cl^- extrusion capacity or KCC2 in neurons (Gagnon et al., 2013; Delpire and Weaver, 2016; Moore et al., 2017). The compound CLP257 was identified in an assay screening for small molecules capable of increasing Cl^- efflux from cultured cells (Gagnon et al., 2013). CLP257 is hypothesized to increase cell surface expression of KCC2 through blocking degradation mechanisms (Delpire and Weaver, 2016), although the efficacy of CLP257 in improving KCC2 function in neurons remains debated (Cardarelli et al., 2017; Gagnon et al., 2017). Therefore, CLP257 could potentially be utilized to increase the Cl^- extrusion capability of RT neurons, providing a new therapeutic approach for treating absence epilepsy.

While my research has largely focused on the implications of intra-RT GABAergic signaling in absence epilepsy, the breakdown of inhibition provided by these same thalamic pathways is also implicated in other, non-epilepsy associated, attentional deficits. GABAergic signaling among RT neurons has long been hypothesized to form a searchlight-like mechanism to only allow selected sensory information to flow from the thalamus to the cortex (Crick, 1984). Experimental evidence supports the important role of the RT nucleus in focusing attention on salient sensory stimuli (McAlonan et al., 2008; Halassa et al., 2014; Wimmer et al., 2015). Interestingly, a selective deletion of the *Ptchd1* gene in the RT nucleus is sufficient to produce attention-deficit hyperactivity disorder-like behavior in mice (Wells et al., 2016). *Ptchd1* deletion is linked to reduced small-

conductance, calcium-activated potassium (***SK***) currents and diminished burst firing in RT neurons. Additionally, the hallucinations and delusions that occur in patients with schizophrenia are thought to result from sensory gating deficits associated with RT neuron dysfunction (Ferrarelli and Tononi, 2011). Both genetic (Ahrens et al., 2015) and pharmacological (Krause et al., 2003; Egerton et al., 2005) disruptions of RT signaling have been linked to schizophrenia-associated deficits in filtering out extraneous sensory stimuli. Furthermore, brain samples from patients with schizophrenia express reduced levels of KCC2 mRNA (Hyde et al., 2011). The important role of proper signaling among RT neurons in preventing ADHD and schizophrenia indicates how critical the thalamic circuitry is for many regular brain functions and suggests that even small disruptions can produce pathological changes. Thus, understanding the mechanisms that regulate $[Cl^-]_i$ in RT neurons appears to have wide applicability beyond just improving our understanding of absence epilepsy.

My dissertation research also provides insight into some technical considerations that are relevant to experiments aiming to link measurements of $[Cl^-]_i$ to an understanding of GABAergic signaling. Two prior studies had utilized gramicidin perforated patch recordings to examine GABAergic responses in RT neurons (Ulrich and Huguenard, 1997; Sun et al., 2012). Divergent reports of an RT E_{GABA} of either -75 mV (Ulrich and Huguenard, 1997) or -45 mV (Sun et al., 2012) sowed confusion about the mechanisms through which GABAergic signaling among RT neurons could provide the desynchronizing drive necessary to sustain a seizure choke point. One of the main methodological differences I noticed in the

Sun et al. study was their use of recording electrodes filled with a CsCl-based internal solution. While the membrane pores formed by gramicidin prevent anions from flowing between the recording electrode and patched neuron, they do not prevent the entry of cations such as Cs^+ (Myers and Haydon, 1972). Although Cs^+ can also be a substrate for the transport of Cl^- by KCC2, Cs^+ translocation through KCC2 occurs at a substantially slower rate and therefore effectively inhibits the rate of Cl^- extrusion (Van Brederode et al., 2001; Williams and Payne, 2004). My data indicates that perforated patch recordings from RT neurons using a CsCl-based internal solution measure a more depolarized E_{GABA} than in recordings utilizing a KCl-based internal solution and that CsCl occludes the ability of VU0463271 to provide any further block of KCC2 (Klein et al., 2018). Therefore, the relatively depolarized E_{GABA} Sun et al. observe in RT neurons appears to be largely an artifact of performing recordings in the presence of Cs^+. Cs^+ is commonly included in electrophysiological recordings as a means to achieve a better space clamp by reducing leak conductances (Jarolimek et al., 1999; Blaesse et al., 2009). However, my research indicates that CsCl-based recording solutions should be avoided in any experiment that is investigating mechanisms that have any dependency on KCC2 function.

Another implication of my research is that solely measuring E_{GABA} does not adequately convey the complicated interaction between GABAergic signaling and dynamic changes in $[Cl^-]_i$. Previous observations (Jin et al., 2005; Blaesse et al., 2009), as well as my own research (Klein et al., 2018), reveal that even limited expression of KCC2 in neurons can maintain a relatively low $[Cl^-]_i$ during basal

periods of sufficiently mild GABAergic signaling. Similar to my recordings from RT neurons, layer V pyramidal neurons in the cortical undercut model of cortical hyperexcitability undergo a downregulation of KCC2 expression that does not produce a corresponding shift in basal E_{GABA} (Jin et al., 2005). However, Cl^- accumulates much faster in both RT and undercut layer V neurons during periods of more intense GABAergic stimulation. Our computational modeling of the RT nucleus indicates that reducing the rate of Cl^- extrusion from a neuron correlates more highly with a susceptibility to undergoing a shift to excitatory responses to GABAergic signaling than does an initially more depolarized E_{GABA}. Therefore, my research emphasizes the need for scientists to contextualize studies on $[Cl^-]_i$ regulatory mechanisms with not only the impact on the basal E_{GABA}, but also in terms of how the capacity of a neuron to extrude Cl^- is altered.

Future Directions

While my dissertation research advances our knowledge regarding the capacity of GABAergic signaling among RT neurons to form a critical seizure choke point, there are several future directions which can further improve our understanding how mechanisms that regulate Cl^- in the thalamus prevent absence seizures. In Chapter 3 of my dissertation, I perform a preliminary set of *in vivo* EEG experiments to examine whether pharmacological manipulation of Cl^- regulation in the thalamus is sufficient to alter seizure frequency. I was unable to observe any alteration in the spontaneous seizure frequency of WAG/Rij rats following a brief, four minute, infusion of compounds to block KCC2 (VU0463271), augment KCC2 (CLP257), block NKCC1 (bumetanide) or reduce $[A]_o$ (ChABC) in an initial sample

of four rats. Similarly brief infusions of VU0463271 (Sivakumaran et al., 2015) or ChABC (Rankin-Gee et al., 2015) into the hippocampus were sufficient to alter seizure susceptibility. However, longer infusions of compounds into the thalamus may be necessary to alter the absence seizure activity of WAG/Rij rats. I also observed that male WAG/Rij rats experience many more seizures than age-matched female rats. Although earlier studies do not report any sex differences in seizure frequency between male and female WAG/Rij rats (Coenen and Van Luijtelaar, 1987; Van Luijtelaar et al., 1996), it is possible that genetic drift has introduced phenotypic differences between our WAG/Rij colony and the originally characterized inbreed strain.

A reanalysis of prior gramicidin perforated patch recordings from thalamic neurons (see **Chapter 2**, **Fig. 2C**) does not reveal any sex-dependent differences in either RT neuron E_{GABA} between female (-63±4.7 mV, n=6) and male rats (-62±4.3 mV, n=7, t(11)=0.097, p=0.92) or in VB neuron E_{GABA} between female (-78±3.2 mV, n=7) and male rats (-81±4.7 mV, n=7, t(12)=0.67, p=0.51, **Fig. 1A**). At P20, a similar age to when E_{GABA} measurements were performed, a reexamination of thalamic KCC2 labeling (see **Chapter 3**, **Fig. 1**) indicated an interaction between the sex and strain of animals (F(1,1,73)=32.91, p<0.001, three-way ANOVA), with more KCC2 expression in the thalamus of male WAG/Rij rats (55±5.4 AU, n=2) than in female WAG/Rij rats (33±2.3 AU, n=2, **Fig. 1B**). Across the strains examined, sex-dependent differences existed in KCC2 expression throughout the thalamus at P150 (F(1,1,77)=18.46, p=0.0001, three-way ANOVA, **Fig 1C**), the age when EEG recordings of seizure activity were performed. At P150, KCC2 expression was higher in the thalamus of male rats (48±2.6 AU, n=2) than in female rats (41±1.9 AU, n=2). However, there was no interaction between KCC2 expression, the sex

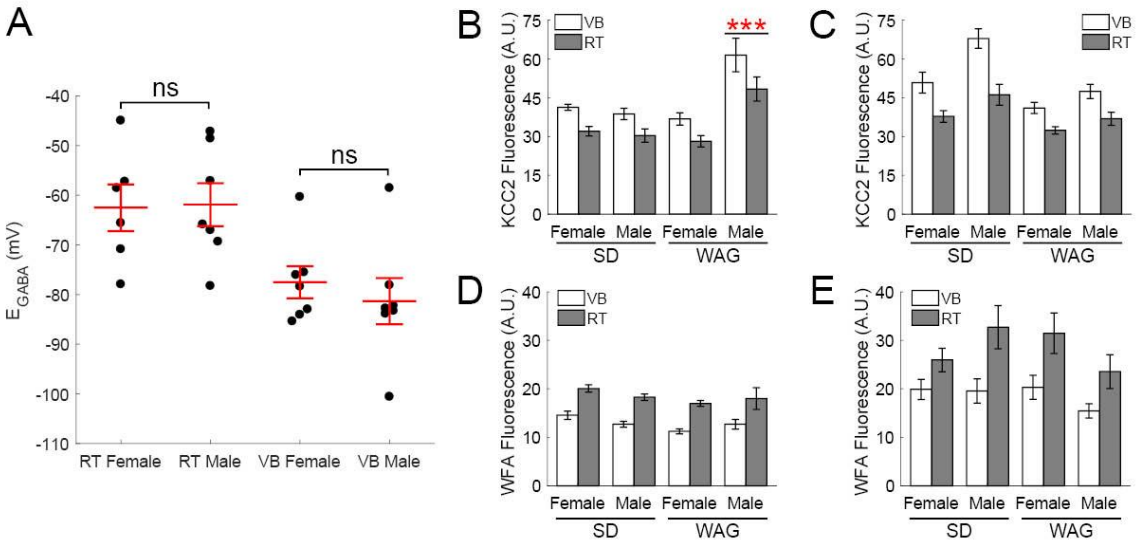

Figure 1. Sex differences among SD and WAG/Rij rats. ***A***, Gramicidin perforated patch recordings of muscimol-induced currents in thalamic neurons from SD rats did not reveal any sex-dependent differences in E_{GABA}. Sex-dependent differences in KCC2 expression were limited at P20 (***B***) and P150 (***C***) in SD and WAG/Rij rats. No sex-dependent differences were observed in WFA labeling of $[A]_o$ at either P20 (***D***) or P150 (***E***) in SD and WAG/Rij rats ***p<0.001.

and the strain of rats at P150 ($F(1,1,77)=2.97$, $p=0.089$, three-way ANOVA), preventing further identification of amongst which strains differences existed. Likewise, reanalysis of thalamic WFA labeling (see **Chapter 3**, **Fig. 2**) across strains did not identify any sex-dependent differences in expression at either P20 ($F(1,1,89)=0.17$, $p=0.68$, $n=2,2$, three-way ANOVA, **Fig. 1D**) or P150 ($F(1,1,87)=0.57$, $p=0.45$, $n=2,2$, three-way ANOVA, **Fig. 1E**). The current analysis is too underpowered to fully address whether sex differences exist in the seizure frequency of WAG/Rij rats and if variability in thalamic $[Cl^-]_i$ may be involved. As the mechanisms underlying seizures may be different between the two sexes of our WAG/Rij rats, sex differences in responses to manipulation of KCC2 need to be considered in EEG recordings performed in a larger number of rats.

Newly emerging tools now enable a direct examination of the relationship between RT $[Cl^-]_i$ and absence seizures in awake and behaving animals. In Chapter 3 of my dissertation, I demonstrate that the Cl^- indicator SuperClomeleon can be used to simultaneously record changes in the $[Cl^-]_i$ of multiple RT neurons in acute brain slices. SuperClomeleon signal has also been recorded *in vivo* using fiber photometry techniques (Wimmer et al., 2015; Wells et al., 2016), although fiber photometry only provides a single measurement of $[Cl^-]_i$ based on changes in the bulk SuperClomeleon signal within a region of the brain. The recent development of miniaturized microscopes that can record fluorescence signals with single cell resolution within deep brain structures of freely behaving animals opens up new possibilities for *in vivo* imaging. Miniaturized fluorescence microscopes, also referred to as Miniscopes, have already been used to record

the activity of hippocampal place cells (Ziv et al., 2013) and ensembles of CA1 neurons that encode contextual memories (Cai et al., 2016). By combining the viral transfection of SuperClomeleon into RT neurons of WAG/Rij rats, Miniscope imaging of SuperClomeleon signal in awake animals and EEG recording of seizure activity, *in vivo* changes in $[Cl^-]_i$ can be correlated with the onset of electrographic seizures. Computational modeling in Chapter 2 of my dissertation predicts that $[Cl^-]_i$ must become sufficiently elevated to enable excitatory GABAergic responses before a seizure-like spread of action potentials can occur among RT neurons. I therefore anticipate that an increase in $[Cl^-]_i$, detectable with SuperClomeleon imaging, will precede all electrographic seizures.

Another exciting question not addressed by my current studies is to what extent there are regional differences in $[Cl^-]_i$ regulation among RT neurons and the ways in which such differences influence the function of the RT nucleus as a seizure choke point. I observe more elevated KCC2 expression in the most anterior and lateral portions of the RT nucleus of both Sprague Dawley and WAG/Rij rats. Additionally, past studies have identified multiple subtypes of RT neurons that display distinct electrophysiological properties (Lee et al., 2007; Halassa et al., 2014; Clemente-Perez et al., 2017). Somatostatin- (***SOM***) and parvalbumin- (***PV***) expressing RT neurons are differentially innervated from outside the thalamus and even project to distinct regions of VB (Clemente-Perez et al., 2017). While gramicidin perforated patch recordings are a prohibitively low throughput technique to examine regional- and subtype- specific differences in $[Cl^-]_i$ regulation among RT neurons, such experiments would be better addressed with

SuperClomeleon imaging of a diverse population of RT neurons. Further computational modeling of interactions among RT neurons that includes new insights into the diversity of RT neuron subtypes will provide more physiologically relevant insights into the ability of the RT nucleus to form a critical seizure choke point.

I am also curious how much other K-Cl cotransporters (***KCCs***), in addition to KCC2, may contribute to $[Cl^-]_i$ regulation in RT neurons. While VU0463271 is a known antagonist of KCC2, non-specific inhibition of the other KCC isoforms KCC1, KCC3 and KCC4 has not been evaluated (Delpire and Weaver, 2016). There is currently little evidence that KCC isoforms other than KCC2 have significant expression in the thalamus (Rivera et al., 1999; Le Rouzic et al., 2006). However, my experiments demonstrate that low expression of a KCC does not necessarily correlate with a low functional contribution to regulating $[Cl^-]_i$. VU0463271 may also have limited off-target impacts on proteins other than KCC2, including the α_{1B} adrenergic receptor (Sivakumaran et al., 2015). Non-specific activation of adrenergic signaling can alter both KCC2 surface expression and transporter efficiency (Hewitt et al., 2009; Mahadevan and Woodin, 2016). Therefore, the main identified off-target interaction of VU0463271 still likely acts indirectly as a modulator of KCC2 activity.

Nevertheless, one method to more specifically reduce functional KCC2 in RT neurons would be through the use of RNA interference (***RNAi***). RNAi is a process through which 20-30 nucleotide long sequences of noncoding RNA initiate molecular mechanisms that silence expression of specific genes (Fire et al., 1998;

Zamore et al., 2000; Wilson and Doudna, 2013). Two major approaches to RNAi are the use of small interfering RNA (***siRNA***) or short hairpin RNA (***shRNA***) (Rao et al., 2009). Exogenous siRNA nonspecifically enters cells within a matter of minutes and produces a reduction of the target gene within around 48 hours. Plasmids encoding for shRNA can be transfected into cells using viral vectors to produce stable, cell-type specific expression that can last for over a year. The timescale over which RNAi could be used to reduce KCC2 expression is too slow for use acutely in gramicidin perforated patch recordings from thalamic slices. However, RNAi may be better suited for EEG experiments where the impact of gene knockdown in the RT nucleus on the seizure frequency of WAG/Rij can be observed over the course of hours or even days. Ideally, an RT neuron specific promoter could be utilized to only express an shRNA targeting KCC2 in RT neurons. The combination of distal-less homeobox 5/6 (***DLX5/6***) -cre mice and a pSico, cre-dependent, shRNA expression vector enables targeted expression of shRNA in RT neurons (Jung et al., 2016). Such RNAi experiments would more specifically isolate the role of KCC2, over other mechanisms, in dynamically regulating $[Cl^-]_i$ in RT neurons and maintaining the inhibitory GABAergic signaling among RT neurons that is required for the RT nucleus to serve as a seizure choke point.

Additional experiments measuring the impact of KCC2 activity on electrographic seizures, the *in vivo* relationship between RT $[Cl^-]_i$ and seizure onset, the differential $[Cl^-]_i$ regulation of RT neuron subtypes, and the selective RNAi knockdown of KCC2 in RT neurons will all further enhance our understanding

of the RT seizure choke point. Altogether, a more complete understanding of the mechanisms that restrict highly synchronized activity from occurring within the thalamus will provide new targets for therapeutic interventions to prevent absence seizures.

References

Ahrens S, Jaramillo S, Yu K, Ghosh S, Hwang G-R, Paik R, Lai C, He M, Huang ZJ, Li B (2015) ErbB4 regulation of a thalamic reticular nucleus circuit for sensory selection. Nat Neurosci 18:104–111.

Blaesse P, Airaksinen MS, Rivera C, Kaila K (2009) Cation-chloride cotransporters and neuronal function. Neuron 61:820–838.

Cai DJ et al. (2016) A shared neural ensemble links distinct contextual memories encoded close in time. Nature 534:115–118.

Cardarelli RA et al. (2017) The small molecule CLP257 does not modify activity of the K+–Cl− co-transporter KCC2 but does potentiate GABAA receptor activity. Nat Med 23:1394–1396.

Clemente-Perez A, Makinson SR, Higashikubo B, Brovarney S, Cho FS, Urry A, Holden SS, Wimer M, Dávid C, Fenno LE, Acsády L, Deisseroth K, Paz JT (2017) Distinct Thalamic Reticular Cell Types Differentially Modulate Normal and Pathological Cortical Rhythms. Cell Rep 19:2130–2142.

Coenen AML, Van Luijtelaar ELJM (1987) The WAG/Rij rat model for absence epilepsy: age and sex factors. Epilepsy Res 1:297–301.

Crick F (1984) Function of the thalamic reticular complex: the searchlight hypothesis. Proc Natl Acad Sci 81:4586–4590.

Delpire E, Weaver CD (2016) Challenges of Finding Novel Drugs Targeting the K-Cl Cotransporter. ACS Chem Neurosci 7:1624–1627.

Egerton A, Reid L, McKerchar CE, Morris BJ, Pratt JA (2005) Impairment in perceptual attentional set-shifting following PCP administration: A rodent

model of set-shifting deficits in schizophrenia. Psychopharmacology (Berl) 179:77–84.

Ferrarelli F, Tononi G (2011) The thalamic reticular nucleus and schizophrenia. Schizophr Bull 37:306–315.

Fire A, Xu S, Montgomery MK, Kostas SA, Driver SE, Mello CC (1998) Potent and specific genetic interference by double-stranded RNA in caenorhabditis elegans. Nature 391:806–811.

Gagnon M, Bergeron MJ, Lavertu G, Castonguay A, Tripathy S, Bonin RP, Perez-Sanchez J, Boudreau D, Wang B, Dumas L, Valade I, Bachand K, Jacob-Wagner M, Tardif C, Kianicka I, Isenring P, Attardo G, Coull J a M, De Koninck Y (2013) Chloride extrusion enhancers as novel therapeutics for neurological diseases. Nat Med 19:1524–1528.

Gagnon M, Bergeron MJ, Perez-Sanchez J, Plasencia-Fernández I, Lorenzo L-E, Godin AG, Castonguay A, Bonin RP, De Koninck Y (2017) Reply to The small molecule CLP257 does not modify activity of the K+–Cl− co-transporter KCC2 but does potentiate GABAA receptor activity. Nat Med 23:1396–1398.

Galanopoulou AS, Mowrey WB (2016) Not all that glitters is gold: A guide to critical appraisal of animal drug trials in epilepsy. Epilepsia Open 1:86–101.

Glauser TA, Ben-Menachem E, Bourgeois B, Cnaan A, Guerreiro C, Kälviäinen R, Mattson R, French JA, Perucca E, Tomson T (2013a) Updated ILAE evidence review of antiepileptic drug efficacy and effectiveness as initial monotherapy for epileptic seizures and syndromes. Epilepsia 54:551–563.

Glauser TA, Cnaan A, Shinnar S, Hirtz DG, Dlugos D, Masur D, Clark PO,

Adamson PC (2013b) Ethosuximide, valproic acid, and lamotrigine in childhood absence epilepsy: Initial monotherapy outcomes at 12 months. Epilepsia 54:141–155.

Gowers WR (1881) Epilepsy and other Chronic Convulsive Diseases, Their Causes, Symptoms and Treatment. London: Churchill.

Halassa MM, Chen Z, Wimmer RD, Brunetti PM, Zhao S, Zikopoulos B, Wang F, Brown EN, Wilson MA (2014) State-dependent architecture of thalamic reticular subnetworks. Cell 158:808–821.

Hewitt SA, Wamsteeker JI, Kurz EU, Bains JS (2009) Altered chloride homeostasis removes synaptic inhibitory constraint of the stress axis. Nat Neurosci 12:438–443.

Hyde TM, Lipska BK, Ali T, Mathew S V, Law AJ, Metitiri OE, Straub RE, Ye T, Colantuoni C, Herman MM, Bigelow LB, Weinberger DR, Kleinman JE (2011) Expression of GABA Signaling Molecules KCC2, NKCC1, and GAD1 in Cortical Development and Schizophrenia. J Neurosci 31:11088–11095.

Jarolimek W, Lewen A, Misgeld U (1999) A furosemide-sensitive K+-Cl- cotransporter counteracts intracellular Cl- accumulation and depletion in cultured rat midbrain neurons. J Neurosci 19:4695–4704.

Jin X, Huguenard JR, Prince DA (2005) Impaired Cl- Extrusion in Layer V Pyramidal Neurons of Chronically Injured Epileptogenic Neocortex. J Neurophysiol 93:2117–2126.

Jung J-Y, Lee SE, Hwang EM, Lee CJ (2016) Neuronal Expression and Cell-Type-Specific Gene-Silencing of Best1 in Thalamic Reticular Nucleus Neurons

Using pSico-Red System. Exp Neurobiol 25:120–129.

Kahle KT et al. (2014) Genetically encoded impairment of neuronal KCC2 cotransporter function in human idiopathic generalized epilepsy. EMBO Rep 15:766–774.

Kelley MR, Deeb TZ, Brandon NJ, Dunlop J, Davies PA, Moss SJ (2016) Compromising KCC2 transporter activity enhances the development of continuous seizure activity. Neuropharmacology 108:103–110.

Klein PM, Lu AC, Harper ME, McKown HM, Morgan JD, Beenhakker MP (2018) Tenuous Inhibitory GABAergic Signaling in the Reticular Thalamus. J Neurosci 38:1232–1248.

Krause M, Hoffmann WE, Hajós M (2003) Auditory sensory gating in hippocampus and reticular thalamic neurons in anesthetized rats. Biol Psychiatry 53:244–253.

Le Rouzic P, Ivanov TR, Stanley PJ, Baudoin FMH, Chan F, Pinteaux E, Brown PD, Luckman SM (2006) KCC3 and KCC4 expression in rat adult forebrain. Brain Res 1110:39–45.

Lee S-H, Govindaiah G, Cox CL (2007) Heterogeneity of firing properties among rat thalamic reticular nucleus neurons. J Physiol 582:195–208.

Löscher W (2017) Animal Models of Seizures and Epilepsy: Past, Present, and Future Role for the Discovery of Antiseizure Drugs. Neurochem Res 42:1873–1888.

Mahadevan V, Woodin MA (2016) Regulation of neuronal chloride homeostasis by neuromodulators. J Physiol 10:1–13.

McAlonan K, Cavanaugh J, Wurtz RH (2008) Guarding the gateway to cortex with attention in visual thalamus. Nature 456:391–394.

Mohanraj R, Brodie MJ (2005) Outcomes in newly diagnosed localization-related epilepsies. Seizure 14:318–323.

Moore YE, Kelley MR, Brandon NJ, Deeb TZ, Moss SJ (2017) Seizing Control of KCC2: A New Therapeutic Target for Epilepsy. Trends Neurosci 40:555–571.

Myers VB, Haydon DA (1972) Ion transfer across lipid membranes in the presence of gramicidin A: II. The ion selectivity. Biochim Biophys Acta 274:313–322.

Paz JT, Huguenard JR (2015) Microcircuits and their interactions in epilepsy: is the focus out of focus? Nat Neurosci 18:351–359.

Rankin-Gee EK, McRae PA, Baranov E, Rogers S, Wandrey L, Porter BE (2015) Perineuronal net degradation in epilepsy. Epilepsia 56:1124–1133.

Rao DD, Vorhies JS, Senzer N, Nemunaitis J (2009) siRNA vs. shRNA: Similarities and differences. Adv Drug Deliv Rev 61:746–759.

Rivera C, Voipio J, Payne JA, Ruusuvuori E, Lahtinen H, Lamsa K, Pirvola U, Saarma M, Kaila K (1999) The K+/Cl- co-transporter KCC2 renders GABA hyperpolarizing during neuronal maturation. Nature 397:251–255.

Sivakumaran S, Cardarelli RA, Maguire J, Kelley MR, Silayeva L, Morrow DH, Mukherjee J, Moore YE, Mather RJ, Duggan ME, Brandon NJ, Dunlop J, Zicha S, Moss SJ, Deeb TZ (2015) Selective Inhibition of KCC2 Leads to Hyperexcitability and Epileptiform Discharges in Hippocampal Slices and In Vivo. J Neurosci 35:8291–8296.

Sun Y-G, Wu C-S, Renger JJ, Uebele VN, Lu H-C, Beierlein M (2012) GABAergic

synaptic transmission triggers action potentials in thalamic reticular nucleus neurons. J Neurosci 32:7782–7790.

Ulrich D, Huguenard JR (1997) Nucleus-specific chloride homeostasis in rat thalamus. J Neurosci 17:2348–2354.

Van Brederode JFM, Takigawa T, Alzheimer C (2001) GABA-evoked chloride currents do not differ between dendrites and somata of rat neocortical neurons. J Physiol 533:711–716.

Van Luijtelaar ELJM, Dirksen R, Vree TB, Van Haaren F (1996) Effects of acute and chronic cocaine administration on EEG and behaviour in intact and castrated male and intact and ovariectomized female rats. Brain Res Bull 40:43–50.

Wells MF, Wimmer RD, Schmitt LI, Feng G, Halassa MM (2016) Thalamic reticular impairment underlies attention deficit in Ptchd1(Y/-) mice. Nature 532:58–63.

Williams JR, Payne JA (2004) Cation transport by the neuronal K(+)-Cl(-) cotransporter KCC2: thermodynamics and kinetics of alternate transport modes. Am J Physiol Cell Physiol 287:C919–C931.